INFORMATION TO USERS

This dissertation was produced from a microfilm copy of the original document. While the most advanced technological means to photograph and reproduce this document have been used, the quality is heavily dependent upon the quality of the original submitted.

The following explanation of techniques is provided to help you understand markings or patterns which may appear on this reproduction.

1. The sign or "target" for pages apparently lacking from the document photographed is "Missing Page(s)". If it was possible to obtain the missing page(s) or section, they are spliced into the film along with adjacent pages. This may have necessitated cutting thru an image and duplicating adjacent pages to insure you complete continuity.

2. When an image on the film is obliterated with a large round black mark, it is an indication that the photographer suspected that the copy may have moved during exposure and thus cause a blurred image. You will find a good image of the page in the adjacent frame.

3. When a map, drawing or chart, etc., was part of the material being photographed the photographer followed a definite method in "sectioning" the material. It is customary to begin photoing at the upper left hand corner of a large sheet and to continue photoing from left to right in equal sections with a small overlap. If necessary, sectioning is continued again — beginning below the first row and continuing on until complete.

4. The majority of users indicate that the textual content is of greatest value, however, a somewhat higher quality reproduction could be made from "photographs" if essential to the understanding of the dissertation. Silver prints of "photographs" may be ordered at additional charge by writing the Order Department, giving the catalog number, title, author and specific pages you wish reproduced.

University Microfilms

300 North Zeeb Road
Ann Arbor, Michigan 48106

A Xerox Education Company

72-20,604

LORES, Manuel Edward, 1942-

A THEORETICAL STUDY OF NONLINEAR LONGITUDINAL COMBUSTION INSTABILITY IN LIQUID PROPELLANT ROCKET ENGINES.

Georgia Institute of Technology, Ph.D., 1972
Engineering, aeronautical

University Microfilms, A XEROX Company, Ann Arbor, Michigan

A THEORETICAL STUDY OF NONLINEAR LONGITUDINAL COMBUSTION INSTABILITY IN LIQUID PROPELLANT ROCKET ENGINES

A THESIS

Presented to

The Faculty of the Division of Graduate

Studies and Research

by

Manuel Edward Lores

In Partial Fulfillment

of the Requirements for the Degree

Doctor of Philosophy

in the School of Aerospace Engineering

Georgia Institute of Technology

March, 1972

A THEORETICAL STUDY OF NONLINEAR LONGITUDINAL COMBUSTION INSTABILITY IN LIQUID PROPELLANT ROCKET ENGINES

Approved:

Ben T. Zinn

Ben T. Zinn, Chairman

Warren C. Strahle

Warren C. Strahle

Eugene A. Powell

Eugene A. Powell

Date approved by Chairman: Feb. 25, 1972

In presenting the dissertation as a partial fulfillment of the requirements for an advanced degree from the Georgia Institute of Technology, I agree that the Library of the Institute shall make it available for inspection and circulation in accordance with its regulations governing materials of this type. I agree that permission to copy from, or to publish from, this dissertation may be granted by the professor under whose direction it was written, or, in his absence, by the Dean of the Graduate Division when such copying or publication is solely for scholarly purposes and does not involve potential financial gain. It is understood that any copying from, or publication of, this dissertation which involves potential financial gain will not be allowed without written permission.

Manuel E. Jones

7/24/68

ACKNOWLEDGMENTS

I would like to express my appreciation to Dr. Ben T. Zinn for his suggestion of the topic and for his guidance during the course of this research. A word of thanks is due to Dr. Eugene A. Powell who, under the direction of Dr. Zinn, laid the foundation of the research reported in this dissertation. I would also like to thank Drs. Zinn, Powell, and Strahle for their careful examination of this manuscript and for their many useful suggestions.

This research could not have been completed without the support given by the staff of the Rich Electronic Computer Center. Their help is gratefully acknowledged. The encouragement of Mr. Paul E. Browne of the Vought Aeronautics Division, L. T. V. Inc., must not go unmentioned. The educational leave of absence and the doctoral fellowship awarded to me by L. T. V. made the completion of this research possible. The financial support of the National Aeronautics and Space Administration, the National Science Foundation, and the Georgia Institute of Technology is gratefully acknowledged.

I wish to express my appreciation to Mrs. Peggy Weldon for the typing of this report.

I wish to thank my parents, Dr. Manuel C. Lores and Mrs. Laura Elby Lores for their moral and financial support during the years of my education.

Finally, a very special word of thanks is due to my family for their understanding and patience in somewhat trying circumstances. The cooperation and encouragement of my wife Lynda is very deeply appreciated.

TABLE OF CONTENTS

TABLE OF CONTENTS (Continued)

LIST OF TABLES

LIST OF ILLUSTRATIONS

LIST OF ILLUSTRATIONS (Continued)

NOMENCLATURE

$A_n(t)$	mode-amplitude function of the n^{th} mode
$B_n(t)$	mode-amplitude function of the n^{th} mode
$C_n(t)$	mode-amplitude function of the n^{th} mode
c	speed of sound
F_b	nozzle boundary term
h	specific enthalpy, or numerical integration step size
$\underline{J}$	perturbation mass flux vector
K_p	linear mode-amplitude
L	combustor length (dimensional)
ℓ	summation index
M	Mach number
m	summation index
N	summation limit
n	summation index
$\underline{n}$	unit normal vector
$\hat{n}$	interaction index
$\hat{n}_{min}$	critical value of the interaction index
$O(\ )$	order of magnitude
P_n	linear pressure mode-amplitude of the n^{th} mode
p	pressure
Q_1	coefficient of the linear boundary term
Q_2	coefficient of the nonlinear boundary term
Q_m'	unsteady mass source representing the nozzle
q	acoustic-type wave velocity

T	oscillation period
t	time
t_o	time parameter in correlation technique
U_n	linear velocity mode-amplitude of the n^{th} mode
u	velocity
w	combustion mass source
z	axial space dimension
z_c	axial station at which combustion is completed
z_r	axial station at which experimental pressure correlation is made
γ	specific heat ratio
$\Delta p'_{max}$	maximum peak-to-peak pressure amplitude
$\delta\hat{n}$	displacement at constant $\bar{\tau}$ in $n - \bar{\tau}$ plane
ε	order of magnitude parameter
v	specific volume
ρ	density
τ	time lag
$\bar{\tau}$	sensitive time lag
φ	velocity potential
ω	reduced frequency, $\omega^* L/\bar{c}_o^*$
1L	first longitudinal mode
2L	second longitudinal mode

Superscripts

$(\ )'$	perturbation quantity or time derivative
$(\bar{\ })$	steady state quantity
$(\ )^*$	dimensional quantity
$(\tilde{\ })$	approximate solution

Subscripts

e	evaluated at combustor exit
i	initial conditions
ℓ	ℓ^{th} longitudinal mode, or liquid phase quantity
R	retarded variable, evaluated at time $t - \bar{\tau}$
s	stagnation condition
t	time derivative
z	space derivative
0	injection face stagnation condition
1	first longitudinal mode
2	second longitudinal mode

Note: The notation used in Chapter II differs from that defined in this list. The symbols used in Chapter II are defined in the text of that chapter.

SUMMARY

Nonlinear analyses of the stability of moderate and large amplitude high frequency longitudinal combustion-driven oscillations in liquid propellant rocket motors are presented. The objective of these investigations is to provide rocket design engineers with straightforward analytical techniques for the nonlinear analysis of longitudinal combustion instability. The resulting methodology (1) provides physical insight into the phenomenon of longitudinal combustion instability, (2) clarifies certain ambiguities in previous investigations of the problem, and (3) requires a minimum of mathematical computations. It is believed that the techniques developed in this dissertation can also be used to investigate axial mode combustion instability problems in solid propellant rocket motors and air-breathing propulsion devices.

The mathematical techniques are developed by investigating the nonlinear behavior of axial mode combustion instability oscillations in liquid propellant rocket motors having a high impedance injector and a short nozzle. The mean flow Mach number is assumed to be small. The combustion process is distributed throughout the combustor, and it is assumed to be completed at the nozzle entrance. Crocco's time lag hypothesis is used to represent the unsteady combustion process.

The undetermined function version of the Galerkin method is used to find solutions. This approach considers the stability of a number of modes simultaneously, and it yields both the transient and final periodic behavior of the combustion instability oscillations.

The salient results of this investigation are summarized in the following paragraphs:

1. Instability of a mode cannot be triggered at engine operating conditions under which another mode is linearly unstable.

2. For moderate amplitude instabilities, the regime of unstable engine operating conditions, in the $\hat{n}$ - $\overline{\tau}$ plane, can be predicted by a linear analysis.

3. For most unstable engine operating conditions the flow oscillations exhibit a shock-type behavior with the number of shocks determined by the characteristics of the engine operating conditions.

4. When only a single mode is linearly unstable, the resulting nonlinear waveforms depend upon the proximity of the engine operating conditions to resonance. Based on this dependence of the nonlinear waveforms upon engine operating conditions, a correlation technique is developed which permits the analytical solutions to be related to experimental data.

5. In a majority of cases, the nonlinear behavior of unstable engines can be approximated by second order solution .

6. Increasing the mean flow Mach number is destabilizing.

7. Increasing the combustor length is stabilizing for above resonant conditions, and destabilizing for below resonant conditions.

CHAPTER I

INTRODUCTION

Description of the Problem

In recent years the occurrence of combustion-driven oscillations has hampered the development of many rocket motors and jet engines. The complex phenomenon involving the interaction of an unsteady combustion process with flow oscillations inside an engine is known as combustion instability. Combustion instability is usually initiated by a flow disturbance which results in a perturbation of the steady state combustion process. Consequently, the rate of energy released by the combustion process may increase, and part of the excess energy may feed back into the initial flow disturbance. Under the proper phase relationship, a closed energy feedback loop is established between the combustion process and the flow oscillations, resulting in self-sustained, organized oscillations of the gas within the combustor. The organized nature of the combustion instability oscillations distinguishes them from the nondestructive random oscillations characteristic of rough engine operation. The amplitudes of combustion instability oscillations are usually large, and the occurrence of combustion instability frequently results in the destruction of the engine or the failure of the mission supported by the motor.

Combustion instabilities are usually categorized according to the frequency of the oscillations. Low frequency combustion instability, or chugging, is characterized by low frequency oscillations, and by a nearly spacially uniform flow field at each instant of time. The driving

mechanism of these low frequency oscillations is primarily through coupling with the propellant feed system. At present, chugging is not considered to be a major problem, and means of preventing its occurrence are relatively well understood.

Combustion instabilities in an intermediate frequency range of several hundred cycles per second have also been investigated. This type of instability is associated with the appearance of entropy waves. In practice, the occurrence of entropy wave instability is rare.

High frequency or acoustic instability is the most destructive form of combustion instability. As the name implies, the frequencies of this type of combustion instability are close to those of the natural acoustic modes of a closed-ended chamber of the same geometry as the rocket combustor. The driving mechanism of these high frequency oscillations is the energy feedback loop formed by the interaction of the energy released by the unstable combustion process with the flow oscillations and with the resonant properties of the combustor. This dissertation is concerned with the investigation of high frequency axial combustion instability.

Experimental data[1] show that high frequency combustion instability oscillations are frequency selective, and that the frequency of oscillation is usually within a few percent of one of the natural acoustic modes of the combustion chamber. The existence of a preferred frequency range indicates that there is a characteristic time associated with the unsteady combustion process, and that unstable engine operation results when this characteristic time is properly related to the period of one of the chamber modes. These observations form the basis of the Crocco sensitive

time lag theory of combustion instability.[1] This theory is briefly discussed in a subsequent section of this thesis.

In an intrinsically unstable motor, combustion instability results spontaneously from perturbations of the engine steady state operating conditions. Because the amplitude of the initial disturbances are very small, the conditions of incipient instability in an intrinsically unstable motor can be predicted by a linear analysis. Consequently, an intrinsically unstable engine is often said to be linearly unstable.

Experimental observations show that instability may be initiated in an intrinsically stable motor by a sufficiently large amplitude perturbation of the steady state engine operating conditions. Because the instability is "triggered" by a finite amplitude disturbance, the engine is said to be nonlinearly unstable. When a large amplitude disturbance is introduced inside a combustor, the pressure and temperature of the flow increase. Consequently, an acceleration of the various rate processes, such as the rates of vaporization and reaction rates, results. If a sufficient change in the rate processes occurs, and if the characteristic time of the unsteady combustion process is conducive to unstable engine operation, then the interaction of the nonlinear flow oscillations with the combustion process results in combustion instability.

Regardless of the manner in which the instability is initiated, the combustion instability oscillations undergo a transient phase prior to the establishment of stable, periodic waves. When the combustor length-to-diameter ratio is sufficiently large, the frequency of the instability is close to the frequency of one of the chambers axial modes; usually the fundamental mode. In this case, the combustion instability oscillations

are longitudinal waves. Fully developed longitudinal combustion instability oscillations are usually discontinuous waves.

This dissertation deals with the development of a mathematical technique for investigating the transient and periodic (i.e., limit cycle) behavior of high frequency longitudinal combustion instability. Specifically, this research is concerned with the study of high frequency axial combustion instability in liquid propellant rocket motors. However, it is believed that the techniques developed herein will also be applicable to the study of combustion driven longitudinal oscillations in solid propellant rockets as well as in jet engines.

Previous Work in the Field

Due to the complex nature of combustion instability, the development of theoretical models capable of describing the flow conditions inside unstable combustors proved to be a difficult task. The difficulties centered about (1) the analytical representation of the unsteady combustion process and its interaction with the flow oscillations, (2) the solution of the partial differential equations that result from the formulation of the problem, and (3) the theoretical description of the unsteady boundary condition imposed by the presence of the nozzle. Over the past two decades considerable effort has been devoted to the investigation of each of these problem areas.

The presence of a nozzle introduces a complicated boundary condition at the combustor exit plane. However, when the subsonic flow portion of the nozzle is short in comparison with the combustor length, the gas residence time inside the nozzle is much shorter than the period of

the wave in the chamber. Under these conditions the nozzle flow instantaneously adjusts itself to flow oscillations within the combustor. That is, the nozzle behaves in a quasi-steady manner. It has been shown[2] that the quasi-steady response of a short nozzle can be expressed analytically by requiring that the Mach number at the nozzle entrance remain constant at all times, that is:

$$\frac{u_e^*}{c_e^*} = \frac{\bar{u}_e^* + u_e^{*\prime}}{\bar{c}_e^* + c_e^{*\prime}} = \text{constant} \qquad (1.1)$$

The quasi-steady short nozzle boundary condition has been extensively used in both linear and nonlinear analyses of combustion instability. In related studies,[3,4] it has been well established that increasing the length of the convergent section of the nozzle has a stabilizing effect on the system. Consequently, the stability behavior predicted using the quasi-steady short nozzle boundary condition is conservative.

After injection, the liquid droplets undergo a complicated process during which the propellant elements mix (bi-propellants), vaporize, and react to form hot gas combustion products. The physical processes involved in the conversion of liquid propellants into gas products are not well understood. In particular, the dependence of the overall reaction rate upon the combustor geometry and on the engine operating conditions has yet to be determined. In the absence of such information, it is impossible to develop a precise analytical description of the unsteady combustion process. As a result, recourse must be made to the use of semi-empirical unsteady combustion models which hopefully incorporate the

important physical characteristics of the unsteady combustion process.

By far the most successful unsteady liquid propellant combustion model was developed by Crocco in the $\hat{n} - \bar{\tau}$ theory of combustion instability. In a monograph published in 1956,[3] Crocco and Cheng discussed the development of the $\hat{n} - \bar{\tau}$ theory and its application in the linear analysis of a variety of liquid propellant longitudinal combustion instability problems. Briefly, in the $\hat{n} - \bar{\tau}$ model Crocco postulates that the complex transformation of propellant elements into combustion products can be represented by a discontinuous process. It is assumed that the vaporization and burning of the propellants can be simulated by a process in which the propellants remain in liquid form over some time periods, at the conclusion of which the elements are instantaneously converted into hot gas products. The time period from the injection to the reaction is called the total time lag, τ_t^*. According to the $\hat{n} - \bar{\tau}$ theory, during a portion of τ_t^* the propellant elements accumulate energy and are insensitive to local flow oscillations, while over the remaining portion of τ_t^* the propellant elements are affected by the flow oscillations. These time periods are referred to as τ_i^* and τ^*, respectively. It is postulated in the theory that during the sensitive portion of the time lag, τ^*, the rate of the combustion process, f^*, is related to the instantaneous local pressure, p^* by the relationship:

$$f^* \sim (p^*)^{\hat{n}}$$

where the parameter $\hat{n}$ is called the interaction index. Using this postulate, a linear analysis was used[3] to derive the following relation between the unsteady mass generation, $\frac{\partial w^{*\prime}}{\partial z^*}$, and the flow pressure perturbations:

$$\frac{\partial w^*}{\partial z^*} = \frac{d\bar{w}^*}{dz^*}\,\hat{n}\left[\frac{p^{*\prime}(z^*, t^*) - p^{*\prime}(z^*, t^* - \bar{\tau}^*)}{\bar{p}^*}\right] \qquad (1.2)$$

Because of the rudimentary nature of the $\hat{n} - \bar{\tau}$ theory, it is appropriate to consider $\hat{n}$ and $\bar{\tau}$ as correlation parameters. In an engine there is a limit cycle oscillation associated with each set of $\hat{n}$ and $\bar{\tau}^*$. Consequently, in principal it is possible to determine $\hat{n}$ and $\bar{\tau}^*$ by observing the behavior of the limit cycle combustion instability oscillations. It is important to note that since the overall reaction rate of the combustion process may be affected by the presence of flow oscillations, or by the introduction of a disturbance, the characteristic time, which is a measure of the susceptibility of the engine to combustion instability, may take on a value different from that corresponding to steady state conditions. In particular, it is to be expected that an increase of the pressure and temperature inside the combustor will result in an acceleration of the combustion rate processes, and that $\bar{\tau}^*$ will consequently decrease. This behavior of $\bar{\tau}^*$ has been argued on physical grounds[5] and has been observed experimentally.[6] If $\bar{\tau}^*$ is in fact changed by a variation of engine operating conditions, brought about, for instance, by the introduction of energy in the form of a triggering disturbance, then the $\hat{n} - \bar{\tau}$ theory is not capable of defining the conditions (e.g., the amount of energy input) required to trigger an instability in an intrinsically stable engine. However, once limit cycle conditions have been reached the relative instability of the engine can be determined in terms of the correlation parameters $\hat{n}$ and $\bar{\tau}^*$.

The usefulness of the $\hat{n} - \bar{\tau}$ theory has been demonstrated in numerous linear and nonlinear analyses of combustion instability. Linear analyses

are concerned with the prediction of the range of engine operating conditions under which combustion instability can be initiated by infinitesimal amplitude disturbances. In the $\hat{n}$ - $\bar{\tau}$ theory it is customary to present the loci of points of neutral linear stability on an $\hat{n}$ - $\bar{\tau}$ coordinate system, as demonstrated in Figure 1a. The regions of linear instability and linear stability are referred to as regions (A) and (B), respectively.

Nonlinear stability limits can also be defined in an $\hat{n}$ - $\bar{\tau}$ coordinate system. Hypothetical nonlinear stability limits are drawn in a broken line in Figure 1a. Instability will result for engine operating conditions between the linear and nonlinear stability limits when the amplitude of the initial disturbance is larger than a critical minimum amplitude. For example, Figure 1b shows the variation of the amplitude of the combustion instability oscillations with displacement from the neutral stability curve, for a given value of $\bar{\tau}^*$. Positive displacement is taken to be into the unstable region of Figure 1a. At $\bar{\tau}^* = \bar{\tau}_1^*$ it is assumed that the linear and nonlinear limits coincide. Hence, in this case the amplitude of the limit cycle oscillations is zero for $\delta\hat{n} \leq 0$. Growth or decay of disturbances is indicated by the arrows in Figure 1b. On the other hand, the nonlinear stability limit is assumed to lie in a linearly stable region at $\bar{\tau}^* = \bar{\tau}_2^*$. The critical amplitude required for unstable engine operation at $\bar{\tau}_2^*$ is shown as a broken line in the region $\delta\hat{n} < 0$ in Figure 1b. The amplitude of the stable limit cycle oscillations is shown as the solid line.

Nonlinear analyses are required to determine nonlinear stability limits and to investigate the behavior of finite amplitude combustion

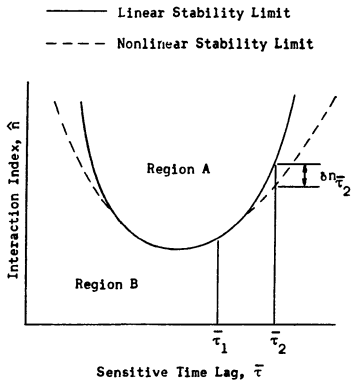

Figure 1a

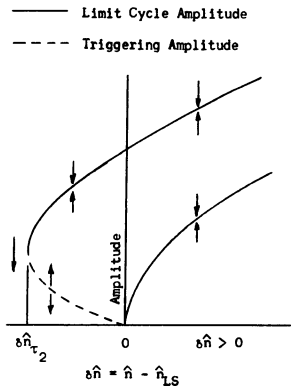

Figure 1b

Figure 1. Concepts of Stability.

instability oscillations. Nonlinear studies of longitudinal combustion instability in liquid propellant rockets have been conducted by Sirigano[8] and Mitchell.[9] The quasi-steady short nozzle boundary condition and the Crocco $\hat{n}$ - $\bar{\tau}$ unsteady combustion model are used in these investigations. Complex perturbation techniques are used to find nonlinear solutions in combustors having low Mach number mean flows.

A serious limitation of these investigations is that they consider the behavior of periodic solutions only and they can only analyze the stability of a single longitudinal mode at a time. As a result it is impossible to use these theories to predict the longitudinal stability of liquid rockets in ranges of operating conditions where more than one mode (e.g., the first and second longitudinal modes) are linearly unstable. Such a region is shown on an $\hat{n}$ - $\bar{\tau}$ plane in Figure 2. In the crossed hatched region of Figure 2 a first longitudinal mode analysis using the results of Reference (8) or (9) would predict a first-longitudinal-type instability, while a second longitudinal analysis would predict a second-longitudinal-type oscillation; results that are in complete contradiction.

References (8) and (9) are concerned with the nonlinear behavior of fundamental mode axial oscillations. The nonlinear stability limits predicted by these two analyses are in complete disagreement. Briefly, Sirignano[8] predicts that second order nonlinearities broaden the range of possible unstable engine operation for all off-resonant conditions. This result is based upon the computed instability of the nonlinear solutions found in regions of linear stability. The limit cycle waveform cannot be predicted by Sirignano's analysis. The extent of the broadening

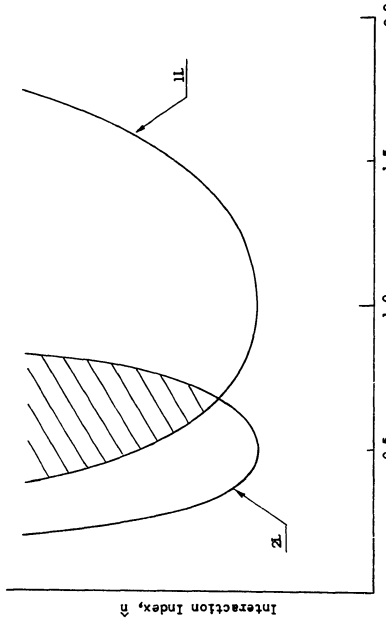

Figure 2. Typical Linear Stability Limits for the First Two Longitudinal Modes.

of the unstable region by nonlinearities is not precisely defined by Sirignano.

On the other hand, Mitchell[9] concluded that nonlinear effects broaden the range of possible instability only in limited regions of the $\hat{n} - \bar{\tau}$ stability plane. Mitchell establishes these regions using deductive arguments concerning the stability of the nonlinear solutions resulting from his analysis. It can be shown that the fundamental mode nonlinearly unstable regions found by Mitchell lie in regions of the $\hat{n} - \bar{\tau}$ stability plane in which the second axial mode is linearly unstable. These results are shown schematically in Figure 3. In the crossed-hatched regions of this figure, the fundamental mode analysis of Reference 9 predicts the possibility of first longitudinal nonlinear instability, while an analysis of the second longitudinal mode will predict a second-longitudinal type oscillation.

The ambiguities discussed in the preceding paragraphs can be clarified by an analysis in which the behavior of a number of modes is considered simultaneously, and in which no a priori knowledge of the limit cycle oscillation is required. A technique which incorporates these features has been developed by Zinn and Powell in References 10 through 14. These analyses apply the Galerkin method, a special application of the Method of Weighted Residuals, in the solution of a variety of combustion instability problems. Because of difficulties encountered in satisfying the complicated boundary conditions associated with combustion instability problems, a modification of the Galerkin method was developed.[14] In this modification, the differential equation residual and the boundary residual are combined in a manner consistent with the flow conservation laws.

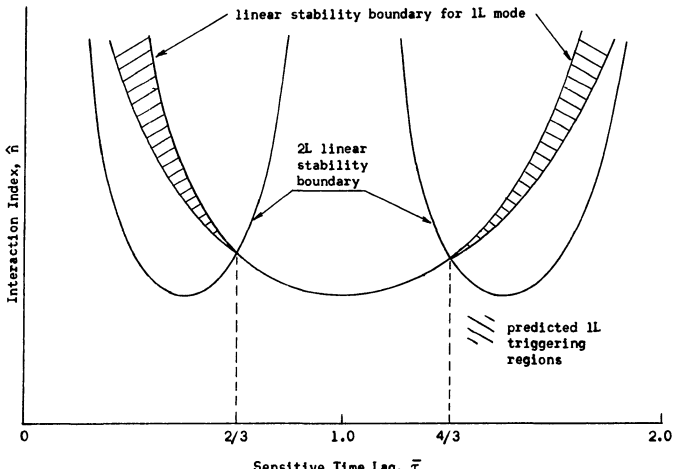

Figure 3. Linear and Nonlinear Stability Maps for the First Longitudinal Mode.

The modified Galerkin method has been used by Zinn and Powell to analyze the linear stability of combustors experiencing incipient longitudinal instability. The predicted stability limits are in excellent agreement with previous results found by a more exact mathematical solution.[3] However, the majority of the solutions obtained to date are concerned with the nonlinear stability of transverse oscillations. The predicted waveforms of the combustion instability oscillations appear to be in good agreement with available experimental data.

In addition to considering the stability of a number of modes simultaneously, the Galerkin method has the advantages of (1) being capable of yielding both the transient and limit cycle behavior of the instabilities, (2) being relatively simple from a mathematical point of view, (3) requiring relatively little computation times, and (4) offering considerable physical insight into the behavior of the instabilities. This dissertation will demonstrate that all of these advantages may be incorporated into the nonlinear analysis of longitudinal combustion instability.

More recently, a similar approach has been used by Culick[15] in the treatment of unstable motions in solid propellant rocket combustors. In Culick's technique an almost linear problem is handled by an application of the Method of Weighted Residuals. The nonlinearities of the problem are associated with localized energy losses, such as wall losses and the interaction between the flow oscillations and the combustion process. This approach is not as general as the method of analysis developed by Zinn and Powell.

Definition of the Problem

The objective of this dissertation is to provide rocket design

engineers with a straightforward analytical technique for the nonlinear analysis of longitudinal combustion instability. The methodology will (1) provide physical insight into the combustion instability phenomenon; (2) clarify the ambiguities arising in the one mode, periodic nonlinear analyses; and (3) retain as much analytical simplicity as possible. A digital computer is required to generate the desired solutions. The numerical techniques used to solve the problem are adaptable to efficient computer programming.

The mathematical techniques are developed by investigating the nonlinear behavior of high frequency longitudinal combustion instability oscillations in liquid propellant rocket combustors. The combustor geometry is shown in Figure 4. The liquid propellants are injected uniformly through a high impedance injector, converted by a complex combustion process into hot gases, and the gas products are exhausted through a short nozzle. The nondimensional coordinate system is defined with the origin at the injector face and the nozzle entrance plane at $z = z^*/L = 1$. The thermodynamic variables are normalized by the appropriate injector face stagnation quantities, the velocity is nondimensionalized by the injector face steady state stagnation sonic velocity, and time is normalized by a characteristic time defined as the ratio of the combustor length to the injector face stagnation sonic velocity. The nondimensional variables are summarized in the following equations:

$$z = z^*/L \qquad t = t^*\bar{c}_o^*/L \qquad u = u^*/\bar{c}_o^* \qquad \rho = \rho^*/\bar{\rho}_o^*$$
$$p = p^*/\bar{p}_o^* = \gamma p^*/\bar{\rho}_o^*\bar{c}_o^{*2} \qquad h = \frac{\gamma-1}{\bar{c}_o^*} h^* \qquad w = w^*/\bar{\rho}_o^*\bar{c}_o^* \tag{1.3}$$

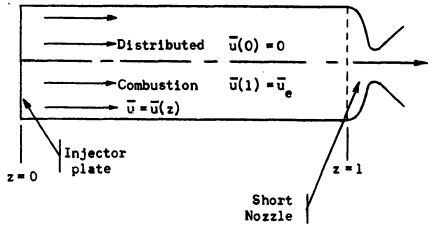

Injector plate boundary conditions:

$$u'(0,t) = 0$$

Quasi-steady short nozzle boundary condition

$$\left.\frac{\bar{u}+u'}{\bar{c}+c'}\right|_{z=1} = \text{constant}$$

Figure 4. Combustor Geometry and Boundary Conditions.

The following assumptions are made concerning the flow within the combustor:

1. The flow is one-dimensional, with the velocity vector parallel to the combustor axis.

2. The mean flow Mach number and its derivative are small.

3. The flow consists of a single constituent perfect gas and liquid droplets of negligible volume.

4. Viscosity, diffusion, and heat conduction are negligible.

5. The liquid phase stagnation enthalpy remains constant as the droplets traverse the combustor.

6. The momentum sources arising from gas-droplet interaction are negligible.

The mean flow Mach number is in fact small for many rocket engines. Restricting the analysis to low Mach number mean flows results in a considerable mathematical simplification, while retaining the essential physical characteristics of the problem.

Assumption 5 implies that the loss in droplet kinetic energy as the droplets traverse the combustor is balanced by an increase in the droplet thermal energy.

The last assumption states that the momentum sources arising from the droplet drag and from the acceleration of the just-burned gas to the gas-phase velocity are negligible. The phenomena neglected by assumptions 5 and 6 are expected to have a stabilizing effect on the system; consequently the stability behavior predicted when these terms are neglected is conservative.

The equations describing the behavior of the two phase flow field

inside the combustor have been developed using a standard control volume approach in Reference 3. The equations derived in Reference 3 are simplified in Appendix A using assumptions (1) through (6). The procedure used in Appendix A follows the development employed in References 3 and 14.

The equations governing the perturbed flow are derived from Equations (A-38) through (A-42) by assuming that the flow variables can be described as the sum of steady state condition and a perturbation term, that is:

$$u = \bar{u} + u' \tag{1.4}$$
$$p = \bar{p} + p'$$
$$\rho = \bar{\rho} + \rho'$$
$$w = \bar{w} + w'$$
$$h = \bar{h} + h'$$

The substitution of Equations (1.4) into Equations (A-38) through (A-42) and separating the steady and unsteady terms produces the equations describing the behavior of the unsteady flow inside the combustor. In performing this operation it is assumed that because the mean flow Mach number is small, terms involving the product of an $O(\bar{u}^2)$ quantity with a perturbation parameter are negligible. In Appendix A it is shown that $\bar{p} = 1 + O(\bar{u}^2)$ and that $\bar{\rho} = 1 + O(\bar{u}^2)$. Using these results and the fact that $\bar{h}_s - h_{\ell_s} = 0$ (Eq. (A-28)) the equations describing the behavior of the perturbed flow field can be written as follows:

1. Continuity:

$$\frac{\partial \rho'}{\partial t} + \bar{u}\frac{\partial \rho'}{\partial z} + \frac{\partial u'}{\partial z} + \rho'\left[\frac{d\bar{u}}{dz} + \frac{\partial u'}{\partial z}\right] + u'\frac{\partial \rho'}{\partial z} - \frac{\partial w'}{\partial z} = 0 \tag{1.5}$$

2. Momentum:

$$(1+\rho')\frac{\partial u'}{\partial t} + \bar{u}\frac{\partial u'}{\partial z} + (u'+\bar{u}\rho'+u'\rho')\left[\frac{d\bar{u}}{dz} + \frac{\partial u'}{\partial z}\right] + \frac{1}{\gamma}\frac{\partial p'}{\partial z} = 0 \quad (1.6)$$

3. Energy:

$$\frac{\partial p'}{\partial t} + (\bar{u}+u')\frac{\partial p'}{\partial z} + \gamma\frac{\partial u'}{\partial z} + \gamma p'\left[\frac{d\bar{u}}{dz} + \frac{\partial u'}{\partial z}\right] \quad (1.7)$$

$$- \gamma\left[\frac{\partial w'}{\partial z} - \frac{(\gamma-1)}{2}(2\bar{u}u'+u'^2)\left(\frac{d\bar{u}}{dz} + \frac{\partial w'}{\partial z}\right)\right] = 0$$

In writing Equation (1.7) use was made of the result that $\bar{w} = \bar{u} + 0(\bar{u}^2)$. (Refer to Equation (A-35)). It should be noted that the steady state velocity distribution must be specified before Equations (1.5) through (1.7) can be solved, and that $\bar{w} = \bar{u}$ within the restrictions of this analysis.

The unsteady combustion process, $\partial w'/\partial z$, is represented by a distribution of fluctuating mass sources. The unsteady mass generation is related to the gas phase flow properties with the aid of the Crocco $\hat{n}$ - $\bar{\tau}$ theory. The desired relation is given by Equation (1.2). In nondimensional terms this equation can be written as follows:

$$\frac{\partial w'}{\partial z} = \hat{n}\frac{d\bar{u}}{dz}\left[p'(z,t) - p'(z,t-\bar{\tau})\right] \quad (1.8)$$

Equation (1.8) is based upon linear considerations. It is particularly attractive from an analytical standpoint, and comparisons of theoretical results obtained using this relation with experimental data have verified its usefulness. Nonlinear extensions of the $\hat{n}$ - $\bar{\tau}$ theory have been developed in References 8 and 14. The resulting expressions

are quite complex. Since the $\hat{n} - \bar{\tau}$ theory is simply an approximate representation of a very complex combustion process that is not well understood, the additional complexity of the nonlinear combustion model is not warranted. Therefore, this study will use Equation (1.8) to describe the unsteady combustion process.

The problem boundary conditions are the solid wall boundary condition defined by

$$u'(0, t) = 0 \tag{1.9}$$

and the quasi-steady short nozzle boundary condition defined by Equation (1.1). Within the framework of the low Mach number assumption, the constant appearing on the right hand side of Equation (1.1) is simply the steady state exit Mach number; consequently the quasi-steady short nozzle boundary condition is given by the following relation:

$$u' = \bar{u}_e \frac{c'_e}{\bar{c}_e}$$

Assuming that the combustion is completed before the nozzle is reached, isentropic flow relations can be used to relate c'_e to one of the other thermodynamic variables. In this analysis it will prove beneficial to replace c'_e by p'_e. For isentropic flow

$$c = p^{\frac{\gamma-1}{2\gamma}}$$

and for the perturbed flow

$$\frac{c'_e}{\bar{c}_e} = \left[1 + \frac{p'_e}{\bar{p}_e}\right]^{\frac{\gamma-1}{2\gamma}} - 1$$

Using a binomial expansion and retaining up to second order terms, the above equation can be written as

$$\frac{c_e'}{\bar{c}_e} = \frac{\gamma-1}{2\gamma}\frac{p_e'}{\bar{p}_e}\left[1 - \frac{\gamma+1}{4\gamma}\frac{p_e'}{\bar{p}_e}\right]$$

Using this relation, the short nozzle boundary condition becomes:

$$u_e'\bar{p}_e^{\,2} = \frac{\gamma-1}{2\gamma}\bar{u}_e p_e'\left[\bar{p}_e - \frac{(\gamma+1)}{4\gamma}p_e'\right]$$

Recalling that $\bar{p}_e = 1 + O(\bar{u}_e^{\,2})$, it follows that:

$$u_e'[1 + O(\bar{u}_e^{\,2})]^2 = \frac{\gamma-1}{2\gamma}\bar{u}_e[p_e'(1+O(\bar{u}_e^{\,2})) - \frac{(\gamma+1)}{4\gamma}p_e'^2] + \text{H.O.T.}$$

Since p_e' is $O(1)$ or higher, it follows from a comparison of the right and left hand sides of the preceding equation that $u_e' = O(\bar{u}_e)$ or higher. Neglecting terms of $O(\bar{u}_e^{\,3})$ or higher, this equation becomes:

$$u_e' = \frac{\gamma-1}{2\gamma}\bar{u}_e\left[p_e' - \frac{+1}{4\gamma}p_e'^2\right] \tag{1.10}$$

Equation (1.11) is the desired quasi-steady short nozzle boundary condition. In deriving this relation, it has been assumed that $p_e' < \bar{p}_e$ and that terms of $O(\bar{u}_e p_e'^3)$ or $O(p_e'\bar{u}_e^{\,3})$ or higher are negligible.

The Galerkin method is used to find solutions of the problem defined by Equations (1.5) through (1.10). The mathematical techniques used in this dissertation are discussed in Chapter II.

The conservation equations describing the unsteady flow within the combustor (i.e., Equations (1.5) through (1.10)) are very complex.

Because of the large number of terms present in Equations (1.5), (1.6) and (1.7) it is not feasible, due to the excessive computation time requirements, to use the Galerkin method to solve these equations. A possible simplification of the analysis results when the relative importance of the various terms in the governing equations is established using order of magnitude arguments, and terms which do not significantly effect the behavior of the system are neglected. This approach is used in this dissertation.

An analysis of the behavior of moderate amplitude longitudinal combustion instability oscillations is developed in Chapter III. This analysis not only provides a simple problem formulation with which the feasibility of the solution technique is proven, but also lends considerable insight into the combustion instability phenomena. The solutions developed in Chapter III describe the nonlinear behavior of combustion instability oscillations over a broad range of engine operating conditions.

Chapter IV is concerned with the examination of the effect of large amplitude flow oscillations on engine stability. In order to accomplish this task, higher order terms must be retained in the governing equations. Consequently, the analysis developed in Chapter IV is considerably more complex, and requires a great deal more computation time, than the solution technique discussed in Chapter III.

Conclusions are drawn and comparisons are made with experimental observations and previous theoretical studies throughout this report. The salient results of this study are summarized in Chapter V. Also in this chapter, the analyses of Sirignano and of Mitchell are reviewed in

light of results of the current investigation. Recommendations for future research are also included in Chapter V.

As previously mentioned, Appendix A is concerned with the simplification of the conservation laws governing unsteady two-phase flow inside rocket combustors. The derivations included in this appendix follow the approach used by Crocco and Cheng.[3] They are included in this report for the sake of completeness.

A linear study not critical to the continuity of the text is presented in Appendix B. This study is concerned with the development of linear stability limits including the effects of the first and second modes simultaneously. The results of this analysis are discussed in Chapter III.

User's Manuals for the computer programs required to solve the problems formulated in this dissertation are included in Appendices C through E. The User's Manuals describe the following programs:

1. Program LINSTB. This program generates the linear stability limits consistent with the formulation of the problem.

2. Program SPAINT. This program evaluates the space integrals which result from the application of the Galerkin method. The results of this program are used as input in Program WAVES.

3. Program WAVES. This program numerically integrates the ordinary differential equations which describe the behavior of the mode-amplitude functions and computes the perturbation flow field.

CHAPTER II

MATHEMATICAL TECHNIQUE

The Galerkin Method

The Galerkin method, an application of the Method of Weighted Residuals (MWR), is a technique for finding approximate solutions of differential equations. The Galerkin method has been used in the solution of a variety of engineering problems (an extensive list of applications is included in the bibliography of Reference 13) and has been found to yield results which are in excellent agreement with exact solutions and with experimental data. The Galerkin method is mathematically straightforward, and when properly used it provides considerable insight into the physical properties of the problem. This physical insight is usually not provided by numerical solution techniques. In most cases, the Galerkin method requires less computation time than approaches involving the direct application of numerical methods.

The Galerkin method uses the concept of completeness and orthogonality to reduce a partial differential equation either to a system of algebraic equations or to a system of ordinary or partial differential equations. The solution of the resulting system of equations is in most cases easier to solve than the original partial differential equation. Consider a problem defined in a domain D in the following manner:

$$L[\varphi(z_j)] = f(z_j) \tag{2.1}$$

$$Bi[\varphi(z_j)] = g_i(z_j) \tag{2.2}$$

where L is the nonlinear (or linear) differential operator, B_i are the boundary conditions, φ is the dependent variable, and z_j are the independent variables. In the MWR the dependent variables are approximated by series expansions:

$$\Phi(z_j) = \sum_{n=0}^{N} c_n \tilde{\varphi}_n \tag{2.3}$$

where Φ is an expansion representation of φ, and φ_n are the selected trial functions.

In the classical Galerkin method, the trial functions φ_n are usually chosen in such a manner that the boundary conditions are satisfied. Alternately, the approximating series can be written in the form:

$$\Phi(z_j) = \tilde{\varphi}_B + \sum_{n=1}^{N} c_n \tilde{\varphi}_n \tag{2.4}$$

In this case the φ_n are required to vanish on the boundary and the φ_i are chosen to satisfy the boundary conditions.

In most classical applications of the Galerkin method, the φ_n are the first $(N+1)$ terms of a complete set of orthogonal functions in D. If the φ_n include the dependence upon all of the z_j, then the c_n are undetermined constants. On the other hand, if the dependence upon one or more of the z_j is not included in φ_n, then the c_n are undetermined functions.

It will now be assumed that the trial expansion, Equation (2.3), satisfies the boundary conditions, Equation (1.2). Substitution of the assumed form of φ, as defined by Equation (2.3) or Equation (2.4), into

Equation (2.2) in general results in a residual, that is:

$$L[\Phi] = R(z_j) \neq 0 \tag{2.5}$$

One of the properties of a complete set of functions in a domain D is that if a function is orthogonal to every member of the complete set in D, then the function must be identically zero in D. This property is used in the Galerkin method to determine the unknown c_n. Recalling that the φ_n represent members of a complete set, the Galerkin method requires the residual to be orthogonal to $(N + 1)$ φ_n:

$$\int_D R\tilde{\varphi}_n dD = 0 \qquad n = 0,1,\ldots,N \tag{2.6}$$

Performing the integration over the independent variables included in φ_n results either in a set of algebraic equations if the c_n are unknown coefficients or in a set of ordinary or partial differential equations if the c_n are unknown functions. In either case, there result $(N + 1)$ equations that can be solved for the $(N + 1)$ unknowns c_n.

Problems arise when neither the differential equation nor the boundary conditions are satisfied by the expansion of the dependent variable. Forming the differential equation and boundary residuals and applying the Galerkin method yields:

$$\int_D R\tilde{\varphi}_n dD = 0 \qquad n = 0,1,\ldots,N \tag{2.7}$$

$$\int_B R_B\tilde{\varphi}_{n_B} dB = 0 \qquad n = 0,1,\ldots,N \tag{2.8}$$

Equations (2.7) and (2.8) result in $2(N+1)$ equations for the $(N+1)$ c_n. Clearly in order for the method to work, either some of the conditions

must be discarded or a suitable manner of combining the equation and boundary residuals must be found. The former approach has not proven to be satisfactory in the past because of the arbitrary manner in which the conditions are discarded. The latter approach has succeeded when the residuals are combined in such a way that the equation residual, when integrated by parts, cancels identical terms in the boundary residual.[15] An extension of this concept, developed by Zinn and Powell,[11,12,14] has proven to be successful in the analysis of combustion instability problems. This modification of the Galerkin method will be discussed in the section of this chapter entitled "The Modified Galerkin Method."

The proper choice of trial functions (i.e., φ_n in Equation (2.2)) is critical to the success of the Galerkin method, and it is sometimes difficult to determine the "best" expansion. However, some useful guidelines have been established for the selection of trial functions. Ames[16] points out that it is useful to select functions which are (1) linearly independent, (2) members of a complete set, and (3) incorporate special characteristics of the problem. It has also been pointed out[15] that (1) the derived boundary conditions can be used to place restrictions on the approximating functions, and (2) eigenfunctions of a lower-order, simpler yet related problem on the same domain are sometimes useful trial functions. Once the trial functions have been selected, the physical reasonableness of the final solution, the convergence of the solution with increasing number of terms, and the insensitivity of the solution to the form of the approximating functions, lend confidence in the results.

The Modified Galerkin Method

In the application of the Galerkin Method to the study of combustion-

driven oscillations, it is often difficult to select trial function which satisfy the problem boundary conditions, and at the same time are not excessively complicated. It has been shown that difficulties are encountered when both boundary and differential equation residuals arise in the problem formulation. This dilemma can be overcome if the boundary and differential equation residuals can be combined in a consistent manner.

Zinn and Powell[11,12,14] demonstrated that the proper combination of residuals in the analysis of combustion instability problems is the subtraction of the boundary residual from the differential equation residual. This combination of residuals is somewhat analogous to the treatment of natural boundary conditions in the calculus of variations. The results obtained in the application of this method to the study of combustion instability problems yielded results which are in excellent agreement with more exact solutions. Subtracting Equation (8) from Equation (7) yields the modified Galerkin method for the analysis of combustion instability; that is

$$\int_D R\tilde{\Phi}_n \, dD - \int_B R_B\tilde{\Phi}_{n_B} dB = 0, \quad n=0,1,\ldots,N \qquad (2.9)$$

This technique is used in Chapter III to find approximate solutions to a second order, nonlinear wave equation.

Even though the modified Galerkin method permits the use of trial functions which do not satisfy the problem's boundary conditions, the expansions selected must be physically realistic. The criteria stated in the preceding section of this chapter still apply to the proper selection of trial functions. In particular, as many boundary conditions as

possible should be satisfied by the series expansion of the dependent variable.

CHAPTER III

SECOND ORDER ANALYSIS

In this chapter the modified Galerkin method is used to investigate the nonlinear behavior of liquid propellant rocket engines experiencing moderate amplitude combustion instabilities. A comparison is made with the results of previous nonlinear investigations,[8,9] and with the observed behavior of unstable engines. The solutions developed in this chapter describe the combustion instability characteristics of liquid propellant rockets over a broad range of engine operating conditions.

Problem Formulation

Equations (1.5) through (1.10) define the behavior of the unsteady flow inside rocket combustors having low Mach number mean flows and a quasi-steady short nozzle. When the amplitudes of the flow perturbations are of the order of magnitude of the mean flow Mach number, and when terms of order higher than second may be neglected, it has been shown by Zinn and Powell[13,14] that the conservation equations (i.e., Equations (1.5) through (1.8)) can be combined into the following nonlinear wave equation:

$$\varphi_{zz} - \varphi_{tt} - 2\bar{u}\varphi_{zt} - \gamma \frac{d\bar{u}}{dz}\varphi_t - 2\varphi_z\varphi_{zt} - (\gamma - 1)\varphi_t\varphi_{zt} \qquad (3.1)$$

$$+ \gamma\hat{n}\frac{d\bar{u}}{dz}[\varphi_t(z,t) - \varphi_t(z,t-\bar{\tau})] = 0$$

In Equation (3.1), $\varphi(z,t)$ is the velocity potential defined by $u' = \varphi_z$, $\bar{u}$ is the steady state velocity (or Mach number) distribution, and γ is the ratio of specific heats. Equation (3.1) has the form of an inhomogeneous wave equation. The first two terms describe wave motion in a quiescent medium. The third and fourth terms describe, to second order, the effects of the mean flow, and the fifth and sixth terms account for the second order nonlinearities of the problem. The last term represents the unsteady mass source due to the unsteady combustion process.

In terms of φ, the solid wall injector face boundary condition is simply:

$$\varphi_z(0,t) = 0 \tag{3.2}$$

To second order accuracy, the quasi-steady short nozzle boundary condition is given by the following equation:

$$\varphi_z(1,t) + \frac{\gamma-1}{2}\bar{u}_e\varphi_t(1,t) = 0 \tag{3.3}$$

The modified Galerkin method is used to find approximate solutions to the problem defined by Equations (3.1) through (3.3). Since the behavior of axial combustion instability oscillations is known to be similar to the behavior of longitudinal acoustic waves in a closed-ended chamber, the velocity potential is expanded in terms of acoustic eigenfunctions multiplied by unknown time dependent mode-amplitudes, that is:

$$\tilde{\varphi}(z,t) = \sum_{n=1}^{N} A_n(t)\cos(n\pi z) \tag{3.4}$$

The summation index is varied from 1 to N, dropping the spacially

independent (i.e., the chugging) mode. A similar expansion was successfully used by Temkin[20] in a study of the nonlinear behavior of piston-driven axial waves. The trial solution defined by Equation (3.4) satisfies the solid wall boundary condition, Equation (3.2), but not the quasi-steady short nozzle boundary condition, Equation (3.3). In order to use the modified Galerkin method, Equation (3.3) must be written in a manner expressing the conservation of mass at the nozzle entrance.[13,14] The unsteady mass source at the nozzle can be written as:

$$Q_m' = -(\bar{\rho}_e + \rho_e')(\bar{u}_e + u_e') + \bar{\rho}_e \bar{u}_e$$

or to second order:

$$Q_m' = -[\varphi_z - \bar{u}_e \varphi_t - \varphi_z \varphi_t]$$

Substitution of Equation (3.3) into the preceding equation yields to second order:

$$Q_m' = \frac{\gamma+1}{2} \bar{u}_e \varphi_t \tag{3.5}$$

Treating the nozzle as an unsteady mass sink, the quasi-steady short nozzle boundary condition requires that

$$Q_m' + \underline{J}' \cdot \underline{n} = 0 \tag{3.6}$$

where $\underline{J}'$ is the perturbation mass flux vector. Substituting the proper expression for $\underline{J}'$ and using Equations (3.5), Equation (3.6) can be written, to second order as:

$$\left[\frac{\gamma-1}{2} \bar{u}_e \varphi_t + \varphi_z - \bar{u}_e \varphi_t - \varphi_z \varphi_t\right]_{z=1} = 0$$

or

$$\left[\frac{\gamma-1}{2}\,\bar{u}_e\varphi_t - \varphi_z(\varphi_t - 1)\right]_{z=1} = 0 \tag{3.7}$$

Although Equation (3.7) is a statement of the conservation of mass at the nozzle entrance plane, it can be shown[14] that if the combustion is completed upstream of the nozzle entrance plane, Equation (3.7) also expresses the conservation of momentum and energy.

The differential equation residual and the boundary residual are formed by substituting the assumed series expansion of the velocity potential, Equation (3.4), into Equations (3.1) and (3.7). The modified Galerkin orthogonality conditions, Equation (2.9), are then applied to the residuals. The weighting functions are the $\cos(\ell\pi z)$, $\ell = 1,\ldots,N$. Because the zeroth terms, (i.e., $\ell = 0$) has been dropped on physical grounds, the cosine series is no longer complete on the interval 0 to 1. In spite of the fact that the Galerkin method is based on the use of members of a complete set, Finlayson[16] notes that valid results have been found in applications of the Galerkin method in which the leading term of the series expansion were neglected for physical reasons. Applying the modified Galerkin method in this manner results in the following equations:

$$\int_0^1 \Big[\varphi_{zz} - \varphi_{tt} - 2\bar{u}\tilde{\varphi}_{zt} - \gamma\frac{d\bar{u}}{dz}\tilde{\varphi}_t - 2\tilde{\varphi}_z\tilde{\varphi}_{zt} - (\gamma-1)\tilde{\varphi}_t\tilde{\varphi}_{zz} + \gamma n\frac{d\bar{u}}{dz}\left[\tilde{\varphi}_t(z,t) - \tilde{\varphi}_t(z,t-\bar{\tau})\right]\Big]\cos(\ell\pi t)dt - \frac{\gamma-1}{2}\,\bar{u}_e\tilde{\varphi}_t(1,t)\cos(\ell\pi) = 0,\ \ell = 1,\ldots,N \tag{3.8}$$

In deriving the above equation, the boundary residual has been simplified by noting that $\tilde{\varphi}_z(1,t) = 0$. It is interesting to note that the resulting boundary residual can be obtained by forming the residual of Equation (3.3), instead of Equation (3.7). Substitution of Equation (3.4) into Equation (3.8) and performing the required space integration yields the following set of second order quasi-linear ordinary differential equations that describe the behavior of the unknown, time-dependent amplitudes:

$$A_\ell'' = (\ell)^2 A_\ell + 2 \sum_{n=1}^{N} \Big[-\gamma A_n' + \gamma n (A_n' - A_n'(t-\bar{\tau})) \, I(n,\ell) \qquad (3.9)$$

$$+2(n\pi) I_2(n,\ell) A_n' - \frac{\gamma - 1}{2} \bar{u}_e (-1)^{n+\ell} A_n'$$

$$+ \sum_{m=1}^{N} [(\gamma - 1)(m\pi)^2 I_3(n,m,\ell) A_n' A_m$$

$$-2(n\pi)(m\pi) I_4(n,m,\ell) A_n A_m' \Big], \quad \ell = 1,\ldots,N$$

where

$$I_1(n,\ell) = \int_0^1 \frac{d\bar{u}}{dz} \sin(n\pi z) \cos(\ell\pi z) dz \qquad (3.10)$$

$$I_2(n,\ell) = \int_0^1 \bar{u} \sin(n\pi z) \cos(\ell\pi z) dz \qquad (3.11)$$

$$I_3(n,m,\ell) = \int_0^1 \cos(n\pi z) \cos(m\pi z) \cos(\ell\pi z) dz \qquad (3.12)$$

$$I_4(n,m,\ell) = \int_0^1 \sin(n\pi z) \sin(m\pi z) \cos(\ell\pi z) dz \qquad (3.13)$$

The structure of Equation (3.9) will now be briefly investigated The first two terms describe the motion of a classical oscillator, the

third and fifth terms represent mean flow effects, the fourth term represents energy addition from the unsteady combustion process, and the fifth term describes nozzle damping. The terms describing the effects of mean flow, combustion, and the nozzle are all proportional to A_ℓ^*. These terms are analogous to the resistance term that appears in many differential equations that describe the dynamics of mechanical systems.

The nonlinear terms describe the interaction between the various modes. The coefficient space integrals of these terms, that is Equations (3.12) and (3.13), are zero for $n = m = \ell$; therefore, there is no nonlinear self-coupling* in Equation (3.9). Applications of the Galerkin method[12,13,14] to problems of transverse instabilities have indicated that triggering cannot be found unless there is nonlinear self-coupling in the differential equations governing the mode amplitudes. If this result also holds in the present study, then it will not be possible to conduct an investigation of possible triggering of axial oscillations, using this second order formulation of the problem.

Results

The nonlinear behavior of the combustion instability oscillations is found by numerical integration of Equation (3.9). However, in order to properly interpret the nonlinear results, the linear behavior of the system must be established. Besides serving as a reference for the nonlinear analysis, the linear results can be compared with linear solutions found with the aid of more exact mathematical techniques; good agreement

*Nonlinear self-coupling appears in terms of the form $c_{\ell\ell\ell}A_\ell^*(t)A_\ell(t)$. In the present formulation the $c_{\ell\ell\ell}$ of the nonlinear terms are zero for all ℓ.

with existing linear solutions will add confidence in the correctness of the predicted nonlinear behavior of the combustion instability oscillations.

Linear Behavior

Linear stability limits, consistent with the second order formulation of the problem, were established on the $\hat{n}$ - $\bar{\tau}$ plane by using the linear terms of Equation (3.9). Because there is coupling in the resulting equations, the linear stability limits for the first two modes were initially established by considering both modes simultaneously. (See Appendix B.) However, nearly identical stability limits were found when each mode was treated independently. Since the latter approach results in significant mathematical simplifications, further linear results were found by considering each mode separately.

The loci of points of linear neutral stability of the ℓ^{th} longitudinal mode are found by assuming that:

$$A_\ell(t) = K_\ell \exp(i\omega_\ell t) \tag{3.14}$$

and then substituting Equation (3.14) into the linear portion of Equation (3.9). The resulting algebraic expressions are separated into their real and imaginary parts, and the following expressions are obtained:

$$\hat{n}_\ell = \frac{\omega_\ell^2 - (\ell\pi)^2}{2\gamma\omega_\ell I_1(\ell,\ell)\sin(\omega_\ell\bar{\tau}_\ell)} \tag{3.15}$$

$$\tan\left(\frac{\omega_\ell\bar{\tau}_\ell}{2}\right) = \frac{2\omega_\ell}{\omega_\ell^2 - (\ell\pi)^2}\left[\gamma I_1(\ell,\ell) + \frac{(\gamma-1)}{2}\bar{u}_e - 2(\ell\pi)I_2(\ell,\ell)\right]$$

where $I_1(\ell,\ell)$ and $I_2(\ell,\ell)$ are defined respectively by Equations (3.10)

and (3.11). The linear stability limits were established, for various mean flows, by assuming values of ω_ℓ near the acoustic frequency of the ℓ^{th} axial mode, and solving Equation (3.16) for $\bar{\tau}_\ell$ and Equation (3.15) for $\hat{n}_\ell$. The computer program used to calculate the linear stability limits is described in Appendix C.

The critical value of the interaction index, that is the value of $\hat{n}$ below which no linear instability is possible, is a useful parameter in establishing the relative stability of various engines. An analytical expression for $\hat{n}_{min}$ can be found by substituting Equation (3.15) into Equation (3.16) and noting that $\hat{n}_{min}$ occurs at resonant engine operating conditions (i.e. $\omega = \ell\pi$). Performing this operation results in the following expression for $\hat{n}_{min}$:

$$\hat{n}_{min} = \frac{1}{2\gamma I_1}\left[\frac{\gamma-1}{2}\bar{u}_e + \gamma I_1 - 2(\ell\pi)I_2\right] \tag{3.17}$$

where I_1 and I_2 are given by Equations (3.10) and (3.11), respectively. It should be noted that for a given $\bar{u}(z)$, $\hat{n}_{min}$ is independent of $\bar{u}_e$. This result is in agreement with Crocco's[3] linear studies.

The effect of the axial distribution of the steady state combustion on the linear stability can be examined by evaluating Equation (3.17) for various $\bar{u}(z)$. A variable ramp mean flow velocity distribution is considered. That is, $\bar{u}(z)$ is assumed to vary linearly from zero at the injector face to $\bar{u} = .2$ at $z = z_c$, and then remain constant at the value $\bar{u} = .2$ from $z = z_c$ to $z = 1$. The variation of $\hat{n}_{min}$ with z_c for the first two fundamental modes is presented in Figure 5. Based on these results, it is concluded that the stability of an engine is improved when the

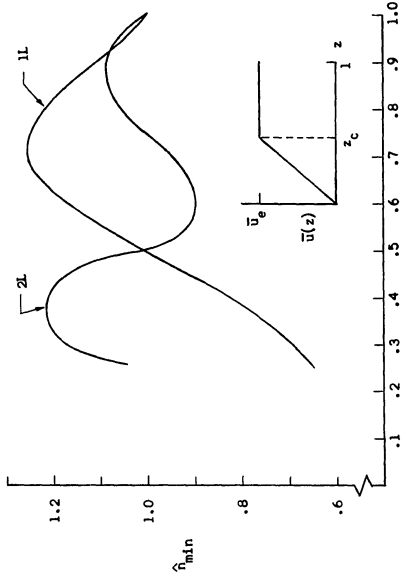

Figure 5. The Effect of the Combustion Distribution on Engine Linear Stability.

combustion processes is completed downstream of a pressure node. This same conclusion is reached by Crocco[3] using a more elaborate analysis.

The dependence of the linear stability limits of the first and second axial modes upon the mean flow Mach number is shown in Figure 6. The mean flow Mach number varies linearly from zero at the injector face to $\bar{u} = \bar{u}_e$ at the combustor exit plane. As was previously noted, for a given $\bar{u}(z)$ the critical value of the interaction index, $\hat{n}_{min}$, is not affected by the mean flow Mach number. However, increasing the mean flow Mach number increases the range of time lags over which the engine may become unstable. That is, increasing the steady state Mach number has a destabilizing effect on a rocket engine.

The linear stability limits for the first three longitudinal modes are presented in Figure 7, for $\bar{u}(z) = .2z$. As pointed out by Crocco,[1] the stability limits of physical interest, that is those encountered in practice, are the limits corresponding to the smallest values of $\omega\bar{\tau}$ which are solutions of Equation (3.16). These limits, shown as solid lines in Figure 7, will be referred to as primary zones of instability. The solution corresponding to the next higher value of $\omega\bar{\tau}$ for the second longitudinal mode is shown as a broken line in Figure 7. These secondary zones of instability arise from the mathematical formulation of the $n-\bar{\tau}$ theory. Experimental results[7] indicate that the secondary zones are not compatible with any physical phenomenon. The linear stability limits presented in Figure 7 will be used later in this paper when the nonlinear results are discussed.

The linear results discussed in the preceding paragraphs are in qualitative agreement with observed experimental behavior and with other

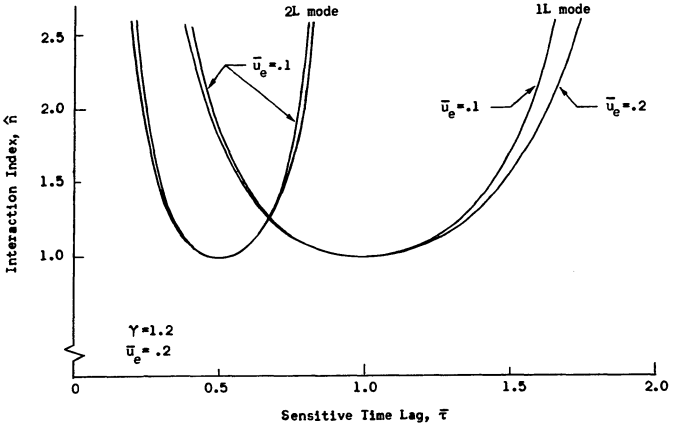

Figure 6. The Effect of the Mean Flow Mach Number on the Linear Stability Limits.

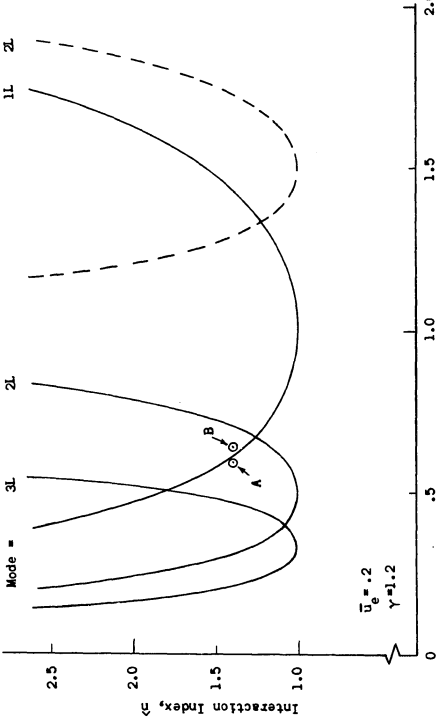

Figure 7. Longitudinal Linear Stability Limits.

analytical solutions. However, when compared with previous investigations, the linear stability limits of the present analysis are displaced downward on the $\hat{n}$ - $\bar{\tau}$ stability plane. In particular, for a linear Mach number distribution, the present study predicts a fundamental mode $\hat{n}_{min} = 1$, while both Mitchell and Crocco predict $\hat{n}_{min} \doteq 1.43$. This discrepancy in linear results probably is not attributable to the modified Galerkin method, since this technique was used by Zinn and Powell[11,14] to find linear stability limits which are in excellent agreement with Crocco's results for the case of a concentrated combustion zone at the injector face. When the combustion is concentrated at the injector face, the combustor mean flow is constant, and the trial functions used by Zinn and Powell very closely approximate the exact unsteady flow variables. On the other hand, in the present study the more realistic problem of distributed combustion is considered, and the series expansion used to represent the velocity potential is not as accurate as the one used in the Zinn-Powell investigation. Furthermore, the perturbation velocity at the combustor exit plane predicted by solutions using Equation (3.4) is zero. As a result, the nozzle boundary condition cannot be satisfied. An examination of the term in Equation (3.9) which arises from the boundary residual (i.e., $-\frac{\gamma-1}{2}\bar{u}_e(-1)^{n+\ell}A_n^*$) reveals that the energy removal by mean flow convection is taken into account, but that energy removal by acoustic radiation (i.e., terms involving $u'(1,t)$) is neglected. Consequently, it is believed that the shift in the linear stability limits in the present study arises from the expansion of the velocity potential in terms of the acoustic eigenvalues and eigenfunctions describing acoustic waves in a quiescent medium.

Nonlinear solutions consistent with the linear stability limits, described in Figure 7, are discussed in the following section. In this nonlinear study a method of correlating experimental data with the analytical solutions is developed. Consequently, the linear stability limits computed in this dissertation can be used to predict the linear stability of rocket engines.

Nonlinear Solutions

The nonlinear behavior of a combustor experiencing a longitudinal mode instability is investigated by specifying the engine operating conditions in terms of $\bar{u}(z)$, γ, and the unsteady combustion parameters n and $\bar{\tau}$, and then performing a numerical integration of Equations (3.9). Both transient and periodic solutions are found for various engine operating conditions in the $n - \bar{\tau}$ stability plane, i.e., Figure 7.

Before Equations (3.9) can be integrated, the integral coefficients defined by Equations (3.10) through (3.14) must be evaluated. Because of the relatively large number of integrations to be performed, the computations were done numerically using a Simpson's rule integration technique (e.g., see Conte[17]). A normalized step size of $h = .02$ was used in all the calculations, and the numerical error of the integration process is of the order of h^5. The Simpson's Rule integration is described in Appendix D.

A fourth order Runge-Kutta technique is used to find the transient and limit cycle solutions of Equations (3.9). The basic Runge-Kutta formulas for integrating the set of second order quasi-linear ordinary differential equations defined by Equations (3.9) were taken from Reference 18. These formulas were then modified to account for the retarded time variable arising from the use of the $n - \bar{\tau}$ theory. In this modification, the retarded variable is treated in the same mathematical manner as the dependent variable

in the Runge-Kutta scheme. The modified Runge-Kutta algorithm is described in Appendix E.

Due to the presence of a retarded time variable, the behavior of the initial disturbance must be specified over the period $t_i - \bar{\tau}$, where t_i is the initial time. In the present study it has been assumed that there are no oscillations present until time t_i, at which time a pressure disturbance is impulsively introduced inside the combustor. The velocity perturbation is taken to be initially zero. Both spacially continuous and spacially discontinuous pressure waveforms have been used as initial conditions. The analytical expressions of these initial conditions, found from a Fourier analysis of the initial disturbance, are given by the following equations:

(1) Spacially Continuous Pulse

$$A_\ell(t_i) = 0, \quad \ell = 1,\ldots,N \tag{3.18}$$

$$\left.\frac{dA_\ell}{dt}\right|_{t_i} = \begin{cases} 0 & n \neq \ell \\ \dfrac{p_i}{\gamma} & n = \ell \end{cases} \tag{3.19}$$

(2) Spacially Discontinuous Pulse

$$A_\ell(t_i) = 0, \quad \ell = 1,\ldots,N \tag{3.20}$$

$$\left.\frac{dA_\ell}{dt}\right|_{t_i} = \frac{4p_i}{\gamma n\pi} \sin\left(\frac{\ell\pi}{n}\right) \tag{3.21}$$

where in both cases,

$$\frac{dA_\ell}{dt} = A_\ell(t) = 0, \quad \ell = 1,\ldots,N \text{ for } -\bar{\tau} \leq t < t_i \tag{3.22}$$

The linear relation $p = -\gamma\varphi_t$ was used in the derivation of Equations (3.19) and (3.21). The peak amplitude of the initial disturbance is

specified by p_i.

The primary drawback of the Runge-Kutta method is the difficulty involved in estimating numerical errors. However, the technique is very stable numerically, and the overall error of the fourth order Runge-Kutta method is of order h^5, where h is the integration step size. In order to determine a satisfactory step size, solutions of Equation (3.9) were found with integration step sizes of h = .02 and h = .05. This study indicated that satisfactory results can be obtained with an integration step size of the order of $h \leq .05$. The fact that the computed waveforms at limit cycle conditions remained unchanged for many cycles indicates that numerical error propagation is minimal for $h \leq .05$.

In order to accurately represent the discontinuous combustion instability oscillations, a sufficient number of terms must be retained in the series expansion of the velocity potential (i.e., in Equation (3.4)). A convergence test in which solutions were found by using series expansions containing five, eight, and ten terms was conducted. The results of this study are summarized in Figures 8 through 10. The pressure data presented in Figure 8 shows the convergence of the solutions with increases in the number of terms retained in the series expansions. The same result is indicated by the mode-amplitude functions shown in Figures 9 and 10. The latter plots also indicate that the behavior of the first two harmonics can, at least in some cases, be predicted using a five term series expansion. The data shown in Figure 8 indicates that for the engine operating conditions in question a five or an eight term series expansion might be used to describe the behavior of discontinuous flow oscillations. However, this conclusion was not found to be valid

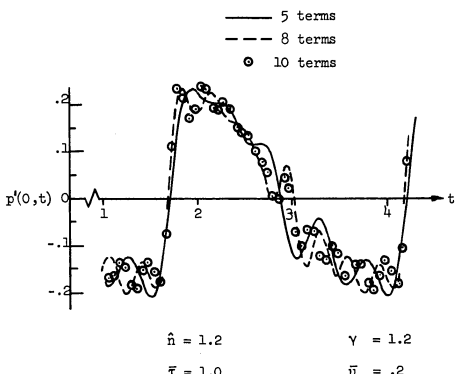

Figure 8. The Effect of the Number of Terms in the Series on the Injector Face Pressure.

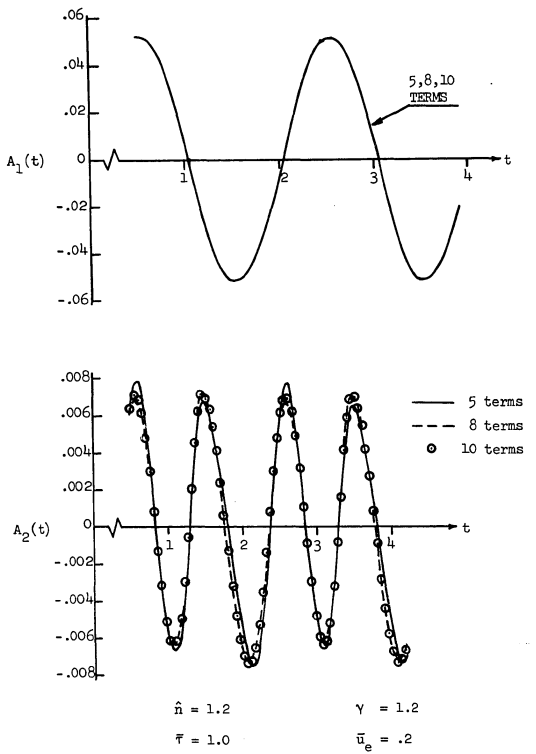

Figure 9. The Effect of the Number of Terms in the Series on the First and Second Harmonics.

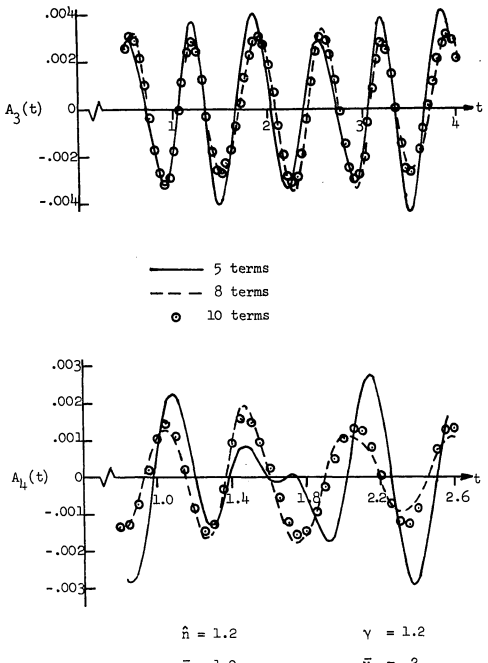

Figure 10. The Effect of the Number of Terms in the Series on the Third and Fourth Harmonics.

for all engine operating conditions. Consequently, a ten term expansion was used in all solutions of Equation (3.9) discussed in this dissertation.

Using a ten term expansion, together with an integration step size of the order h ≤ .05, a maximum of four minutes of computation time is required, on a Univac 1108 digital computer, for reaching stable limit cycle conditions. The solutions are found to be independent of the waveform of the initial disturbance. However, the length of the computations can be reduced if the structure of the initial disturbance is a close approximation of the final limit cycle.

In order to proceed with the nonlinear analysis, the distribution of the steady state velocity, $\bar{u}(z)$, must be specified. For the present study the following convenient and often used distribution has been assumed:

$$\bar{u}(z) = \bar{u}_e z \tag{3.23}$$

The use of this velocity distribution permits a direct comparison to be made with previous nonlinear results as well as with the computed linear stability limits.

Once the combustion parameters $\hat{n}$ and $\bar{\tau}$, the initial conditions, and $\bar{u}(z)$ and γ have been specified, the integration of Equation (3.9) is continued until a stable periodic solution is found, if one exists. The velocity and pressure oscillations are then given by:

$$u'(z,t) = \tilde{\Phi}_z(z,t) \tag{3.24}$$

$$p'(z,t) = \frac{\gamma}{2}\left[\tilde{\Phi}_t(\tilde{\Phi}_t - 2) - \tilde{\Phi}_z(\tilde{\Phi}_z + 2\bar{u})\right] \tag{3.25}$$

where $\tilde{\Phi}$ is given by Equation (3.4) and Equation (3.25) follows from an integral of the second order momentum equation.[14]

The limit cycles have been found to be independent of the form and amplitude of the initial disturbance. Figure 11 presents typical results obtained in the present investigation. In this case, an initially continuous waveform distorts itself into a discontinuous oscillation. This capability of investigating the transient behavior of an oscillation from a continuous to a discontinuous wave, or more importantly, from one mode of oscillation to another, is one of the important features of the present analysis. Because the limit cycle oscillations are independent of the initial disturbance, no a priori knowledge of the stable, periodic behavior of the combustion instability oscillation is required to use the analytical techniques developed in this dissertation. In contrast, previous nonlinear analyses[8,9] are restricted to the investigation of periodic oscillations in a single mode at a time. That is, in the previous analytical techniques the instabilities are not free to change modes of oscillation, nor can the instabilities grow or decay.

Typical resonant behavior of the 1L limit cycle pressure oscillations at the injector face and at a point within the combustor are shown in Figure 12. The discontinuous pressure waves traveling towards and away from the injector face are clearly evident in the plot describing the behavior at z = .3. The spacial dependence of the wave is presented in Figure 13. Typical limit-cycle injector face pressure waveforms for values of $\bar{\tau}$ representing conditions above and below resonance, for the first longitudinal mode (i.e. $\bar{\tau} < 1$, $\bar{\tau} > 1$, respectively), are presented in Figure 14. These waveforms are qualitatively similar to those obtained

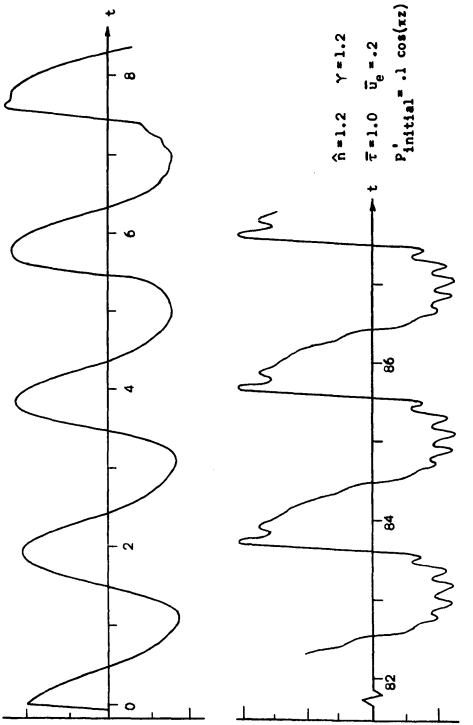

Figure 11. Typical Transient and Periodic Pressure Oscillations.

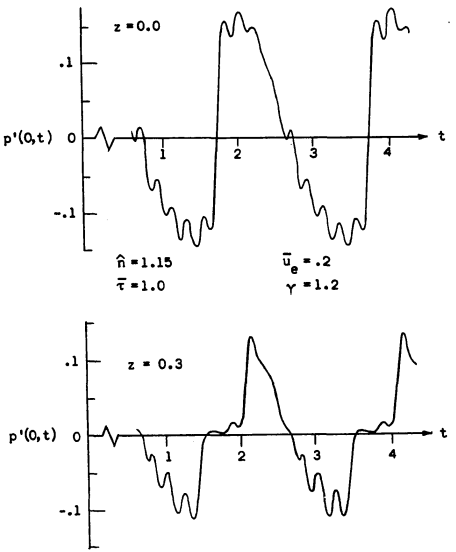

Figure 12. Time Dependence of the Nonlinear Pressure Waveforms at Resonant Conditions.

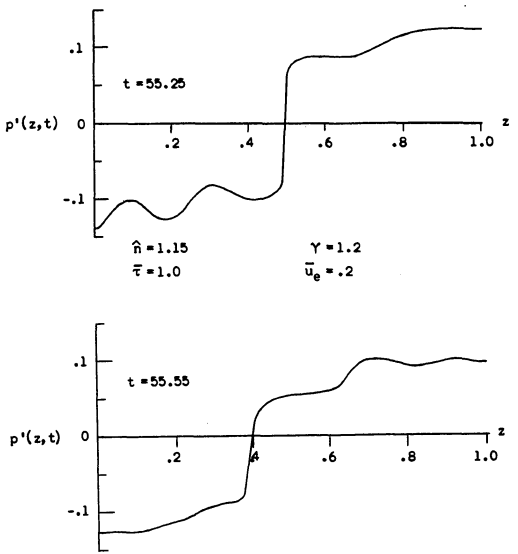

Figure 13. Instantaneous Space Dependence of the Nonlinear Pressure Waveforms.

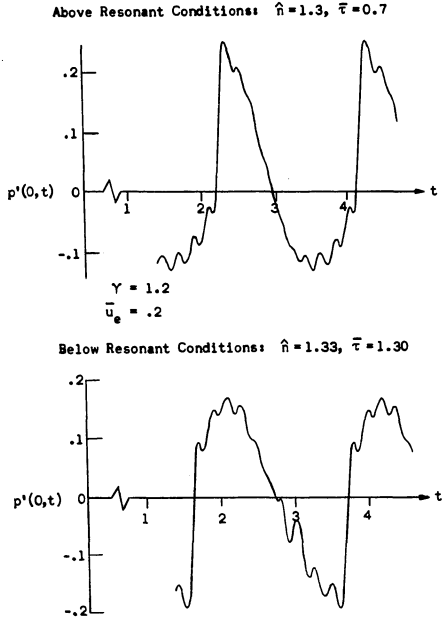

Figure 14. Time Dependence of the Nonlinear Pressure Waveforms for Off-Resonant Conditions.

by Chester[21] in the study of forced oscillations in closed tubes; they are also in qualitative agreement with the solutions found by Mitchell.[9] The computations performed in this study indicate that for the majority of unstable engine operating conditions the resulting limit cycle waveforms are discontinuous; the exception occurs for unstable conditions very near the linear stability limits where the resulting oscillations are continuous. However, if both the 1L and 2L modes are linearly unstable, no continuous, stable, periodic 1L solutions could be found.

The effect of the mean flow Mach number on the combustion instability oscillations is shown in Figure 15. From these results, it appears that the amplitude of the instabilities is strongly dependent upon the steady state Mach number; the peak to peak amplitude increases with increasing Mach number. Therefore, as in the linear results, it is believed increasing the mean flow Mach number has a destabilizing effect upon the engine. This behavior is due to the dependence of the $\hat{n} - \bar{\tau}$ combustion model upon the mean flow Mach number (i.e., see Equation (1.8)).

The present calculations show that the limit cycle behavior obtained for given values of $\hat{n}$ and $\bar{\tau}$ is determined by the corresponding linear stability of the various modes that are present in the series solution. In general, if the first longitudinal (1L) mode is linearly unstable at a given point in the $\hat{n} - \bar{\tau}$ plane, then the resulting limit cycle will exhibit an oscillation that approximates the behavior of the 1L mode. On the other hand, if for a given value of $\hat{n}$ and $\bar{\tau}$ the second longitudinal (2L) mode is linearly unstable and the 1L mode is linearly stable, then the limit cycle will exhibit a 2L-type oscillation. These

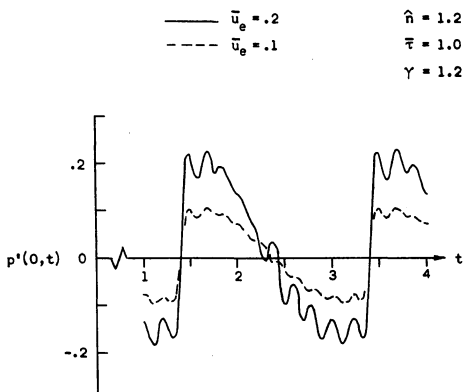

Figure 15. The Effect of the Mean Flow Mach Number on the Nonlinear Pressure Waveforms.

characteristics are evident in Figure 16. In this figure limit-cycle oscillations are presented for a fixed value of $\hat{n}$ and values of $\bar{\tau}$ on either side of the left "branch" of the 1L linear stability limit as shown in Figure 7. At point A, the 2L mode is linearly unstable and the 1L mode is linearly stable, while at point B, both the 1L and 2L modes are linearly unstable.

At point A the combustion instability has evolved into a 2L type oscillation with two shock waves moving back and forth within the chamber. On the other hand, the final limit cycle at point B exhibits a first longitudinal type of oscillation. These limit cycle oscillations evolved from initial disturbances which approximated the spacial dependence of the 1L mode. However, the computation time required to predict the limit cycle at point A is considerably reduced if the initial disturbance has a spacial dependence that resembles the structure of the 2L mode.

It should be noted that point A, for which the present theory predicts a 2L type oscillation, lies in a region of the $\hat{n} - \bar{\tau}$ plane where according to Mirchell a 1L type oscillation may be triggered. These conclusions are in complete disagreement. It should be added, however, that in the present study the final mode of oscillation is not restricted a priori, and the stability of a number of modes is considered simultaneously. On the other hand, Mitchell considers the stability of a single mode at a time. Analysis of the evolution of the initial disturbances at point A clearly shows that the resulting 2L instability is a direct consequence of the linear instability of the 2L mode at this point. It thus appears that the final nature of the instability, at a given point in the $\hat{n} - \bar{\tau}$ plane, strongly depends upon the linear stability of the various modes at this point.

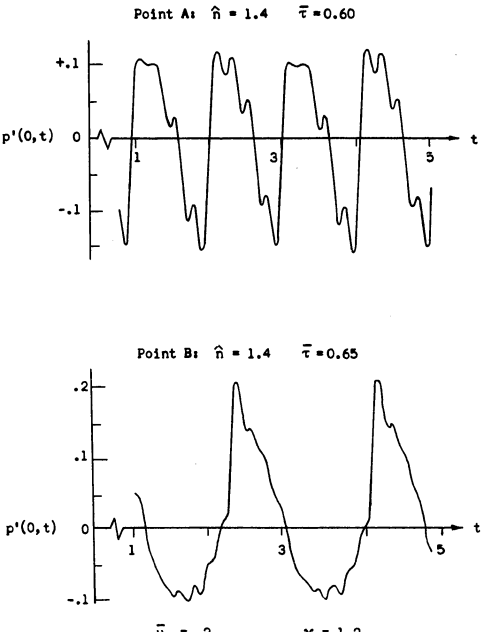

Figure 16. Dependence of Nonlinear Waveforms on $\hat{n}$ and $\bar{\tau}$.

Typical first, second and third-mode amplitude functions for oscillations in regions of 2L instability and of combined 1L and 2L instability are presented in Figures 17 and 18, respectively. When both modes are linearly unstable, the first harmonic is dominant. On the other hand, when the second mode is linearly unstable and the first mode is linearly stable, the second harmonic is an order of magnitude larger than the first harmonic. In this case, the period of the first mode-amplitude is the same as the period of the second axial mode. These results clearly indicated that the second mode is dominant in regions of 2L instability where the 1L mode is linearly stable.

The variation of the peak-to-peak amplitudes of fundamental mode combustion instability oscillations with upward displacement from the linear stability limits is shown in Figure 19. Here, the peak-to-peak injector face pressure amplitudes are presented as functions of $\delta\hat{n} = \hat{n} - \hat{n}_{LS}$ for constant values of $\bar{\tau}$ corresponding to conditions above, below and at resonance. From this figure, it can be seen that for a given $\delta\hat{n}$ the amplitude of the oscillations at $\bar{\tau} = .7$ are larger than those found at $\bar{\tau} = 1.0$ or 1.3. This result reflects the decreasing linear stability of the second axial mode with decreasing $\bar{\tau}$. When both the first and second modes are linearly unstable, the amplitudes of the oscillation are large even for engine operating conditions at which the 1L mode is only slightly unstable. This behavior is shown in Figure 20, and it is due to the unstable nature of the 2L mode at these engine operating conditions. A 2L-type instability is found when the 1L mode becomes linearly stable while the 2L mode is still linearly unstable.

A limit-cycle amplitude map for first longitudinal instabilities

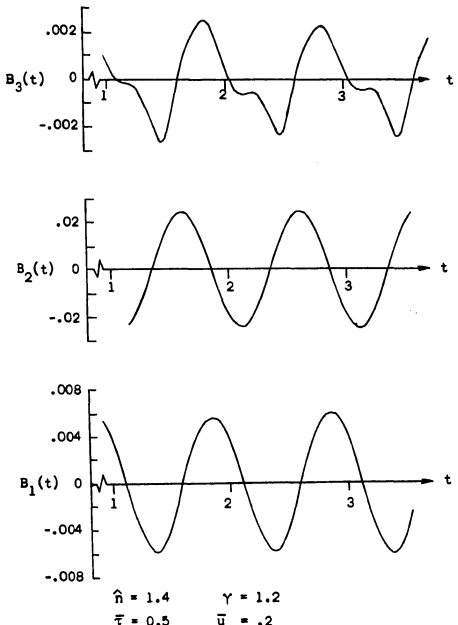

Figure 17. Mode Amplitude Functions for Linearly Unstable 2-L Conditions.

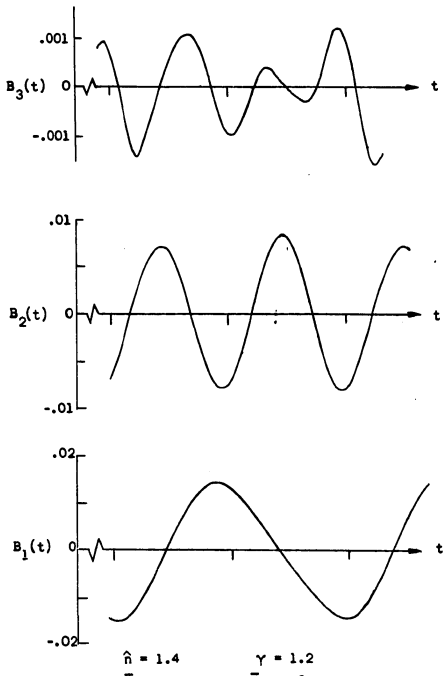

Figure 18. Mode-Amplitude Functions for Linearly Unstable 1L and 2L Conditions.

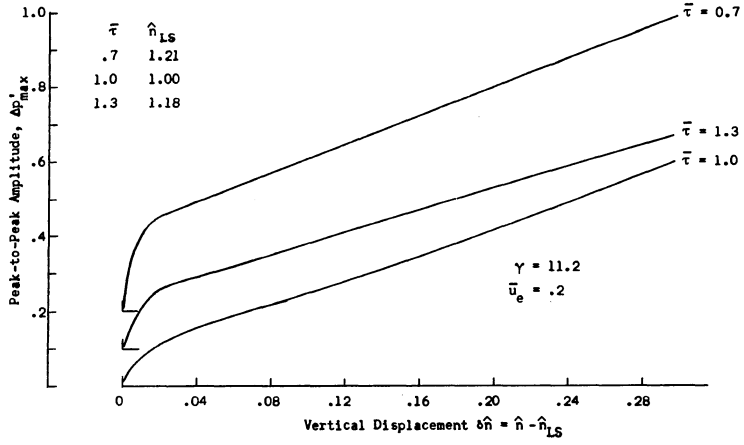

Figure 19. Injector Face Peak to Peak Pressure Amplitudes

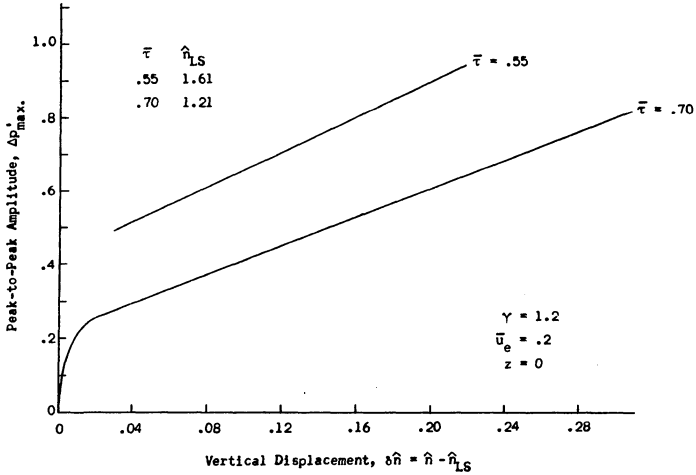

Figure 20. The Effect of the Linear Stability of the First Two Modes on Fundamental Mode Oscillation Peak-to-Peak Amplitudes.

is presented in Figure 21. Here, lines of constant peak-to-peak pressure amplitude are plotted on an $\hat{n} - \bar{\tau}$ plane. No stable 1L solutions could be found in the linearly stable region of the fundamental mode. Therefore, in the present analysis the stability limits of the system are not altered by nonlinear effects. Noting that $\bar{\tau} = \bar{\tau}^* \bar{c}_o^*/L$, it is apparent that for fixed engine operating conditions (i.e., fixed values of $\bar{\tau}^*$ and $\bar{c}_o^*$) an increase in L is stabilizing for above resonant conditions, and destabilizing for below resonant conditions.

It is important to note that in obtaining the results discussed in the preceding paragraphs, a given mode was only allowed to be linearly unstable in the primary zone of instability of that mode. That is, the secondary zones of instability were neglected on the grounds that they result from the mathematical formulation of the $\hat{n} - \bar{\tau}$ theory, and not from any physical phenomenon.

Correlation with Experimental Data

In the $\hat{n} - \bar{\tau}$ theory of combustion instability, the complex unsteady combustion process is represented with the aid of two parameters, the interaction index $\hat{n}$, and the sensitive time lag $\bar{\tau}$. In this section, a method of determining from experimental data the unsteady engine operation conditions in terms of $\hat{n}$ and $\bar{\tau}$ is developed.

Since the amplitude of the combustion instability oscillations is primarily dependent upon $\hat{n}$, a peak-to-peak amplitude map, such as Figure 21, provides one correlation parameter, namely $(\Delta p'_{max})_{z_T}$. This correlation parameter has been widely used in combustion instability research. In previous investigations, the normalized frequency of the oscillations has been used as the second parameter. The frequency is primarily a

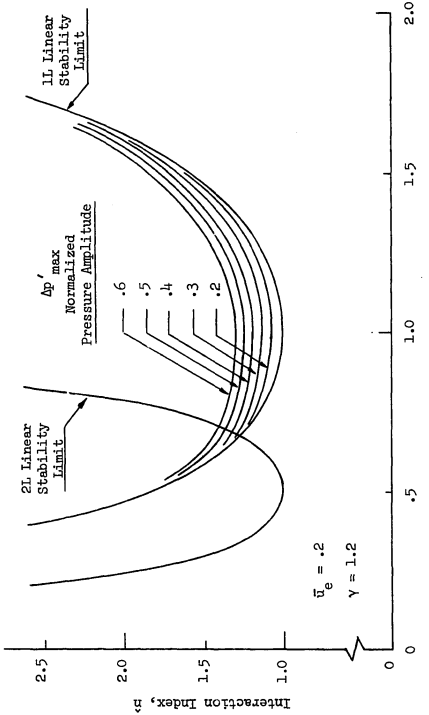

Figure 21. Injector Peak-to-Peak Pressure Amplitudes

function of the characteristic time of the problem, that is $\bar{\tau}$. However, due to the difficulty in determining $\bar{c}_o^*$ experimentally, the normalized frequency of the oscillations cannot be defined precisely.

The problem of determining $\bar{\tau}$ from experimental data can be overcome in the following manner. From Figures 12 and 14 it is apparent that the waveform of the combustion instability oscillation depends on whether $\bar{\tau}$ corresponds to above, below, or at resonant conditions. Define t_o to be the non-dimensional time from the passage of the shock at z_r to the expansion to zero perturbation pressure. Also define T to be the period of the oscillation. These definitions are shown schematically in Figure 22. The ratio t_o/T is now formed, and the results plotted as a function of $\bar{\tau}$, as shown in Figure 23.

Because the numerical solutions are found using a truncated series expansion, the computed pressure waveforms are slightly irregular in nature. In order to determine t_o, a smooth "theoretical" pressure waveform is drawn through the approximate solution, as demonstrated in Figure 24. The value of t_o/T computed in this manner at a given $\bar{\tau}$ lies within the error band shown in Figure 23.

In this correlation approach, only experimental pressure data at one axial location (i.e., at $z = z_r$) is required to determine $\hat{n}$ and $\bar{\tau}$. These parameters are found in the following manner:

1. An analytical t_o/T curve is generated. This task is accomplished by computing the limit cycle pressure waveforms at $z = z_r$ for various values of $\bar{\tau}$. It is best to use a nearly constant $\delta\hat{n}$ (i.e., vertical displacement from the linearly stability limit) in the calculations. The generated plot is then entered at the experimentally determined value

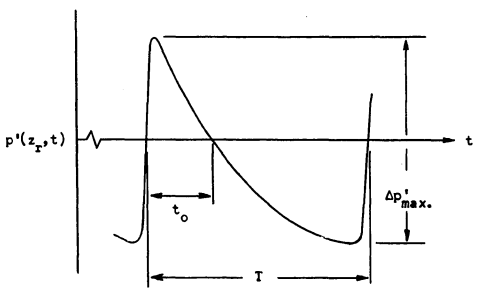

Figure 22. Definition of the Waveform Correlation Parameters.

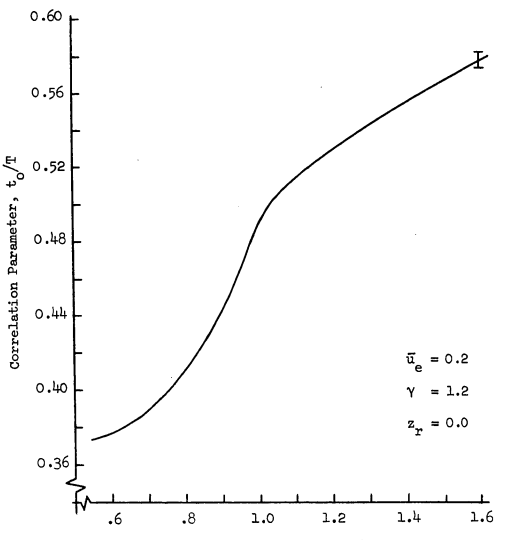

Figure 23. Waveform Correlation Parameter t_o/T.

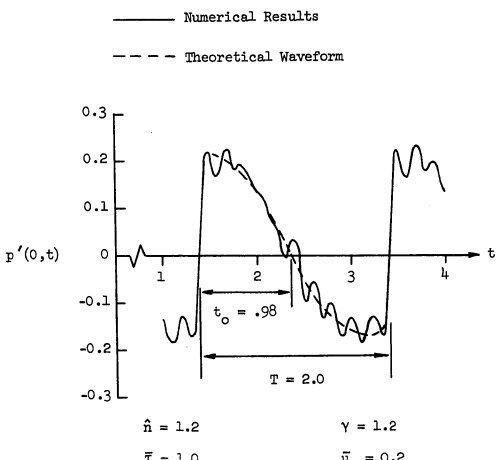

Figure 24. Theoretical Pressure Waveform Used to Determine t_o/T.

of t_o/T, and $\bar{\tau}$ is read from the ordinate.

2. At the calculated value of $\bar{\tau}$, a peak-to-peak pressure plot, similar to the graph shown in Figure 19, is constructed using analytical solutions. This plot is then entered at the experimentally determined $\Delta p'_{max}$, and $\hat{n}$ is read from the abscissa.

It should be noted that because of the nature of experimental pressure data, it may be difficult to use this method to determine $\bar{\tau}$ precisely.

Discussion of the Results

An analysis valid for moderate amplitude longitudinal combustion instability oscillations has been presented. The linear stability of a variety of liquid propellant rocket motors was investigated. Nonlinear solutions were found for first and second mode instabilities. The following conclusions are drawn from the results of this study.

1. The linear results are in qualitative agreement with the observed behavior of rocket motors at the onset of combustion instability, and with analytical solutions found by more exact mathematical techniques.

2. The limit cycle pressure waveforms are usually discontinuous. The waveform is strongly dependent upon $\hat{n}$ and $\bar{\tau}$, and this dependence can be used to correlate the theoretical results with experimental pressure data.

3. Contrary to other available methods of analysis, the present method can predict the behavior of both the transient and final phases of the instability. The ability to analyze the transient phase of the motion adds considerable insight into the understanding of the problem.

This method can predict, without ambiguity, the mode of instability that will occur under various engine operating condition.

4. It has been found that the mode of oscillation depends upon the characteristics of the combustion process. For moderate amplitude instabilities for which the unsteady combustion process can be represented by the $\hat{n} - \bar{\tau}$ model, the mode of oscillation is determined by the linear stability of the various modes at the engine operating condition in question.

5. For moderate amplitude instabilities, the regime of unstable engine operating conditions, in the $\hat{n} - \bar{\tau}$ plane, can be predicted by a linear analysis. Whether or not this conclusion is valid when large amplitude oscillations are present is investigated in the following chapter.

6. Increasing the mean flow velocity has a destabilizing effect on the system.

7. Increasing the combustor length is stabilizing for above resonant oscillations and destabilizing for below resonant oscillations.

8. Engine linear stability is improved when the combustion process is completed downstream of a pressure node of the mode that is unstable for the engine operating conditions in question.

CHAPTER IV

LARGE AMPLITUDE INSTABILITIES

An analysis of moderate amplitude longitudinal combustion instability oscillations has been developed in Chapter III. That analysis is attractive from an analytical point of view because the unsteady flow field is described by one dependent variable, the velocity potential. Consequently, only one partial differential equation need be solved, resulting in a relatively simple mathematical analysis requiring a minimum of computations to find solutions. The results of this analysis indicate that when higher than second order terms are neglected the regions of unstable engine operating conditions can be predicted by a linear analysis.

The effect of large amplitude disturbances on the stability of an engine has not yet been determined. To investigate this question, higher than second order nonlinearities must be retained in the governing equations. In this case the conservation equations can no longer be combined into a single nonlinear wave equation. The mathematical techniques required to successfully apply the Galerkin method to the solution of the conservation equations which describe the behavior of large amplitude oscillations are developed in this chapter. Contrary to the analysis discussed in Chapter III, in the current study both the injector and short nozzle boundary condition are identically satisfied by the series expansions selected to approximate the dependent variables.

The feasibility of the method of solution used to investigate the behavior of large amplitude instabilities is verified by a second order analysis. In this manner, the required analytical techniques are developed by considering a simplified set of equations. The results of this study are found to be in good agreement with the findings of the second order wave equation investigation.

Problem Formulation

The unsteady flow inside a combustor having a low Mach number mean flow is described by Equations (1.5) through (1.7). An examination of Equation (1.6) reveals that this equation is not amenable to solution by a Runge-Kutta integration unless the equation is divided by the term $(1 + \rho')$. This operation is required in order to eliminate the nonlinear coupling in the time derivative term. Unfortunately this division produces terms involving the ratio of unsteady flow variables. Terms of this type are difficult to treat within the framework of the Galerkin method. Since $\rho' < 1$, a binomial expansion of $1/(1+\rho')$ could be used to overcome this difficulty. However, in the present investigation this problem has been overcome by using the following approach. It was observed that the introduction of the specific volume;

$$(\bar{v} + v') = \frac{1}{(\bar{\rho} + \rho')} \tag{4.1}$$

into the conservation laws eliminates the need to use a binomial expansion. In terms of the specific volume, the equations describing the behavior of combustion instability oscillations in combustors having low Mach number mean flows can be written as:

1. Continuity:

$$v'_t + \bar{u} v'_z + u' v'_z - \left[\frac{d\bar{u}}{dz} + u'_z\right] v' - u'_z + w'_z \tag{4.2}$$

$$+ (2v' + v'^2)\left[\frac{d\bar{u}}{dz} + w'_z\right] = 0$$

2. Momentum:

$$u'_t + \bar{u}u'_z + \left[\frac{d\bar{u}}{dz} + u'_z\right]u' + \frac{v'}{\gamma} p'_z + \frac{p'_z}{\gamma} = 0 \tag{4.3}$$

3. Energy:

$$p'_t + \bar{u}p'_z + \gamma\left[\frac{d\bar{u}}{dz} + u'_z\right] + u'p'_z + \gamma u'_z - \gamma w'_z \tag{4.4}$$

$$+ \frac{\gamma(\gamma-1)}{2} (2\bar{u}u' + u'^2) \left[\frac{d\bar{u}}{dz} + w'_z\right]$$

The unsteady mass generation term, w'_z, is defined by Equation (1.8) and the boundary conditions are defined by Equations (1.9) and (1.10).

Moderate Amplitude Analysis

In this section it is assumed that the combustion instability oscillations are of the order of magnitude of the mean flow Mach number, and that terms of $O(\bar{u}_e^3)$ or higher may be neglected. That is, a second order analysis is performed using a system of equations in lieu of the potential equation used in Chapter III. Since the same restrictions are used in both analyses, a direct comparison can be made between the two methods of solution. Contrary to the potential analysis, the boundary conditions will be satisfied by the series expansions used to approximate the flow variables. Subsequently, the methodology developed in this

section will be used to investigate large amplitude combustion instability oscillations.

Neglecting terms of $O(\bar{u}^3)$ or larger, Equations (4.3) and (4.4) can be written as:

1. Energy:

$$p_t' + \bar{u}p_z' + u'p_z' + \gamma u_z' + \gamma \frac{d\bar{u}}{dz} p' + \gamma p' u_z' - \gamma w_z' = 0 \qquad (4.5)$$

2. Momentum:

$$u_t' + \bar{u}u_z' + \frac{d\bar{u}}{dz} u' + u'u_z' + \frac{1}{\gamma} p_z' + \frac{1}{\gamma} v'p_z' = 0 \qquad (4.6)$$

In this system of equations, the specific volume perturbation, v', appears only in the second order term $\frac{1}{\gamma} v'p_z'$ appearing in the momentum equation. Therefore, the continuity equation can be de-coupled from the energy and momentum equations if v' is eliminated from this term. To accomplish this task consider the first order terms of Equations (4.2) and (4.4):

$$v_t' - u_z' = 0$$

$$p_t' + \gamma u_z' = 0$$

The substitution of the second equation into the first results in the following equation:

$$\frac{\partial}{\partial t} \left[v' + \frac{1}{\gamma} p' \right] = 0$$

Therefore,

$$v' + \frac{1}{\gamma} p' = F(z)$$

Since the medium can be considered to be initially at a steady state condition, F(z) can be set equal to zero, and then,

$$v' = -\frac{1}{\gamma} p' + H.O.T. \tag{4.7}$$

After substituting Equation (4.7) into Equation (4.6) and neglecting terms of $O(\bar{u}^3)$ or larger, the flow equations can be written as:

$$E_1' = p_t' + \gamma u_z' + \bar{u} p_z' + \gamma \frac{d\bar{u}}{dz} p' + u' p_z' + \gamma p' u_z' \tag{4.8}$$

$$- \gamma \hat{n} \frac{d\bar{u}}{dz} [p'(t) - p'(t - \bar{\tau})] = 0$$

$$E_2' = u_t' + \frac{1}{\gamma} p_z' + \bar{u} u_z' + \frac{d\bar{u}}{dz} u' + u' u_z' - \frac{1}{\gamma^2} p' p_z' = 0 \tag{4.9}$$

where Equation (1.8) has been used to replace w_z' in Equation (4.8).

The problem boundary conditions have been derived in Chapter I. These are the solid wall boundary condition at the injector face,

$$u'(0,t) = 0 \tag{4.10}$$

and the quasi-steady short nozzle boundary condition, given by Equation (1.10). To second order, Equation (1.10) can be written as:

$$u'(1,t) = \frac{\gamma - 1}{2\gamma} \bar{u}_e p'(1,t) \tag{4.11}$$

The pressure and velocity are now expanded in trial functions which satisfy the boundary conditions given by Equations (4.10) and (4.11). As in the potential analysis of Chapter III, the pressure is expanded in

terms of acoustic eigenfunctions and eigenvalues, that is:

$$\tilde{p}'(z,t) = \sum_{n=1}^{N} B_n(t) \cos(n\pi z) \tag{4.12}$$

The velocity is expanded in the manner indicated by Equation (2.4), that is:

$$\tilde{u}'(z,t) = F_b(z,t) + \sum_{n=1}^{N} c_n(t)\sin(n\pi z) \tag{4.13}$$

or

$$\tilde{u}'(z,t) = F_b(z,t) + \tilde{q}'(z,t) \tag{4.14}$$

where

$$\tilde{q}'(z,t) = \sum_{n=1}^{N} c_n(t)\sin(n\pi z) \tag{4.15}$$

and

$$F_b(0,t) = 0 \tag{4.16}$$

$$F_b(1,t) = \frac{\gamma-1}{2\gamma} \bar{u}_e p'(1,t) \tag{4.17}$$

It is apparent from Equations (4.13) through (4.17) that the velocity has been assumed to consist of an acoustic-type velocity plus a correction term of $O(\bar{u}^2)$. The acoustic-type expansion is zero at $z = 0$ and $z = 1$, and the correction term satisfies the problem boundary conditions. The functional form of $F_b(z,t)$ remains to be specified. Two choices will be

considered in this investigation. These functions, based on acoustic considerations,[22] are:

$$F_b(z,t) = Q_1 p'(1,t) z \tag{4.18}$$

and

$$F_b(z,t) = Q_1 p'(z,t) z \tag{4.19}$$

where

$$Q_1 = \frac{\gamma-1}{2r} \bar{u}_e \tag{4.20}$$

It will be shown that the solutions are insensitive to the choice of $F_b(z,t)$. However, it will be found that the computation time required to reach limit cycle condition is reduced when the $F_b(z,t)$ defined by Equation (4.19) is used. According to Finlayson,[16] the fact that the results are relatively insensitive to the choice of trial functions is an indication of the validity of the solutions. That is, any errors incurred by an improper selection of $F_b(z,t)$ are, in some manner, compensated for by the undetermined mode-amplitudes $B_n(t)$ and $C_n(t)$.

The two conservation equations are written in terms of p' and q' by substituting Equation (4.14) into Equations (4.8) and (4.9). The following equations, to $O(\bar{u}^2)$, result:

$$E_1' = p_t' + \gamma F_{b_z} + \gamma q_z' + \bar{u} p_z' + \gamma \frac{d\bar{u}}{dz} p' + q' p_z' + \gamma p' q_z' \tag{4.21}$$

$$- \gamma \hat{n} \frac{d\bar{u}}{dz} [p'(t) - p'(t - \bar{\tau})] = 0$$

$$E_2' = q_t' + F_{b_t} + \frac{1}{\gamma} p_z' + \bar{u}q_z' + \frac{d\bar{u}}{dz} u' + q'q_z' - \frac{1}{\gamma} p'p_z' = 0 \qquad (4.22)$$

Care must be used in the selection of the weighting functions in the application of the Galerkin method to the solution of Equations (4.21) and (4.22). Recall that the basic concept behind the Galerkin method is that by requiring a residual to be orthogonal to members of a complete set over the domain of the problem, the residual is minimized in some average sense. The weighting functions are selected from the trial functions used to represent the dependent variables. In this problem, the weighting functions are members of either the cosine series, $\cos(\ell\pi z)$, or the sine series, $\sin(\ell\pi z)$. In order to take advantage of the orthogonal properties of these series, Equation (4.2) is weighted by the cosine series and Equation (4.22) is weighted by the sine series. That is, the Galerkin orthogonality conditions are applied in the following manner:

$$\int_0^1 \bar{E}_1' \cos(\ell\pi z)dz = 0, \quad \ell = 1,\ldots,N \qquad (4.23)$$

$$\int_0^1 \bar{E}_2' \sin(\ell\pi z)dz = 0, \quad \ell = 1,\ldots,N \qquad (4.24)$$

where the spacially independent (chugging) mode has been deleted.

Applying the Galerkin method in the manner indicated by Equations (4.23) and (4.24) decouples the time derivatives of the mode-amplitude functions, a result that simplifies the numerical integration of the resulting ordinary differential equations. It is also intuitively appealing to consider Equation (4.21) as the governing differential equation for p_t', and since p' is expanded in terms of a cosine series, the $\cos(\ell\pi z)$

should be used as weighting functions for the residual arising from Equation (4.21). A similar argument applies to Equation (4.22). These arguments are by no means rigorous, and only the correctness of the final solutions can justify this procedure.

A comparison of the results obtained using the two definitions of F_b will now be made. A linear mean flow velocity distribution, defined by

$$\bar{u}(z) = \bar{u}_e z \tag{4.25}$$

will be used in this study. Because only two terms are affected by the definition of F_b, it is convenient to write Equations (4.21) and (4.22) in the following manner:

$$E_1' = \left[p_t' + \gamma q_z' + \bar{u} p_z' + \gamma \frac{d\bar{u}}{dz} p' + q' p_z' + \gamma p' q_z'\right. \tag{4.26}$$

$$\left. - \gamma \hat{n} \frac{d\bar{u}}{dz}\left[p'(t) - p'(t-\bar{\tau})\right]\right] + \begin{bmatrix} \gamma Q_1 p'(1,t) \\ \gamma Q_1 p'(z,t) + \gamma Q_1 p_z'(z,t) z \end{bmatrix} = 0$$

$$E_2' = \left[q_t' + \frac{1}{\gamma} p_z' + \bar{u} q_z' + \frac{du}{dz} u' + q' q_z' - \frac{1}{\gamma} p' p_z'\right] \tag{4.27}$$

$$+ \begin{bmatrix} \gamma Q_1 p_t'(1,t) z \\ \gamma Q_1 p_t'(z,t) z \end{bmatrix} = 0$$

In the second bracketed expressions in Equations (4.26) and (4.27), the upper term corresponds to F_b defined by Equation (4.18), and the lower term corresponds to F_b defined by Equation (4.19). This notation will be used throughout this section.

The series expansions given by Equations (4.12) and (4.15) are now substituted into Equations (4.26) and (4.27). Applying the Galerkin orthogonality conditions defined by Equations (4.23) and (4.24) to the resulting expressions produces the following set of first order, quasi-linear ordinary differential equations governing the behavior of the mode-amplitudes:

$$\frac{dB_\ell}{dt} = F_\ell^{(1)} = -\gamma[\ell\pi c_\ell + \bar{u}_e B_\ell - \hat{n}\,\bar{u}_e(B_\ell - B_{\ell_R})] \tag{4.28}$$

$$+ 2\sum_{n=1}^{N}\left[\bar{u}_e(\ell\pi)I_1(\ell,n)B_n + \sum_{m=1}^{N}[(m\pi)I_2(n,\ell,m)c_n B_m - \gamma(m\pi)I_3(n,m,\ell)B_n C_m]\right]$$

$$+ \begin{bmatrix} 0 \\ \gamma Q_1 \dfrac{B_\ell}{2} - \gamma Q_1 \displaystyle\sum_{n=1}^{N}(n\pi)I_1(\ell,n)B_n \end{bmatrix}$$

$$\frac{dC_\ell}{dt} = -\bar{u}_e C_\ell + \frac{\ell\pi}{\gamma} B_\ell - 2\sum_{n=1}^{N}\left[\bar{u}_e(n\pi)I_1(n,\ell)C_n\right. \tag{4.29}$$

$$\left. + 2\sum_{m=1}^{N}[(m\pi)I_2(n,m,\ell)C_n C_m + \frac{1}{\gamma^2}(n\pi)I_2(n,m,\ell)B_n B_m]\right]$$

$$+ \begin{bmatrix} -Q_1 \dfrac{(-1)^\ell}{\ell\pi}\displaystyle\sum_{n=1}^{N}(-1)^n F_n^{(1)} \\ + Q_1 \displaystyle\sum_{n=1}^{N} I_1(n,\ell)F_n^{(1)} \end{bmatrix}$$

where

$$I_1(n,\ell) = \int_0^1 z\cos(n\pi z)\sin(\ell\pi z)dz \tag{4.30}$$

$$I_2(n,m,\ell) = \int_0^1 \sin(n\pi z)\cos(m\pi z)\sin(\ell\pi z)dz \tag{4.31}$$

$$I_3(n,m,\ell) = \int_0^1 \cos(n\pi z)\cos(m\pi z)\cos(\ell\pi z)dz \tag{4.32}$$

The linear stability limits are found by considering the linear terms of Equations (4.28) and (4.29). From these linear terms, it appears that the choice of F_b affects the linear behavior of the system. Consequently, the linear stability limits, in the $\hat{n}$ - $\bar{\tau}$ plane, must be established, and a comparison must be made between the two results. Using linear mode-amplitude coefficients defined by

$$B_n = P_n e^{i\omega_n t}$$

and

$$C_n = U_n e^{i\omega_n t}$$

the linear differential equations can be written as:

$$\gamma(n\pi)U_n + i\omega_n P_n + \begin{bmatrix} \frac{\gamma+1}{2}\,\bar{u}_e \\ \frac{\gamma-1}{4}\,\bar{u}_e \end{bmatrix} P_n - \gamma\hat{n}\bar{u}_e[1 - e^{-i\omega_n\tau}]P_n = 0 \tag{4.33}$$

$$i\omega_n U_n + \frac{\bar{u}_e}{2}U_n - \frac{n\pi}{\gamma}P_n - i\omega_n\bar{u}_e \begin{bmatrix} \frac{\gamma-1}{\gamma(n\pi)} \\ \frac{\gamma-1}{4\gamma(n\pi)} \end{bmatrix} P_n = 0 \tag{4.34}$$

Noting that

$$1 - e^{-i\omega_n\bar{\tau}} = 1 - \cos(\omega_n\bar{\tau}) + i\sin(\omega_n\bar{\tau})$$

Equations (4.33) and (4.34) can be written in the following form:

$$\begin{bmatrix} \left[\frac{2\gamma+1}{2}\bar{u}_e\right] - \gamma\hat{n}\bar{u}_e(1-\cos(\omega_n\bar{\tau}) + i(\omega_n - \gamma\hat{n}\bar{u}_e\sin(\omega_n\bar{\tau})) & [n\pi\gamma] \\ \left[-\frac{n\pi}{\gamma} - \omega_n\bar{u}_e\right] & \left[\frac{\bar{u}_e}{2} + i\omega_n\right] \end{bmatrix} \begin{bmatrix} P_n \\ U_n \end{bmatrix} = 0 \qquad (4.35)$$

$$\left[\begin{matrix} \frac{\gamma-1}{\gamma(n\pi)} \\ \frac{\gamma-1}{4\gamma(n\pi)} \end{matrix}\right]$$

$$\left[\frac{\frac{7\gamma-1}{4}\bar{u}_e}{}\right]$$

In order for Equation (4.35) to be valid for every P_n and U_n, the determinant of the coefficient matrix must be set equal to zero. Because terms involving the product of a term of $O(\bar{u}_e^2)$ with a flow perturbation are neglected in this analysis, terms of $O(\bar{u}_e^2)$ are neglected in the evaluations of the determinant. Performing this operation and separating the real and imaginary parts of the resulting equation yields the following relations:

$$\hat{n} = \frac{\omega_n^2 - (n\pi)^2}{\gamma\bar{u}_e\omega_n\sin(\omega_n\bar{\tau})} \qquad (4.36)$$

$$\tan\left(\frac{\omega_n\bar{\tau}}{2}\right) = \frac{2\gamma\omega_n\bar{u}_e}{\omega_n^2 - (n\pi)^2} \qquad (4.37)$$

These relations are the same as the equations defining the linear stability limits for $\bar{u}$ for $\bar{u}_e z$ found in the second order wave equation

analysis (i.e., Equations (3.15) and (3.16)). Consequently, within the accuracy of this investigation, the linear stability limits are not affected by the definition of the boundary term.

A comparison of the nonlinear solutions will now be made. The desired solutions are found by numerical integration of Equations (4.28) and (4.29). The procedures used to solve these equations are identical to those used in the analysis discussed in Chapter III, except that in this case the system of ordinary differential equations is of first order. A description of the computer programs used in the solution of the equations is described in Appendix E.

In Figure 25 typical injector face pressure waveforms are presented for resonant and below resonant oscillations. The fundamental mode pressure and velocity mode amplitudes of the below resonant (i.e. $\bar{\tau} = 1.3$) oscillation are shown in Figure 26. Based on these results, it is concluded that the choice of F_b has a negligible effect on the nonlinear limit cycle solutions. However, the computation time required to reach limit cycle conditions is reduced when $F_b = Q_1 p(z_1 t) z$ (i.e., Equation (4.19)) is used. Furthermore, solutions of driven axial acoustic considerations waves[22] in a closed-ended chamber indicate this to be the more proper choice of a boundary term. Therefore, Equation (4.19) will be used as the boundary correction term when the second order nozzle admittance condition is to be satisfied. A similar relation will be used in the large amplitude analysis.

A comparison of results obtained in the wave equation analysis of Chapter III with results obtained in the second order conservation equation analysis is presented in Figure 27. Here, injector face pressure

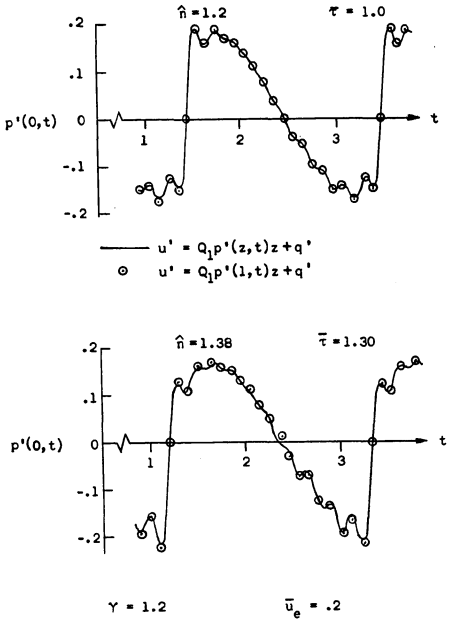

Figure 25. The Effect of the Choice of the Boundary Term on the Pressure Waveforms.

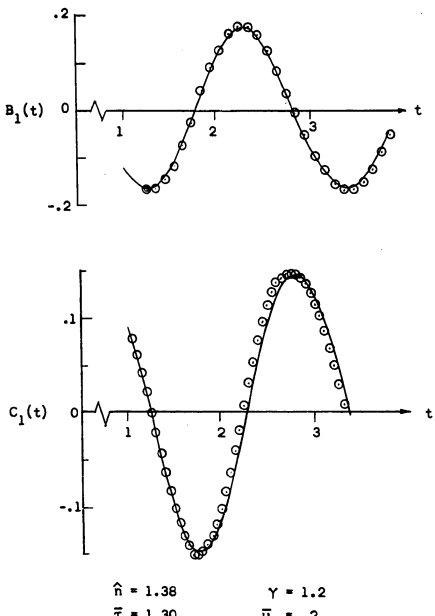

Figure 26. The Effect of the Choice of the Boundary Term on the Mode-Amplitude Function

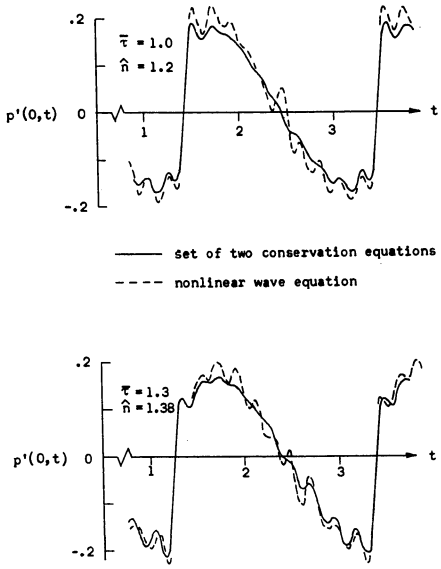

Figure 27. A Comparison of Second Order Solutions.

waveforms are compared. From these data it is concluded that the results are qualitatively similar although the wave equation solutions predict a larger peak-to-peak amplitude, and that the potential solutions are of a more irregular nature.

Since in these studies the same assumptions are made concerning the gasdynamics and the unsteady combustion process, these differences are probably due to the different treatment of the quasi-steady short nozzle boundary condition. A small but finite perturbation velocity at the nozzle entrance is required to satisfy the nozzle boundary condition. The expansion used, Equation (3.4), in the solution of the wave equation results in a zero perturbation velocity at the nozzle entrance. Consequently, the boundary condition cannot possibly be satisfied, and the error thus incurred must be distributed throughout the combined differential equation and boundary residual. Because the perturbation velocity at the combustor exit is zero, it is hypothesized that the boundary term of Equation (3.8) accounts for energy removal through the nozzle by mean flow convection, but does not account for acoustic radiation. This difficulty can probably be overcome if a trial function which includes a non-zero perturbation velocity is used in lieu of Equation (3.4).

It is also apparent from Figure 27 that the nonlinear solutions of the second order conservation equation analysis exhibit the characteristic waveform dependence upon $\bar{\tau}$ as observed in Chapter III.

The effect of the magnitude of the mean flow Mach number on the nonlinear solutions can be seen in the results presented in Figure 28. The reduction in peak-to-peak pressure amplitude evident in this figure is in agreement with the potential analysis result shown in Figure 15.

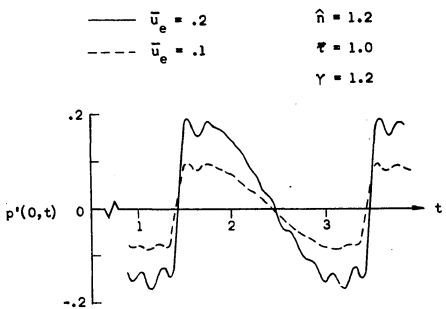

Figure 28. The Effect of the Mean Flow Mach Number on the Pressure Waveforms.

From the results of this second order conservation equation analysis, it can be concluded that:

1. It is feasible to satisfy the problem boundary conditions by a judicious selection of trial functions. Furthermore, when physically realistic boundary terms are used in the series expansions the results of the analysis are insensitive to the form of the boundary terms. It is concluded that the more proper choice of the second order boundary term is $F_b = Q_1 p(z,t)z$. A similar term will be used in the large amplitude analysis.

2. The results of the second order potential analysis of Chapter III and the second order conservation equation analysis discussed in this chapter are in good agreement. However, it appears that when using the modified Galerkin method a non-zero perturbation velocity at the nozzle entrance should be included in the trial function expansion.

Large Amplitude Instability Analysis

Experimental data show that large amplitude oscillations are often present inside unstable liquid propellant rocket combustors. It is also known that the presence of large amplitude disturbances can change the stability characteristics of rocket combustors. This phase of the investigation is concerned with extending the methodology developed in the first section of this chapter to the study of large amplitude instabilities in combustors having low Mach number mean flows. The analysis is not valid for arbitrarily large amplitude oscillations; however, oscillations with amplitudes an order of magnitude larger than the exit Mach number are considered.

In order to accomplish this task, two ordering parameters are

used. One parameter, $\bar{u}_e$, is a measure of the deviation of the flow field from the behavior of oscillations in a quiescent medium. The second parameter, ε, is a measure of the amplitude of the flow oscillations. The flow field is represented by Taylor's series expansions in the two ordering parameters about the unperturbed quiescent state. For example, the pressure is expanded in the following form:

$$p(z,t,\varepsilon,\bar{u}_e) = p(z,t,0,0) + \left[\varepsilon \frac{\partial p}{\partial \varepsilon} + \bar{u}_e \frac{\partial p}{\partial \bar{u}_e}\right]_{z,t,0,0}$$

$$+ \frac{1}{2}\left[\varepsilon^2 \frac{\partial^2 p}{\partial \varepsilon^2} + 2\varepsilon \bar{u}_e \frac{\partial^2 p}{\partial \varepsilon \partial \bar{u}_e} + \bar{u}_e^2 \frac{\partial^2 p}{\partial \bar{u}_e^2}\right]_{z,t,0,0}$$

$$+ \frac{1}{6}\left[\varepsilon^3 \frac{\partial^3 p}{\partial \varepsilon^3} + 3\varepsilon^2 \bar{u}_e \frac{\partial^3 p}{\partial \varepsilon^2 \partial \bar{u}_e} + 3\varepsilon \bar{u}_e^2 \frac{\partial^3 p}{\partial \varepsilon \partial \bar{u}_e^2} + \bar{u}_e^3 \frac{\partial^3 p}{\partial \bar{u}_e^3}\right]_{z,t,0,0}$$

$$+ \ldots .$$

The flow field has previously been assumed to consist of a steady state flow (e.g., $\bar{p}(z,t,\bar{u}_e)$) and a perturbation flow (e.g., $p'(z,t,\varepsilon,\bar{u}_e)$). The steady and perturbation terms in the Taylor's series expansions can be separated from one another. For example, the perturbation pressure can be represented by the following series expansion:

$$p'(z,t,t,\bar{u}_e) = \left[\varepsilon \frac{\partial p'}{\partial \varepsilon} + \bar{u}_e \frac{\partial p'}{\partial \bar{u}_e}\right]_{z,t,0,0}$$

$$+ \frac{1}{2}\left[\varepsilon^2 \frac{\partial^2 p'}{\partial \varepsilon^2} + 2\bar{u}_e \frac{\partial^2 p'}{\partial \bar{u}_e \partial \varepsilon} + \bar{u}_e^2 \frac{\partial^2 p'}{\partial \bar{u}_e^2}\right]_{z,t,0,0} +$$

$$+ \frac{1}{6}\left[\varepsilon^3 \frac{\partial^2 p'}{\partial \varepsilon^3} + 3\varepsilon^2 \bar{u}_e \frac{\partial^2 p'}{\partial \varepsilon^2 \partial \bar{u}_e} + 3\varepsilon \bar{u}_e^2 \frac{\partial^3 p'}{\partial \varepsilon \partial \bar{u}_e^2} + \bar{u}_e^3 \frac{\partial^3 p'}{\partial \bar{u}_e^3}\right]_{z,t,0,0}$$

$$+ \ldots$$

Similar expressions can be derived for v' and u'.

In this analysis it is assumed that $\bar{u}_e$ is small, and that terms of order higher than $O(\bar{u}_e^2)$ are negligible. However, the amplitudes of the flow oscillations may be large. Consequently, terms of $O(\bar{u}_e \varepsilon^2)$ must be retained in the formulation of the problem. The terms that must be retained in the governing equations (i.e., Equations (4.2) through (4.4)) are found by substituting the series expansions of the p',u', and v' into the individual terms of these equations and neglecting those terms of order higher than $O(\bar{u}_e^2)$ or $O(\bar{u}_e \varepsilon^2)$. Consider, for example, the term $\frac{d\bar{u}}{dz} v'$ in Equation (4.2):

$$\frac{d\bar{u}}{dz} v' = \frac{d\bar{u}}{dz}\left[\varepsilon \frac{\partial v'}{\partial \varepsilon} + \bar{u}_e \frac{\partial v'}{\partial \bar{u}_e}\right]_{z,t,0,0} + \ldots$$

Since terms of $O(\bar{u}_e \varepsilon)$ and of $O(\bar{u}_e^2)$ are not negligible, terms of this type must be retained in the governing equations.

Next consider the term $2\bar{u} \frac{d\bar{u}}{dz} u'$ in Equation (4.4):

$$2\bar{u} \frac{d\bar{u}}{dz} u' = 2\bar{u} \frac{d\bar{u}}{dz}\left[\varepsilon \frac{\partial u'}{\partial \varepsilon} + \bar{u}_e \frac{\partial u'}{\partial \bar{u}_e}\right]_{z,t,0,0} + \ldots$$

Terms of this type are neglected in the analysis.

Ordering all of the terms in Equations (4.2) through (4.4) in this manner, and neglecting the appropriate terms, results in the

following equations describing the behavior of large amplitude oscillations in a low Mach number mean flow:

1. Continuity:

$$v_t' + \bar{u}v_z' + \frac{d\bar{u}}{dz}v' - v'u_z' - u_z' + w_z' + 2v'w_z' + \frac{d\bar{u}}{dz}v'^2 = 0 \qquad (4.38)$$

2. Momentum:

$$u_t' + \bar{u}u_z' + \frac{d\bar{u}}{dz}u' + u'u_z' + \frac{1}{\gamma}v'p_z' + \frac{1}{\gamma}p_z' = 0 \qquad (4.39)$$

3. Energy:

$$p_t' + \bar{u}p_z' + u'p_z' + \gamma u_z' - \gamma w_z' + \gamma\frac{d\bar{u}}{dz}p' + \gamma p'u_z' + \frac{\gamma(\gamma-1)}{2}\frac{d\bar{u}}{dz}u'^2 = 0 \qquad (4.40)$$

where w_z' is defined by Equation (1.8), and the boundary conditions are defined by Equations (1.9) and (1.10). It should be emphasized that a linear unsteady combustion model is used in this investigation. That is, only higher order flow nonlinearities are taken into account. This approach was taken becaus of the lack of a proven nonlinear unsteady combustion model.

In order to satisfy the nozzle boundary condition, a new velocity variable, q', is defined in a manner similar to the approach used in the second order analysis. That is;

$$u' = [Q_1p'(z,t) + Q_2p'^2(z,t)]z + q' = F_bz + q' \qquad (4.41)$$

where

$$Q_1 = \frac{\gamma-1}{2\gamma}\,\bar{u}_e \tag{4.42}$$

$$Q_2 = -\frac{\gamma^2-1}{8\gamma^2}\,\bar{u}_e = -Q_1\,\frac{\gamma+1}{4\gamma} \tag{4.43}$$

and q' is expanded in terms of acoustic eigenfunctions and eigenvalues, such that $q'(0,t) = q'(1,t) = 0$. Therefore, both of the problem boundary conditions are identically satisfied by the assumed solutions. Equation (4.41) is substituted into Equations (4.38) through (4.40) and the following set of partial differential equations results:

$$E_1 = v'_t - q'_z + \bar{u}v'_z + \frac{d\bar{u}}{dz}\,v' + q'v'_z - v'q'_z + \frac{d\bar{u}}{dz}\,v'^2 + Q_1 zp'v'_z \tag{4.44}$$

$$- Q_1 zp'_z v' - Q_1 v'p' + 2v'w'_z + w'_z - F_b - F_{b_z} z = 0$$

$$E_2 = \rho'_t + \gamma q'_z + \bar{u}p'_z + \gamma\,\frac{d\bar{u}}{dz}\,p' + q'p'_z + \gamma p'q'_z + \frac{\gamma(\gamma-1)}{2}\,\frac{d\bar{u}}{dz}\,q'^2 \tag{4.45}$$

$$+ \gamma Q_1 p'^2 + (\gamma+1)Q_1 zp'p'_z - \gamma[w_z - F_b - F_{b_z} z] = 0$$

$$E'_3 = q'_t + \frac{p'_z}{\gamma} + \bar{u}q'_z + \frac{d\bar{u}}{dz}\,q' + \frac{1}{\gamma}\,v'p'_z + q'q'_z + Q_1 zp'q'_z \tag{4.46}$$

$$+ Q_1 zp'_z q' + Q_1 p'q' + F_{b_t} z = 0$$

The dependent variables are expanded in terms of acoustic eigenfunctions and eigenvalues:

$$\tilde{v}'(z,t) = \sum_{n=1}^{N} A_n(t)\,\cos(n\pi z) \tag{4.47}$$

$$\tilde{p}'(z,t) = \sum_{n=1}^{N} B_n(t)\,\cos(n\pi z) \tag{4.48}$$

$$\tilde{q}'(z,t) = \sum_{n=1}^{N} C_n(t)\ \sin(n\pi z) \tag{4.49}$$

As was the case in both of the second order analyses, the spacially independent (n = 0) "chugging" mode has been omitted from the series expansions.

The Galerkin method is now applied to the solution of Equations (4.44) through (4.46) in the same manner which proved successful in the second order analysis. That is, it is required that the following expressions are satisfied:

$$\int_0^1 \tilde{E}_1' \cos(\ell\pi z)dz = 0, \quad \ell=1,\ldots,N \tag{4.50}$$

$$\int_0^1 \tilde{E}_2' \cos(\ell\pi z)dz = 0 \tag{4.51}$$

$$\int_0^1 \tilde{E}_3' \sin(\ell\pi z)dz = 0 \tag{4.52}$$

Carrying out the operations indicated by Equations (4.50) through (4.52) and assuming a linear velocity distribution, $\bar{u} = \bar{u}_e z$, results in the following set of quasi-linear ordinary differential equations:

$$\begin{aligned}\frac{dA_\ell}{dt} = F_{1_\ell} = {} & (\ell\pi)C_\ell + Q_1 B_\ell - \bar{u}_e A_\ell - \hat{n}\bar{u}_e(B_\ell - B_{\ell_R}) \\ & + 2\sum_{n=1}^{N}\left[\left[\bar{u}_e(n\pi)I_1(n,\ell)A_n - Q_1(n\pi)I_1(n,\ell)B_n\right]\right. \\ & + \sum_{m=1}^{N}\left[(m\pi)I_2(n,m,\ell)C_n A_m + (m\pi)I_3(n,m,\ell)A_n C_m\right.\end{aligned} \tag{4.53}$$

$$-\bar{u}_e I_3(n,m,\ell)A_n A_m + Q_1(m\pi)I_4(n,m,\ell)B_n A_m$$

$$-Q_1(m\pi)I_4(n,m,\ell)A_n B_m + Q_1 I_3(n,m,\ell)A_n B_m$$

$$-2\hat{n}\bar{u}_e I_3(n,m,\ell)(B_n - B_{n_R})A_m$$

$$+ Q_2 I_3(n,m,\ell)B_n B_m - 2Q_2(m\pi)I_4(n,m,\ell)B_n B_m\Big]\Big]$$

$$\frac{dB_\ell}{dt} = F_{2_\ell} = -\gamma(\ell\pi)C_\ell - \gamma\bar{u}_e B_\ell - \gamma Q_1 B_\ell + \gamma\hat{n}\bar{u}_e(B_\ell - B_{\ell_R}) \qquad (4.54)$$

$$+ 2\sum_{n=1}^{N}\Big[\bar{u}_e(n\pi)I_1(n,\ell)B_n + \gamma Q_1(n\pi)I_1(n,\ell)B_n$$

$$+ \sum_{m=1}^{N}[(m\pi)I_2(n,m,\ell)C_n B_m - \gamma(m\pi)I_3(n,m,\ell)B_n C_m$$

$$- \frac{\gamma(\gamma-1)}{2}\bar{u}_e I_2(n,m,\ell)C_n C_m - \gamma Q_1 I_3(n,m,\ell)B_n B_m$$

$$+ (\gamma+1)Q_1(m\pi)I_4(n,m,\ell)B_n B_m - \gamma Q_2 I_3(n,m,\ell)B_n B_m$$

$$+ 2\gamma Q_2(m\pi)I_4(n,m,\ell)B_n B_m\Big]\Big]$$

$$\frac{dC_\ell}{dt} = -2\sum_{n=1}^{N}\Big[Q_1 I_1(n,\ell)F_{2_n} + 2Q_2\sum_{m=1}^{N}I_4(n,\ell,m)B_n F_{2_m}\Big] + F_{3_\ell} \qquad (4.55)$$

where

$$F_{3_\ell} = \frac{\ell\pi}{\gamma}B_\ell - \bar{u}_e C_\ell + 2\sum_{n=1}^{N}\Big[-\bar{u}_e(n\pi)I_1(\ell,n)C_n \qquad (4.55a)$$

$$+ \sum_{m=1}^{N}[\frac{1}{\gamma}(m\pi)I_2(\ell,m,n)A_n B_m - (m\pi)I_2(n,\ell,m)C_n C_m$$

$$- Q_1(m\pi)I_4(n,\ell,m)B_nC_m + Q_1(n\pi)I_5(n,\ell,m)B_nC_m$$
$$- Q_1I_2(\ell,m,n)B_nC_m\Big]\Big]$$

and where the following definitions have been made:

$$I_1(n,\ell) = \int_0^1 z\ \sin(n\pi z)\ \cos(\ell\pi z)dz \tag{4.56}$$

$$I_2(n,m,\ell) = \int_0^1 \sin(n\pi z)\sin(m\pi z)\cos(\ell\pi z)dz \tag{4.57}$$

$$I_3(n,m,\ell) = \int_0^1 \cos(n\pi z)\cos(m\pi z)\cos(\ell\pi z)dz \tag{4.58}$$

$$I_4(n,m,\ell) = \int_0^1 z\ \cos(n\pi z)\sin(m\pi z)\cos(\ell\pi z)dz \tag{4.59}$$

$$I_5(n,m,\ell) = \int_0^1 z\ \sin(n\pi z)\sin(m\pi z)\sin(\ell\pi z)dz \tag{4.60}$$

Linear Results

An examination of Equations (4.53) through (4.55) reveals that the linear parts of Equation (4.54) and (4.55) are independent of Equation (4.53), and that they are identical to the linear equations used to establish the linear stability limits in the preceding second order analysis. Consequently, the linear stability limits for the large amplitude analysis are the same as the linear stability limits of the second order analysis. These limits are shown in Figure 7.

Nonlinear Solutions

The method used in Chapter III to find nonlinear solutions is also employed in this study. That is, engine operating conditions are specified

in terms of $\bar{u}_e$, Υ, $\hat{n}$ and $\bar{\tau}$, the space integrals given in Equations (4.56) through (4.60) are numerically integrated, an initial disturbance is introduced, and Equations (4.53) through (4.55a) are integrated numerically using a fourth order Runge-Kutta method until a stable periodic solution is found, if one exist (refer to Appendix E). An examination of these equations show that there are a great many more terms involved in the integration than was the case in the second order analyses. The presence of these additional terms results in a substantial increase in computation time. The number of equations in the system and the number of terms in each equation can be significantly reduced if fewer terms are retained in the series expansions of the dependent variables. Fortunately, it has been demonstrated in Chapter III that at least in the case of moderate amplitude oscillations the behavior of the first and second harmonics can be found using five term expansions. Since longitudinal instabilities are most often encountered in the first and second modes, these modes are of primary interest. A convergence test, using five, seven, and ten term expansions were conducted using the solutions describing the behavior of large amplitude oscillations to determine if nonlinear discontinuous pressure waveforms can be approximated with a reduced number of terms in the series expansions. An integration step size of h = .05 was used in this investigation. The resulting waveforms are presented in Figure 29. The approximate run time required on a U-1108 computer to generate these solutions is listed below:

No. of Cycles	No. of Terms	Run Time, minutes
15	5	2
15	7	4.5
15	10	11

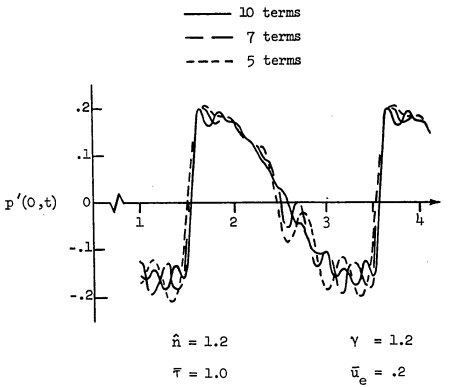

Figure 29. The Effect of the Number of Terms in the Series on the Injector Face Pressure.

Based on these data and on the results of the convergence test conducted in the second order analysis discussed in Chapter III, it is concluded that the essential characteristics of the oscillations can be found using five term expansions. This approach results in a significant reduction in computation time.

When some critical characteristic of the combustion instability oscillation was not satisfactorily represented by a five term expansion (e.g., when there was a question as to whether the waveform was continuous or discontinuous) a solution was found using additional terms in the series expansions. In these cases, the initial disturbance was based on the results of the five term expansion solutions. This approach minimized the computation time required to reach limit cycle conditions.

A comparison of the pressure waveforms resulting from the large amplitude analysis with those found using the moderate amplitude conservation equations is made in Figure 30. Here, injector face pressure oscillations at resonant conditions are presented for two values of $\hat{n}$. When the engine operating conditions are only moderately unstable, the results of the two analyses are in good agreement. As the instability of the engine increases, the large amplitude analysis predicts slightly larger peak-to-peak amplitudes than does the second order analysis. That is, the two theories are in good agreement for moderate amplitude instabilities, and the agreement deteriorates as the amplitude increases. This result, of course, is to be expected.

The results of the large amplitude instability analysis are compared with the results of the second order potential equation analysis in Figure 31. The variation of the peak-to-peak amplitude at resonant conditions

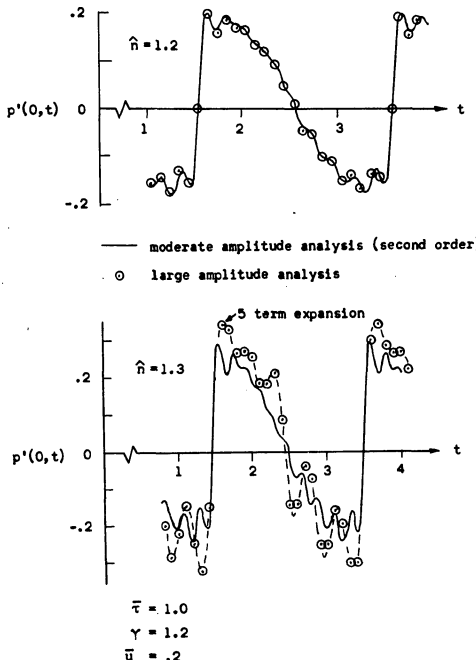

Figure 30. The Effect of the Order of the Solution on the Pressure Waveforms.

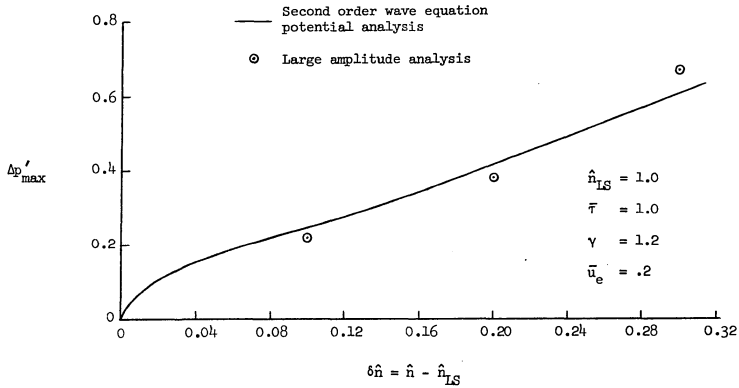

Figure 31. A Comparison of the Large Amplitude Analysis with Second Order Wave Equation Solutions.

with unstable displacement from the linear stability limits is presented in this figure. These data indicate that the large amplitude analysis predicts smaller peak-to-peak amplitudes for moderate amplitude oscillations, and larger peak-to-peak amplitudes for larger amplitude waves. This result, together with the comparison discussed in the preceding paragraph, is consistent with the previously made comparison of the two second order theories. The discrepancy in the peak-to-peak amplitudes at moderately unstable engine operating conditions is believed to be due to the manner in which the nozzle boundary condition was treated in the two analyses.

The primary reason for performing the large amplitude analysis is to determine if the presence of large amplitude oscillations alters the region of unstable engine operating conditions. The engine operating conditions, in terms of $\hat{n}$ and $\bar{\tau}$, for which an engine is linearly unstable are defined in Figure 7. It should be recalled that to second order these stability limits are not changed by the flow nonlinearities. Referring to Figure 1, when the nonlinearities of the system broaden the region of possible unstable engine operation an initially small amplitude oscillation will grow to a finite amplitude stable limit cycle for values of $\hat{n}$ and $\bar{\tau}$ corresponding to linearly stable engine operating conditions. This behavior was used to determine if the regime of fundamental mode linear instability was broadened by nonlinearities when all the higher modes are linearly stable (i.e., when $\bar{\tau} > 2/3$). In this study, small amplitude disturbances were initiated at neutrally stable (in a linear sense) engine operating conditions, and the transient behavior of the disturbance was observed. If the amplitude of the oscillation increased, a broadening of

the unstable region is indicated. In this case, the limit cycle oscillation was found by continuing the time integration. If, on the other hand, the amplitude of the initial disturbance decayed, a smaller disturbance was initiated, and the transient behavior of the smaller disturbance was observed. This was done to insure that the amplitude of the initial disturbance was smaller than the amplitude of the possible limit cycle oscillation. If the initial disturbance decayed for all initial amplitudes investigated, it is concluded that no finite amplitude oscillations are possible at the engine operating conditions in question. Consequently, the nonlinearities do not change the unstable region at the $\bar{\tau}$ location under consideration.

The results of this study are summarized in Figure 32. In this figure, the variation with $\bar{\tau}$ of the peak-to-peak amplitudes of the limit cycle oscillations at linearly stable engine operating conditions is presented. Based on this data it is evident that (1) in the approximate range $1 \leq \bar{\tau} \leq 1.36$ the nonlinearities of the system do not broaden the range of possible unstable engine operation; and (2) because the limit cycle amplitudes are small for $\bar{\tau} < 1$, the extent of the broadening of the unstable region is most probably small.

It is concluded that triggering of axial instabilities can be predicted when higher than second order effects are accounted for in the formulation of the problem.

The extent of the displacement of the stability limits by the flow nonlinearities can be determined by an examination of the behavior of the nonlinear oscillations in regions of linear stability. This was done at $\bar{\tau} = 1.623$ by establishing the variation of the peak-to-peak limit cycle

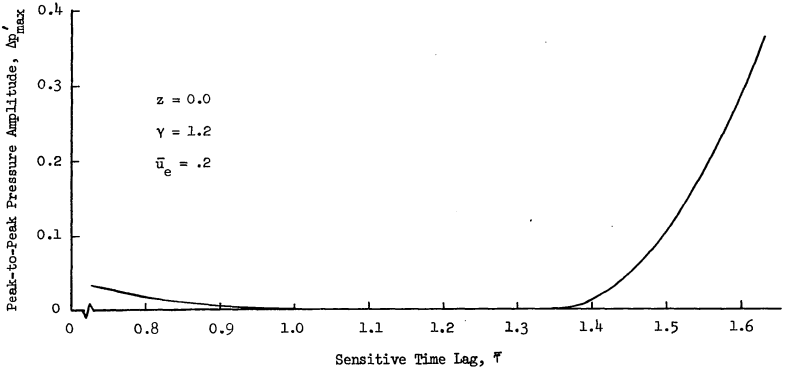

Figure 32. Peak-to-Peak Injector Face Pressure on the Linear Stability Limit.

amplitude with $\delta\hat{n} = \hat{n} - \hat{n}_{LS}$. The maximum negative $\delta\hat{n}$ for which a limit cycle was found is considered to be the boundary of the unstable region.

The critical minimum amplitude required to produce unstable oscillations in the linearly stable region was found by decreasing the amplitude of the initial disturbance at the value of $\delta\hat{n} < 0$ in question until decay of the initial disturbance was noted.

The results of the investigation at $\bar{\tau} = 1.623$ are summarized in Figure 33. Here the variation of the peak-to-peak pressure amplitude with vertical displacement (i.e., $\delta\hat{n}$) is presented. The approximate amplitude of the critical disturbance above which unstable engine operation will result is drawn in a broken line. The solid line represents the resulting limit cycle amplitudes. The small broadening of the region of instability by flow nonlinearities is evident in this figure.

It is believed that the use of a nonlinear unsteady combustion model would significantly change the results of this large amplitude analysis. Unfortunately, a proven unsteady combustion model incorporating nonlinear effects has not yet been developed. Consequently, the investigation of the behavior of large amplitude oscillations in a linearly stable region was not pursued.

A second region of interest in the stability plane is that region where the fundamental mode is linearly stable, and the second mode is linearly unstable ($\bar{\tau} < 2/3$). In this region Mitchell predicts the possibility of triggering fundamental mode instability. The behavior of the combustion instability oscillations was examined in the same manner as used in Chapter III. That is, the transient and limit cycle behavior of the oscillations was found for engine operating conditions at a fixed $\hat{n}$ on either

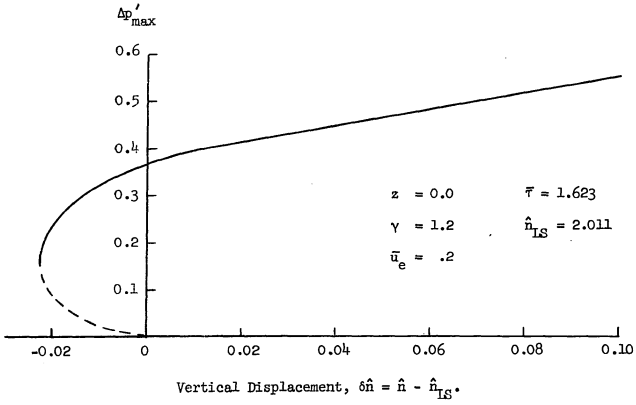

Figure 33. The Effect of Large Amplitude Oscillations on Engine Stability

side of the left branch of the 1L linear stability limit (see Figure 25). A discontinuous 1L disturbance was impulsively introduced within the combustor, and the behavior of the oscillation was examined. The injector face pressure waveforms found at $\hat{n} = 1.4$ are presented in Figure 34. As was the case in the moderate amplitude analysis of Chapter III, the mode of oscillation is determined by the linear characteristics of the system. In the region where Mitchell reports the possibility of triggering 1L oscillations, the current investigation clearly shows the resulting instability to be a 2L-type oscillation. This point is discussed in greater detail in the following chapter.

Discussion of the Results

In reviewing the conclusions reached in this chapter, it is important to note that a linear unsteady combustion model was used in all the calculations. Such a model is rigorous within the framework of the second order investigations. However, in the presence of large amplitude flow oscillations the unsteady combustion process most likely exhibits nonlinear characteristics. Unfortunately, because an appropriate nonlinear model was not available at the time, a linear unsteady combustion model was used in all phases of this research. With these comments in mind, the salient conclusions of this chapter are summarized in the following paragraphs:

1. The pressure waveforms found when the short nozzle boundary condition is satisfied by the assumed solutions are in good agreement with those resulting from the modified Galerkin method solution of the potential solution. Moreover, the former waveforms are somewhat smoother,

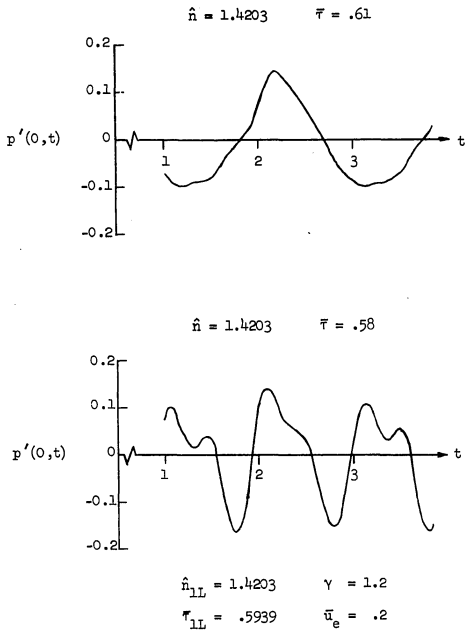

Figure 34. Dependence of Nonlinear Waveforms on $\hat{n}$ and $\bar{\tau}$ (Large Amplitude Analysis).

indicating improved convergence of the solutions. These discrepancies are probably attributable to the choice of series expansion used in the potential analysis. Since in the perturbation velocity component is always zero in this expansion, the nozzle boundary condition cannot be even approximately satisfied, and the resulting errors must be reflected in the time-dependent mode-amplitudes.

2. When compared with the large amplitude solutions, the second order results slightly underestimate the peak amplitude of large amplitude combustion instability oscillations. The discrepancies between the waveforms predicted by these analyses increase with increasing values of $\hat{n}$. However, in most cases the salient features of the waveforms are adequately described the second order analyses.

3. The regime of unstable engine operating conditions was not changed by nonlinear effects in either of the two second order analyses. However, for some off-resonant conditions the presence of large amplitude flow oscillations slightly broadens the range of possible unstable engine operation. It is believed that in a majority of cases the regions of longitudinally unstable engine operating conditions can be predicted by a linear analysis.

5. The large amplitude analysis is considerably more involved than the second order studies. It also requires more computation time to establish periodic solutions. Furthermore, from a practical point of view the large amplitude analysis does not generate any significant new knowledge about the problem. It is therefore recommended that a second order analysis be used in engineering applications of the methodology developed in this report.

CHAPTER V

DISCUSSION AND CONCLUDING REMARKS

The Galerkin method has been used to investigate the behavior of liquid propellant rocket motors experiencing high frequency longitudinal combustion instability. The method of analysis developed in this report reduces the mathematical complexity associated with previous studies of the problem, and at the same time provides considerable insight into the physics of combustion instability oscillations. Unlike other solution techniques, the methodology developed in this investigation is not restricted to the study of a single mode at a time, and no a priori knowledge of the final waveform of the combustion instability oscillation is required. Fundamental to the usefulness of the analytical technique is its ability to describe the transient as well as the final periodic behavior of the oscillations. Using this capability the growth or decay of a disturbance, or the transition from one mode of oscillation to another, can be studied. In this manner, the ambiguities that could arise in interpreting the one mode, periodic solutions of Sirignano and of Mitchell are clarified. Before proceeding with the discussion of the results of the present investigation, it is beneficial to review some of the salient points of these previous nonlinear studies.

Mitchell and Sirignano investigated the behavior of longitudinal combustion instability oscillations in liquid propellant rocket combustors with very short nozzles. Crocco's $\hat{n} - \bar{\tau}$ unsteady combustion model is used to represent a concentrated combustion zone at the injector face. Mitchell's

analysis is also extended to include the case of a uniformly varying steady state combustion distribution. In this case, the result are qualitatively similar to those found using a concentrated combustion zone. The following discussion is concerned with comparisons of the methods of analysis used in these theories, and the conclusions reached by the two authors. The comparison is based on the results found using the concentrated combustion zone study.

In these analyses, perturbation schemes are used to find solutions of a set of conservation equations in which the dependent variables are u and c. The unsteady sources of energy addition and removal are concentrated at the injector face and at the nozzle entrance plane, respectively. Sirignano works in a characteristic coordinate system, while Mitchell uses a physical coordinate system. For off-resonant conditions, Sirignano's analysis is restricted to the behavior of continuous oscillations; as a result only the behavior of combustion instability oscillations at engine operating conditions close to the linear stability limit can be investigated. On the other hand, Mitchell's analysis is not restricted in this manner. Both investigations are concerned with the periodic behavior of the fundamental mode of longitudinal oscillations; second and higher mode oscillations are not considered. Both solution techniques are incapable of predicting the transient behavior of the combustion instability oscillations.

In these analyses, the dependent variables are expanded in power series of the following form:

$$u = u_0 + \varepsilon u_1 + \varepsilon^2 u_2 + \ldots$$

$$a = a_0 + \varepsilon a_1 + \varepsilon^2 a_2 + \ldots$$

where ε is a measure of the amplitude of the flow oscillations, and $\varepsilon \ll 1$. Mitchell makes the additional assumption that $u_o = O(\varepsilon)$. These expansions are substituted into the governing equations and the boundary conditions, and the resulting equations are separated into powers of ε. Because of the different treatment of u_o, certain dissimilarities arise in the resulting equations:

1. The $O(1)$ equations are the same in both theories.

2. In the $O(\varepsilon)$ equations and boundary conditions, Sirignano retains terms of $O(u_o\varepsilon)$, while in Mitchell's analysis these terms are included in the second order equations. Recall that the boundary conditions can be written in the form $u(0,t) = u_o F_{b_1}[a(0,t)]$ and $u(1,t) = u_o F_{b_2}[a(1,t)]$. Consequently, to $O(\varepsilon)$, Mitchell's boundary conditions are $u_1(0,t) = u_1(1,t) = 0$. Sirignano, on the other hand, has non-zero u_1's at the boundaries.

3. To $O(\varepsilon^2)$, Sirignano retains terms of $O(u_o\varepsilon^2)$. These terms are considered to be of third order by Mitchell (the same assumption is used in the current study) and hence they are neglected. There are again differences in the boundary conditions. The important point to note is that Sirignano's second order analysis includes some effects which are considered to be of third order by Mitchell and in the present investigations.

In both analyses, second order solutions generate the nonlinear combustion instability oscillation waveforms. Sirignano demonstrates that a third order analysis is required to determine the stability of the oscillations. This does not imply that a third order analysis is required to find unstable nonlinear solutions. It does imply that to mathematically determine the stability of the nonlinear periodic solution requires a

third order analysis. Mitchell does not perform this third order analysis. Instead, he uses deductive arguments to predict the stability of the second order solutions. The conclusions reached by the two authors will be discussed shortly.

In addition to the conservation equation and boundary conditions, initial conditions are in general required to completely describe the problem. In both studies, the initial conditions are replaced by a cyclic condition on the oscillations. The imposed cyclic condition is that the period of oscillation is approximately the fundamental axial mode acoustic period. Furthermore, Mitchell requires the solution to be continuous within the period of the fundamental mode oscillation. That is, only one discontinuity can be present within the combustor.

Sirignano finds continuous small amplitude periodic solutions in a narrow region on both sides of the linear stability limits, for off-resonant conditions. A third order stability study shows the solution in the linearly unstable region to be stable. Since linear theory predicts that growth of infinitesimal disturbances in this region, it is concluded that the stable small amplitude solutions are the limit cycle waveform of the combustion instability oscillations in this region. In the linearly stable region, Sirignano's solutions are found to be unstable. In this region linear theory predicts the decay of infinitesimal disturbances. Since the small but finite amplitude solutions are unstable, it is concluded that the nonlinearities broaden the region of possible unstable engine operating conditions.

Sirignano's solution is not capable of predicting the final waveform attained by oscillations which grow from the small amplitude wave.

That is, the final wave may be in the first or second or some higher mode of oscillation. It is important to note that Sirignano predicts a broadening of the unstable region of the $\hat{n} - \bar{\tau}$ plane using a second order analysis. However, Sirignano's second order solution contains terms which are considered to be third order by Mitchell and in the present investigation. In the present study it is found that to second order accuracy the regions of 1L instability are not changed by the nonlinearities of the problem. When higher order terms (e.g., terms like Sirignano's second order term $u_o u_2$) are included in the present study, a broadening of the 1L stable region is found for certain off-resonant conditions.

In Mitchell's second order analysis, which is equivalent to the current second order studies, a broadening of the 1L unstable region is predicted only in regions where the 2L mode is linearly unstable (i.e., for $\bar{\tau} < 2/3$, and $\bar{\tau} > 4/3$, in the range of $\bar{\tau}$ that is of interest). The secondary zones of instability are included in his analysis. In these regions, Mitchell finds two periodic solutions. Mitchell argues that the calculated small amplitude solutions are unstable, and represent the critical amplitude required to trigger unstable 1L oscillations in this region. Mitchell bases this conclusion on the statement that "Clearly, the discontinuous oscillations cannot be the final result of the growth of infinitesimal perturbations in this case, simply because infinitesimal perturbations do not grow but rather decay to zero in this region." (See pg. 56, reference 7.) This statement only applies to 1L oscillations. In fact, in this region the 2L mode is linearly unstable, and linear theory predicts an unbounded growth of infinitesimal 2L oscillations in this region. The current theory clearly shows that regardless of the

order of the nonlinearities included in the solution, the limit cycle oscillation in this region is in the 2L mode. This conclusion is independent of the form of the initial disturbance.

The mechanism involved in the change from one mode of oscillation to another is an energy exchange through coupling between the modes. Once energy is transferred into the second harmonic, the 2L mode must grow, in accordance with the predictions of linear theory. Since the second mode is in general highly unstable near the 1L linear stability region, the final oscillation is usually discontinuous, with two shock waves moving back and forth along the combustors. Mitchell's theory, as developed in Reference 9, is incapable of predicting such an oscillation. In spite of this fact, it is interesting to note that the oscillation argued by Mitchell to be unstable exhibits 2L characteristics, even though there is only one discontinuity in the wave.

It is also important to note that Mitchell's second order theory does not predict a broadening of the 1L unstable region when the 2L mode is linearly stable (i.e., for values of $\bar{\tau}$ in the range $2/3 \leq \bar{\tau} \leq 4/3$). The current second order theories clearly show that the second order nonlinearities do not broaden the 1L unstable region predicted by a linear analysis for any value of $\bar{\tau}$.

The following conclusions can be drawn from the preceding discussion:

1. A comparison of Mitchell's results and the results of the current second order theories indicates that the broadening of the 1L unstable region reported by Mitchell does not occur. Instead, 2L oscillations result in this region. It is therefore concluded that to second order

accuracy, the nonlinearities of the system do not change the region of fundamental mode instability predicted by a linear analyses. It is also concluded that it is not physically reasonable to consider the triggering of a linearly stable mode for operating conditions at which another mode is linearly unstable.

2. The broadening of the 1L instability regime reported by Sirignano is in fact due to the inclusion in the second order theory of terms that in the present analysis are considered to be of higher order. These higher order effects do slightly broaden the range of fundamental mode instability. Unless a higher mode is linearly unstable at the value of $\hat{n}$ and $\bar{\tau}$ under consideration, the limit cycle oscillation in the nonlinearity unstable region will be in the fundamental mode. It should also be noted that $\hat{n}_{min}$ is not changed by the nonlinearities of the system.

A serious shortcoming of the perturbation schemes of Sirignano and Mitchell is that they consider the periodic behavior of a single mode at a time. They cannot provide the transient behavior of an oscillation. Consequently, in using these theories some a priori knowledge of the mode of the limit cycle oscillation is required. This is not the case in the present study. In fact, the capability of studying the transient behavior of the oscillation is of paramount importance in clarifying some of the ambiguities of the previous investigations.

The preceding discussions of the mathematically elegant works of Sirignano and of Mitchell are not meant to be derogatory; their development greatly aided the understanding of nonlinear longitudinal instabilities. The discussion presented here is intended to point out the pitfalls that are associated with interpretation of results obtained by use of

mathematical techniques which consider only the periodic behavior of a single mode at a time.

Conclusions

The following conclusions can be drawn from the results of the present study.

1. In most instances, the limit cycle oscillations of longitudinal instabilities are discontinuous waves. Near the linear stability limit, small amplitude continuous oscillations can be found. The oscillations become discontinuous as their amplitude increases.

2. The number of shock waves present within the combustor (i.e., the mode of oscillation) is determined by the "relative linear stability" of the various modes at the engine operating conditions in question. That is, in the majority of cases for which the first and second modes are linearly unstable, the flow oscillation will be in the first mode. On the other hand, when the first mode is linearly stable and the second mode is linearly unstable, the flow oscillation will be in the second mode, and so on.

3. Increasing the mean flow Mach number is destabilizing. Increasing the combustor length is stabilizing for above resonant oscillations, and destabilizing for below resonant oscillations.

4. To second order, the nonlinearities of the system do not change the regions (in the $\hat{n}$ - $\bar{\tau}$ plane) of instability predicted by a linear analysis. There is a slight broadening of the unstable region when higher order terms are included in the analysis; that is, in this case triggering of axial instabilities is predicted. However, the change in the unstable

region is very small and probably will not seriously effect the applicability of the linear stability limits. Moreover, the values of $\hat{n} - \bar{c}$ cannot be determined, based on the current state of the art, to a sufficient degree of accuracy to distinguish between the linear and nonlinear stability limits.

5. The nonlinear waveforms are in most cases adequately represented by the second order solutions. The second order solutions require considerably less computation time than do the large amplitude analysis solutions.

6. Based on observations 4 and 5 it is concluded that in the majority of cases a second order analysis will adequately describe the behavior of liquid propellant rocket experiencing high frequency longitudinal instability.

7. The technique developed in Chapter IV satisfies the quasi-steady short nozzle boundary condition. It may be difficult to extend this approach to the case of a more general nozzle boundary condition. In this case, it may be advisable to use a second order potential analysis incorporating a more realistic expansion of the velocity potential to study more general longitudinal instability problems.

Recommendations for Further Research

The Galerkin method has proven to be a useful technique for the analysis of combustion instability problems. Its usefulness in the study of transverse instability has been demonstrated by Zinn and Powell, and its applicability to the analysis of longitudinal instability has been shown in this dissertation. It is hoped that the Galerkin method will be used to study more general problems of combustion instability than those

treated to date. A few of the areas of interest will now be discussed.

In this study the Crocco linear $\hat{n} - \bar{\tau}$ theory is used to describe the unsteady combustion process. Although this theory has produced results which are in good agreement with experimental data, it is basically an empirical representation of a complex combustion process. It is highly desirable that a more realistic combustion model, supported by both experimental and theoretical evidence be developed. One possibility might be a vaporization rate controlled model, similar to the one developed by Priem.[23]

Axial mode instabilities frequently appear in solid propellant rockets having high combustor length-to-diameter ratio. It is believed that the techniques developed in this thesis can be adapted to the study of axial instabilities in solid propellant rockets.

The following refinements in the analysis presented in this dissertation are suggested:

1. Use a series expansion of the velocity potential in the analysis developed in Chapter III which permits a nonzero perturbation velocity of the nozzle entrance plane.

2. Incorporate a more realistic nozzle admittance relation in lieu of the quasi-steady short nozzle boundary condition.

3. Perform an analysis valid for moderate amplitude instabilities and an arbitrary Mach number mean flow. This study is of interest in light of the trend towards lower contraction ratio nozzles in the design of newer rocket motors.

4. An effort to correlate the results presented in this dissertation with experimental data should be performed.

It is hoped that this dissertation, in conjunction with the solutions of the suggested problems, will provide rocket design engineers with a useful methodology for determining the stability behavior of rocket engines.

APPENDIX A

SIMPLIFICATION AND NON-DIMENSIONALIZATION OF THE CONSERVATION EQUATIONS

In this appendix the equations describing the combustor flow will be written in a form amendable to analytic solution. The one-dimensional, unsteady conservation equations describing a two phase flow can be written as follows:[3]

1. Conservation of Mass:

$$\frac{\partial \rho^*}{\partial t^*} + \frac{\partial(\rho^* u^*)}{\partial z^*} = \frac{\partial w^*}{\partial z^*} = -\frac{\partial \rho_\ell^*}{\partial t^*} - \frac{\partial(\rho_\ell^* u_\ell^*)}{\partial z^*} \tag{A.1}$$

2. Conservation of Momentum:

$$\frac{\partial(\rho^* u^*)}{\partial t^*} + \frac{\partial(\rho^* u^{*2})}{\partial z^*} + \frac{\partial p^*}{\partial z^*} = -\frac{\partial(\rho_\ell^* u_\ell^*)}{\partial t^*} - \frac{\partial(\rho_\ell^* u_\ell^{*2})}{\partial z^*} \tag{A.2}$$

3. Conservation of Energy:

$$\frac{\partial(\rho^* e_s^*)}{\partial t^*} + \frac{\partial(\rho^* u^* h_s^*)}{\partial z^*} = -\frac{\partial}{\partial t^*}\left[\rho_\ell^* (n_\ell^* + \tfrac{1}{2} u_\ell^{*2})\right] - \frac{\partial}{\partial z^*}\left[\rho_\ell^* u_\ell^* (h_\ell^* + \tfrac{1}{2} u_\ell^{*2})\right] \tag{A.3}$$

The following assumptions were made in writing these equations:

1. The flow is one-dimensional, with the velocity vector parallel to the combustor axis.

2. The flow is inviscid, consisting of burnt gases and liquid droplets of negligible volume.

3. There is no heat exchange through the combustor walls.

4. The liquid phase internal energy is equal to the liquid phase enthalpy; and h_{ℓ}^{*} includes the chemical energy of the propellants.

The gas phase is assumed to be both thermally and calorically perfect. In this case, the equation of state for the gas phase is:

$$h_s = \frac{\gamma}{\gamma-1}\frac{p^*}{\rho^*} + \frac{u^{*2}}{2} \tag{A.4}$$

Assuming that the velocity difference between the gas and liquid phases is small, and therefore that the force exerted by the gases on the liquid droplets is inversely proportional to the Reynolds number, a droplet dynamic equation can be written:

$$\frac{\partial u_{\ell}^{*}}{\partial t^{*}} + u_{\ell}^{*}\frac{\partial u_{\ell}^{*}}{\partial z^{*}} = k^{*}(u^{*} - u_{\ell}^{*})$$

where k^{*} will be assumed to be constant.

As a propellant droplet travels through the gas phase, it will be assumed that changes in the droplet thermal and kinetic energy are small, and that the total energy of the droplets remains constant:

$$h_{\ell}^{*} + \frac{1}{2}u_{\ell}^{*2} = \text{constant} = h_{\ell_s}^{*} \tag{A.6}$$

The momentum equation, Equation (A.2), and the energy equation, Equation (A.3), will now be rearranged into a more convenient form. Using Equation (A.1) and Equation (A.5), the momentum equation can be written as:

$$\rho^* \left[\frac{\partial u^*}{\partial t^*} + u^* \frac{\partial u^*}{\partial z^*}\right] + \frac{\partial p^*}{\partial z^*} + (u^* - u_\ell^*)\left[\frac{\partial w^*}{\partial z^*} + K^*\right] = 0 \qquad (A.7)$$

where $K^* = \rho^* K^*$. The last term in Equation (A.7) represents the momentum source arising from the acceleration of the just burned gas to the gas phase velocity, and from the droplet drag. Experience has shown that these momentum sources have a small, stabilizing effect on the flow field. Therefore, neglecting these terms will result in conservative estimates of stability limits. The momentum equation is:

$$\rho^* \left[\frac{\partial u^*}{\partial t^*} + u^* \frac{\partial u^*}{\partial z^*}\right] + \frac{\partial p^*}{\partial z^*} = 0 \qquad (A.8)$$

The energy equation is simplified by noting that:

$$e_s^* = h_s^* - \frac{p^*}{\rho^*} \qquad (A.9)$$

and using the results presented in Equation (A.6), indicating that

$$\frac{D}{bt}\left[h_\ell^* + \frac{1}{2} u_\ell^{*2}\right] = 0 \qquad (A.10)$$

Using these results, together with Equation (A.1), the energy equation can be rewritten as:

$$\frac{\partial}{\partial t^*}\left[\rho^* h_s^*\right] + \frac{\partial}{\partial z^*}\left[\rho^* u^* h_s^*\right] - \frac{\partial p^*}{\partial t^*} = h_{\ell_s} \frac{\partial w^*}{\partial z^*} \qquad (A.11)$$

Using Equations (A.1), (A.8), and (A.4), Equation (A.11) can be written as:

$$\frac{\partial p^*}{\partial t^*} + u^* \frac{\partial p^*}{\partial z^*} + p^*\left[\frac{\partial u^*}{\partial z^*} - \frac{1}{\rho^*}\frac{\partial w^*}{\partial z^*}\right] + (\gamma - 1)(h_s^* - h_{\ell_s}^*)\frac{\partial w^*}{\partial z^*} = 0 \qquad (A.12)$$

Writing the last term in Equation (A.12) in terms of the stagnation enthalpy will prove to be convenient in subsequent manipulations of the energy equation.

Before proceeding with the formulation of the unsteady problem, some useful information will be found by considering the steady state solution. The steady state equations are:

1. Continuity

$$\frac{\partial(\bar{\rho}^*\bar{u}^*)}{\partial z^*} = \frac{\partial \bar{w}^*}{\partial z^*} \tag{A.13}$$

$$\frac{\partial(\bar{\rho}_\ell^*\bar{u}_\ell^*)}{\partial z^*} = -\frac{\partial \bar{w}^*}{\partial z^*} \tag{A.14}$$

2. Momentum

$$\frac{\partial(\bar{\rho}^*\bar{u}^{*2})}{\partial z^*} + \frac{\partial \bar{p}^*}{\partial z^*} = -\frac{\partial}{\partial z^*}(\bar{\rho}_\ell^*\bar{u}_\ell^{*2}) \tag{A.15}$$

3. Energy

$$\frac{\partial(\bar{\rho}^*\bar{u}^*\bar{h}_s^*)}{\partial z^*} = -\frac{\partial}{\partial z^*}(h_{\ell_s}^*\bar{\rho}_\ell^*\bar{u}_\ell^*) \tag{A.16}$$

4. Equation of State

$$\bar{p}^* = R\bar{\rho}^*\bar{T}^* \tag{A.17}$$

5. Droplet heat balance

$$\bar{h}_{\ell_s}^* = \text{constant} \tag{A.18}$$

The steady state boundary conditions at the injector face are:

$$\bar{w}^*(0) = 0 \tag{A.19}$$

$$\bar{u}^*(0) = 0 \tag{A.20}$$

$$\bar{p}^*(0) = p_o^* \tag{A.21}$$

$$u_\ell^*(0) = \bar{u}_{\ell_o}^* \tag{A.22}$$

$$\bar{\rho}_\ell^* \bar{u}_\ell^*(0) = \bar{w}_i^* \tag{A.23}$$

$$\bar{h}_{\ell_s}^*(0) = \bar{h}_{\ell_{s_o}} \tag{A.24}$$

When Equations (A.13) through (A.16) are integrated subject to these boundary conditions, the following solutions are obtained.

$$\bar{\rho}^* \bar{u}^* = \bar{w}^* \tag{A.25}$$

$$\bar{\rho}_\ell^* \bar{u}_\ell^* = \bar{w}_i^* - \bar{w}^* \tag{A.26}$$

$$\bar{p}^* = p_o^* - [(\bar{u}^* - \bar{u}_\ell^*)\bar{w}^* + (\bar{u}_\ell^* - \bar{u}_{\ell_o}^*)\bar{w}_i^*] \tag{A.27}$$

$$\bar{h}_s^* = \bar{h}_{\ell_{s_o}}^* \tag{A.28}$$

Equation (A.28) can also be written as:

$$\bar{T}^* = T_o^* \left(1 - \frac{\gamma-1}{2} \frac{\bar{u}^{*2}}{\bar{c}_o^{*2}}\right) \tag{A.29}$$

The steady state flow field can be found by specifying the steady state velocity, $\bar{u}^*(z)$, and using the steady state droplet dynamic equation (from Equation (A.5)), together with Equations (A.25), (A.26), (A.27) and (A.29). However, a considerable simplification results when $\bar{u}^*(z)$ is

significantly smaller than $\bar{c}_o^*$. Under these conditions, terms of the order $O[(\bar{u}^*/\bar{c}_o^*)^2]$ or higher may be neglected. It then follows from Equation (A.29) that

$$\bar{T}^* \approx \bar{T}_o^* \tag{A.30}$$

while the equation of state, Equation (A.17), yields:

$$\frac{\bar{p}^*}{\bar{\rho}_o^*} \approx \frac{\bar{p}^*}{\bar{\rho}_o^*} \tag{A.31}$$

Equation (A.27) can be written as:

$$\frac{\bar{\rho}^*}{\bar{\rho}_o^*} = 1 - \frac{\bar{\rho}^*}{\bar{\rho}_o^*}\left[\left(\frac{\bar{u}^*}{\bar{c}_o^*}\right)^2 - \frac{\bar{u}_\ell^*\bar{u}^*}{\bar{c}_o^{*2}}\right] - \frac{\gamma\bar{\rho}_\ell^*}{\bar{\rho}_o^*}\left[\frac{\bar{u}_\ell^{*2}}{\bar{c}_o^{*2}} - \frac{u_{\ell_o}^*\bar{u}_\ell^*}{\bar{c}_o^{*2}}\right] \tag{A.32}$$

Since the droplet velocity is the same order of magnitude as the gas phase velocity, and since $\bar{\rho}^*/\bar{\rho}_o^*$ and $\bar{\rho}_\ell^*/\bar{\rho}_o^*$ are first order terms, it follows from Equation (A.32) that:

$$\frac{\bar{\rho}^*}{\bar{\rho}_o^*} = 1 + O\left(\frac{\bar{u}^*}{\bar{c}_o^*}\right)^2 \tag{A.33}$$

Equations (A.31) and (A.32) yield:

$$\frac{\bar{\rho}^*}{\bar{\rho}_o^*} = 1 + O\left(\frac{\bar{u}^*}{\bar{c}_o^*}\right)^2 \tag{A.34}$$

while from Equation (A.25)

$$\bar{w}^* = \bar{\rho}_o^*\bar{u}^* + O\left(\frac{\bar{u}^*}{\bar{c}_o^*}\right)^2 \tag{A.35}$$

Therefore, provided the mean flow velocity is small enough so that second order terms in $\bar{u}^*/c_o^*$ may be neglected, the steady combustion distribution is proportional to the mean flow velocity distribution. The steady state thermodynamic variables are then given by:

$$\frac{\bar{p}^*}{\bar{p}_o^*} = \frac{\bar{\rho}^*}{\bar{\rho}_o^*} = \frac{\bar{T}^*}{\bar{T}_o^*} = 1 + O\left(\frac{\bar{u}^*}{\bar{c}_o^*}\right)^2 \tag{A.36}$$

The governing equations will now be nondimensionalized by the steady state stagnation conditions at the injector face. The characteristic space dimension of the problem will be the combustor length. The nondimensional variables are defined as:

$$z = \frac{z^*}{L} \quad t = \frac{\bar{c}_o^*}{L} t^* \quad u = \frac{u^*}{\bar{c}_o^*} \quad \rho = \frac{\rho^*}{\bar{\rho}_o^*} \tag{A.37}$$

$$p = \frac{\gamma}{\bar{\rho}_o^* \bar{c}_o^{*2}} p^* \quad h = \frac{\gamma - 1}{\bar{c}_o^{*2}} h^* \quad w = \frac{w^*}{\bar{\rho}_o^* \bar{c}_o^*}$$

Using these definitions, the nondimensional conservation equations can be written as:

1. Continuity:

$$\frac{\partial \rho}{\partial t} + \frac{\partial \rho u}{\partial z} = \frac{\partial w}{\partial z} \tag{A.38}$$

2. Momentum:

$$\rho\left[\frac{\partial u}{\partial t} + u \frac{\partial \bar{u}}{\partial z}\right] + \frac{1}{\gamma} \frac{\partial p}{\partial z} = 0 \tag{A.39}$$

3. Energy

$$\frac{\partial p}{\partial t} + u \frac{\partial p}{\partial z} + \gamma p \frac{\partial u}{\partial z} - \gamma \frac{p}{\rho} \frac{\partial w}{\partial z} + \gamma [h_s - h_{\ell_{s_o}}] \frac{\partial w}{\partial \bar{z}} = 0 \qquad (A.40)$$

and the nondimensional equation of state is given by:

$$h_s = \frac{p}{\rho} + \frac{\gamma - 1}{2} u^2 \qquad (A.41)$$

The droplet heat balance equation is simply

$$h_{\ell_{s_o}} = \text{constant} \qquad (A.42)$$

Equations (A.38) through (A.42), together with an expression relating the mass generation to the gas dynamical flow variables, describe the unsteady flow field within the rocket combustor. It is interesting to note that in this problem formulation, the liquid phase appears only through the constant term representing the liquid phase stagnation enthalpy, and indirectly through the mass source term. It is a solution of this system of equations that is the objective of this investigation.

APPENDIX B

COMBINED 1L AND 2L LINEAR STABILITY LIMITS

In this appendix it is demonstrated that the linear behavior of longitudinal combustion instability oscillations can be determined by treating each mode independently. Linear stability limits are established by considering the 1L and 2L modes simultaneously, and the results are compared to the linear stability limits described in Chapter III. A linear velocity distribution is assumed.

For the first two modes, the linear portion of Equation (3.14) is given by the following equation:

$$A_\ell'' = -(\ell\pi)^2 A_\ell - \gamma \bar{u}_e A_\ell^{\#} + \gamma \bar{u}_e \hat{n}[A_\ell' - A_\ell'(t-\bar{\tau})] \qquad (B.1)$$

$$+ 2 \sum_{n=1}^{2} [(2n\pi I(n,\ell) - \frac{\gamma-1}{2}(-1)^{n+\ell})\bar{u}_e A_n'] \, , \ell = 1,2$$

where

$$I(n,\ell) = \int_0^1 z \sin(n\pi z)\cos(\ell\pi z)dz$$

For the case of $I(n,\ell) = \int_0^1 z \sin(n\pi z)\cos(\ell\pi z)dz$ y stable engine operating conditions, the time-dependent mode-amplitudes can be written as follows:

$$A_n(t) = K_n \exp[iwt] \qquad (B.2)$$

Equation (B.2) is substituted into Equation (B.1), and $I(n,\ell)$ is

evaluated. After some manipulations, the resulting equations can be written as:

$$\begin{bmatrix} (A_R^{(1)} + i\,A_i^{(1)}) & i\,A_i^{(2)} \\ i\,B_i^{(1)} & (B_R^{(2)} + i\,B_i^{(2)}) \end{bmatrix} \begin{bmatrix} K_1 \\ K_2 \end{bmatrix} = 0 \qquad (B.3)$$

where

$$A_R^{(1)} = \frac{\omega^2 - \kappa^2}{\omega \bar{u}_e} - \gamma \hat{n} \sin(\omega\bar{\tau})$$

$$A_i^{(1)} = \gamma\hat{n}(1 - \cos(\omega\bar{\tau})) - 2\gamma$$

$$A_i^{(2)} = \gamma + \frac{13}{3}$$

$$B_i^{(1)} = \gamma - \frac{7}{3}$$

$$B_R^{(2)} = \frac{\omega^2 - 4\kappa^2}{\omega \bar{u}_e} - \gamma \hat{n} \sin(\omega\bar{\tau})$$

$$B_i^{(2)} = \gamma\hat{n}(1 - \cos(\omega\bar{\tau})) - 2\gamma = A_i^{(1)}$$

For this system of equations to have a non-trivial solution, the determinant of the coefficient matrix must be identically zero. Evaluating the determinant and setting where the real and imaginary components equal to zero, results in the following set of equations.

$$A_R^{(1)} B_R^{(2)} - (A_i^{(1)})^2 + A_i^{(2)} B_i^{(1)} = 0 \qquad (B.4)$$

$$[A_R^{(1)} + B_R^{(2)}] A_i^{(1)} = 0 \qquad (B.5)$$

Assume for the moment that $A_i^{(1)} \neq 0$. In this case Equation (B.5) requires that $A_k^{(1)} = -B_k^{(2)}$, and consequently Equation (B.4) can be written as

$$-(B_R^{(2)})^2 - (A_i^{(1)})^2 + A_i^{(2)} B_i^{(1)} = 0$$

Since $A_i^{(2)} > 0$ and $B_i^{(1)} < 0$, and since all the terms are real, this equation cannot possibly be satisfied. Consequently the assumption that $A_i^{(1)} \neq 0$ must be incorrect. Therefore, Equation (B.5) requires that:

$$\hat{n} = \frac{2}{1 - \cos(\omega\bar{\tau})} \tag{B.6}$$

Equations (3.20) and (3.21), for $\bar{u} = \bar{u}_e z$, can be combined to yield exactly the same expression for n as that given by Equation (B.6).

Equation (B.4) becomes:

$$A_R^{(1)} B_R^{(2)} + A_i^{(2)} B_i^{(1)} = 0 \tag{B.7}$$

After substituting the appropriate expressions for $A_R^{(1)}$, $B_R^{(2)}$, $A_i^{(2)}$ and $B_i^{(1)}$ into Equation (B.7) and manipulating the resulting expression yields the following equation:

$$c_1 \tan^2(\frac{\omega\bar{\tau}}{2}) + c_2 \tan(\frac{\omega\bar{\tau}}{2}) + 4\gamma^2 = 0 \tag{B.8}$$

where

$$c_1 = \frac{(\omega^2 - \pi^2)(\omega^2 - 4\pi^2)}{(\omega\bar{u}_e)^2} + (\gamma + \tfrac{13}{3})(\gamma - \tfrac{7}{3})$$

and

$$c_2 = -\frac{2\gamma}{\omega \bar{u}_e}\left[2\omega^2 - 5\pi^2\right]$$

Solving Equation (B.8) gives:

$$\tan\left[\frac{\omega\bar{\tau}}{2}\right] = \frac{-c_2 \pm \sqrt{c_2^2 - 4(4\gamma)^2 c_1}}{2c_1} \qquad (B.9)$$

Equations (B.6) and (B.9) must be solved for $\hat{n}$ and $\bar{\tau}$. This is accomplished by specifying values of ω near the fundamental mode frequency, (i.e., $\omega \triangleq \pi$) solving Equation (B.9) for $\bar{\tau}$, and then solving Equation (B.6) for $\hat{n}$. The process is repeated for values of ω near the second mode frequency (i.e., $\omega \triangleq 2\pi$) solving Equation (B.9) for $\bar{\tau}$, and then solving Equation (B.6) for $\hat{n}$. The process is repeated for values of ω near the second mode frequency (i.e., $\omega \triangleq 2\pi$). Because of the two roots in Equation (B.9), there are two possible sets of $\bar{\tau}$ and n for each set of ω's (neglecting, of course, the secondary zones of instability). For one root, n is of the order of 10^2, while in the other case n is of O(1). The latter case is of practical interest. For $\omega \triangleq \pi$, the solution of interest corresponds to the negative root, while for $\omega \triangleq 2\pi$, the solution of interest corresponds to the positive root.

The linear stability limits found from the solution of Equations (B.6) and (B.7) are compared to the linear stability limits predicted by the independent analysis of each mode (i.e., Equations (3.20) and (3.21)) in Figure B.1. Based on these results, it is concluded that the linear stability of the system can be determined by considering the behavior of each mode independently. The resulting mathematical simplification of the analysis is important when the linear stability limits are established using a set of conservation equations.

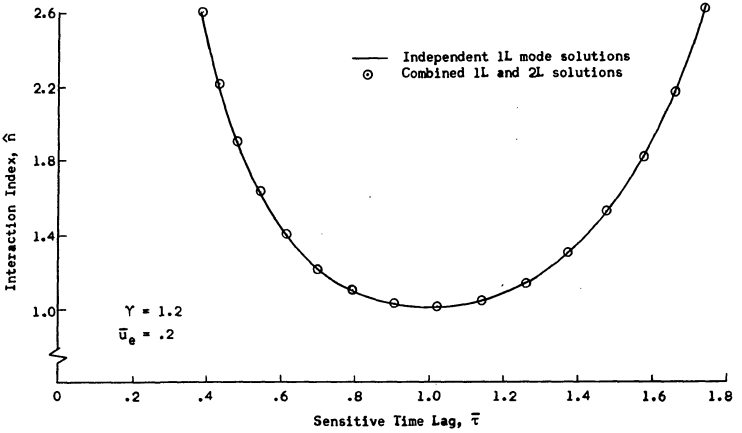

Figure B-1. A Comparison of Linear Stability Limits.

APPENDIX C

PROGRAM LINSTB: COMPUTES THE AXIAL MODE
LINEAR STABILITY LIMITS

Statement of the Problem

Program LINSTB is used to compute the axial mode linear stability limits. The loci of points of neutrally stable engine operating conditions, on the $\hat{n}$-$\bar{\tau}$ stability plane, are found by solving Eqs. (3.15) and (3.16). The mean flow Mach number is assumed to vary linearly from zero at the injector face to $\bar{u}(z) = \bar{u}_e$ at $z = z_c$, and to remain constant at $\bar{u} = \bar{u}_e$ from $z = z_c$ to the nozzle entrance. The exit Mach number, $\bar{u}_e$, is assumed to be small. Under these conditions, Eqs. (3.15) and (3.16) can be written as follows:

$$\tan\left(\frac{\omega\bar{\tau}}{2}\right) = \frac{2\omega\bar{u}_e}{\omega^2-(\ell\pi)^2}\left\{\frac{\gamma-1}{2} + \frac{\gamma}{z_c} I_1 - \frac{2(\ell\pi)}{z_c}\left[I_2^{(1)} + z_c I_2^{(2)}\right]\right\} \qquad (C.1)$$

$$\hat{n} = \frac{\omega^2-(\ell\pi)^2}{\frac{2\gamma\omega\bar{u}_e}{z_c} I_1 \sin(\omega\bar{\tau})} \qquad (C.2)$$

The critical value of the interaction index is given by the following equation:

$$\hat{n}_{min} = \frac{1}{2\gamma I_1}\left[\frac{\gamma-1}{2} z_c + \gamma I_1 - 2(\ell\pi) I_2\right] \tag{C.3}$$

In writing Eqs. (C.1) through (C.3), the following definitions have been made:

$$I_1 = \int_0^{z_c} \cos^2(\ell\pi z)\, dz = \frac{1}{2\ell\pi}\left[\ell\pi z_c + \sin(\ell\pi z_c)\cos(\ell\pi z_c)\right] \tag{C.4}$$

$$I_2^{(1)} = \int_0^{z_c} z \sin(\ell\pi z)\cos(\ell\pi z)\, dz \tag{C.5}$$

$$= \frac{1}{4(\ell\pi)^2}\left\{\sin(\ell\pi z_c)\left[\cos(\ell\pi z_c) + 2(\ell\pi z_c)\sin(\ell\pi z_c)\right] - \ell\pi z_c\right\}$$

$$I_2^{(2)} = \int_{z_c}^{1} \sin(\ell\pi z)\cos(\ell\pi z)\, dz = -\frac{1}{2\ell\pi}\sin^2(\ell\pi z_c) \tag{C.6}$$

and

$$I_2 = I_2^{(1)} + z_c I_2^{(2)} \tag{C.7}$$

The values of $\hat{n}$ and $\bar{\tau}$ corresponding to neutrallly stable engine operation are determined by performing the following calculations:

1. $\bar{u}_e$, γ, and z_c are specified.

2. Eqs. (C.4) through (C.7) are used to evaluate I_1, $I_2^{(1)}$, $I_2^{(2)}$, and I_2.
3. For specified values of ω, Eq. (C.1) is solved for $\bar{\tau}$, and then $\hat{n}$ is computed from Eq. (C.2).

The ω's for which $\hat{n}$ and $\bar{\tau}$ are to be found are specified in the following manner. Noting that ω_ℓ is within a few percent of $(\ell\pi)$, where ℓ is the axial mode number, a $\Delta\omega$ and a $(\Delta\omega)_i$ are specified. Computations are performed for values of $(\ell\pi-\Delta\omega) \leq \omega \leq (\ell\pi+\Delta\omega)$ in increments of $(\Delta\omega)_i$. That is, calculations are made at $\omega = \ell\pi - \Delta\omega$, $\omega = \ell\pi - \Delta\omega + \Delta\omega_i$, $\omega = \ell\pi - \omega + 2\Delta\omega_i$, and so on until $\omega = \ell\pi + \Delta\omega$.

Input and Output

The following input data are required:

Card 1

Column*	Term	Type	Format	Comments
1-10	NEQ	Integer	I10	the number of modes for which stability limits are sought.
11-20	NZ	Integer	I10	the number of different combustion distributions (i.e., no. of ZC).
21-30	KSTOP	Integer	I10	the maximum number of points to be computed for each mode. KSTOP is a safely cut-off number.
31-40	GAMMA	Floating	F10.0	specific heat ratio.
41-50	UE	Floating	F10.0	exit Mach number.
51-60	DELTA 1	Floating	F10.0	$\Delta\omega$, the frequency band.

*For integer data, indicates the column in which the data is right justified.

Column	Term	Type	Format	Comments
61-70	DELTA 2	Floating	F10.0	$(\Delta\omega)_i$, the incremental frequency.

Card 2

Column	Term	Type	Format	Comments
1-10	ZC	Floating	F10.0	axial location at which combustion is completed, ZC ≤ 1. There are NZ number of cards of this type in the data set.

The output symbols are defined as follows:

Term	Description
UBAR	$\bar{u}(z)$, the steady state Mach number distribution
UE	$\bar{u}_e$, the steady state combustor exit Mach number
Z	z, axial location
ZC	z_c, axial location at which combustion is completed
GAMMA	γ, the specific heat ratio
L	axial mode number
OMEGA	ω, frequency
N	$\hat{n}$, interaction index
TAU	$\bar{\tau}$, sensitive time lag
NMIN	$\hat{n}_{min}$, critical value of the interaction index

A sample input data set and a sample program output are presented in Tables C.1 and C.2, respectively.

Recommendations on Program Usage

The execution of this program requires very little computation time. Good results have been obtained using values of DELTA 1 = .3 and DELTA 2 = .02. In this case, approximately .4 seconds, not

including program collection time (about 1 second), are required on the U-1108 computer to compute the linear stability limits of a particular engine.

TABLE C-1. Sample Input For Program LINSTB

COLUMN							
1-10	11-20	21-30	31-40	41-50	51-60	61-70	71-80
2	2	40	1.2	.2	.30	.02	
1.0							
.75							

TABLE C-2. Sample Output From Program LINSTB

LINEAR STABILITY LIMITS

UBAR = UE*Z/ZC FOR Z LESS THAN OR EQUAL TO ZC
UBAR = UE FOR Z GREATER THAN ZC

L= 1 GAMMA= 1.20000 UE= .20000 ZC= 1.00000

OMEGA	N	TAU
.29216+01	.19047+01	.15958+01
.29416+01	.17425+01	.15516+01
.29616+01	.15972+01	.15051+01
.29816+01	.14686+01	.14563+01
.30016+01	.13563+01	.14052+01
.30216+01	.12600+01	.13518+01
.30416+01	.11794+01	.12963+01
.30616+01	.11140+01	.12389+01
.30816+01	.10637+01	.11799+01
.31016+01	.10282+01	.11201+01
.31216+01	.10070+01	.10598+01
.31616+01	.10069+01	.94125+00
.31816+01	.10274+01	.88425+00
.32016+01	.10613+01	.82960+00
.32216+01	.11084+01	.77774+00
.32416+01	.11683+01	.72896+00
.32616+01	.12409+01	.68343+00
.32816+01	.13259+01	.64119+00
.33016+01	.14232+01	.60217+00
.33216+01	.15324+01	.56625+00
.33416+01	.16535+01	.53325+00
.33616+01	.17862+01	.50297+00
.33816+01	.19303+01	.47520+00

CRITICAL INTERACTION INDEX IS NMIN = .100000+01

FORTRAN Listing of Program LINSTB

```
C
C         THIS PROGRAM CALCULATES THE LINEAR STABILITY LIMITS
C
C    NOTATION
C         NEQ = NO. OF MODES FOR WHICH STABILITY LIMITS ARE TO BE FOUND
C         NZ = NO. OF DIFFERENT COMBUSTION DISTRIBUTIONS
C         KSTOP = MAXIMUM NO. OF POINTS AT WHICH STABILITY LIMITS
C                 ARE TO BE FOUND
C         GAMMA = SPECIFIC HEAT RATIO
C         UE = EXIT MACH NUMBER
C         DELTA1 = MAXIMUM FREQUENCY DELTA FROM RESONANT FREQUENCY
C         DELTA2 = INCREMENTAL FREQUENCY
C         L = MODE NUMBER
C         OMEGA = FREQUENCY
C         N = ANB = INTERACTION INDEX
C         TAU = SENSITIVE TIME LAG
C         NMIN = CRITICAL VALUE OF THE INTERACTION INDEX
C
  400 FORMAT (3I10,5F10.0)
  410 FORMAT (2F10.0)
  401 FORMAT (10X,3E15.5)
  402 FORMAT ( /,10X,3HL= ,I3,5X,7HGAMMA= ,F8.5 ,5X,4HUE= ,F8.5,
     15X,4HZC= ,F8.5,/)
  403 FORMAT (1H1,/ ,10X,'LINEAR STABILITY LIMITS',/)
  404 FORMAT (/,10X,'       OMEGA                N              TAU',/)
  405 FORMAT (10X,'UBAR = UE*Z/ZC  FOR Z LESS THAN OR EQUAL TO ZC',/,
     1        10X,'UBAR = UE       FOR Z GREATER THAN ZC',/)
  420 FORMAT (/,10X,'CRITICAL INTERACTION INDEX IS NMIN =',E12.6)
C
      READ (5,400) NEQ,NZ,KSTOP,GAMMA,UE   ,DELTA1,DELTA2
C
      T =    .5*UE*(GAMMA-1.)
      DO 300 KZ =1,NZ
      READ (5,410) ZC
      DO 100 L=1,NEQ
      KOUNT = 1
      WRITE (6,403)
      WRITE (6,405)
      WRITE (6,402) L,GAMMA,UE,ZC
      WRITE (6,404)
      PIL = 3.1415927*L
      PIL2 = PIL*PIL
      A = PIL*ZC
      CF = UE/ZC
      S = SIN(A)
      C = COS(A)
      R1 = .5*(A + S*C) /PIL
      R2T1 = (S*(C + 2.*A*S) - A)*.25/PIL2
      R2T2 = -.5*S*S/PIL
      R2 = R2T1 + ZC*R2T2
      X = T/CF + GAMMA*R1 - 2.*PIL*R2
      ANMIN = .5*X/(GAMMA*R1)
      OMEGA = 3.1415927*L - DELTA1
      TEST = PIL + DELTA1
  120 CONTINUE
```

```
      T1 = 2.*OMEGA*(T + GAMMA*CF*R1 - 2.*PIL*R2*CF)
      T2 = OMEGA*OMEGA - PIL2
      IF (ABS(T2).LE.0.00001) GO TO 110
      AT = ATAN( ABS(T1)/ABS(T2))
      IF (T1.GT.0.0.AND.T2.GT.0.0)  AT = AT
      IF (T1.GT.0.0.AND.T2.LT.0.0)  AT = 3.14159-AT
      IF (T1.LT.0.0.AND.T2.LT.0.0)  AT = 3.14159 + AT
      IF (T1.LT.0.0.AND.T2.GT.0.0)  AT = 6.28318 - AT
      TAU = 2.*AT/OMEGA
      S = SIN(OMEGA*TAU)
      IF (ABS(S).LE.0.00001) GO TO 110
      ANB = T2/(2.*GAMMA*OMEGA*S*R1*CF)
      WRITE (6,401) OMEGA,ANB,TAU
  110 CONTINUE
      IF (OMEGA.GE.TEST) GO TO 200
      IF (KOUNT.GE.KSTOP) GO TO 200
      OMEGA = OMEGA + DELTA2
      KOUNT = KOUNT + 1
      GO TO 120
  200 CONTINUE
      WRITE (6,420) ANMIN
  100 CONTINUE
  300 CONTINUE
      STOP
      END
```

APPENDIX D

PROGRAM SPAINT: EVALUATES THE SPACE INTEGRALS RESULTING FROM THE APPLICATION OF THE GALERKIN METHOD

Statement of the Problem

Program SPAINT uses a Simpson's rule integration algorithm to evaluate the space integrals resulting from the application of the Galerkin method. A linear ramp Mach number distribution, $\bar{u}(z) = \bar{u}_e \times z$, is used. The computed integrals are stored in a data file which is used as input data in Program WAVES. The program user must specify the step size to be used in the numerical integration, and the number of terms retained in the series expansion(s) of the dependent variable(s).

The space integrals to be evaluated are given in Eqs. (4.56) through (4.60). The following definitions are made for the purpose of computer storage assignment:

Array	Integral	Index (K)	
T2(1,N,L)	$= \int_0^1 z \sin(n\pi z)\cos(\ell\pi z)\,dz$	0	(D.1)
T3(1,N,M,L)	$= \int_0^1 \sin(n\pi z)\sin(m\pi z)\cos(\ell\pi z)\,dz$	1	(D.2)
T3(2,N,M,L)	$= \int_0^1 \cos(n\pi z)\cos(m\pi z)\cos(\ell\pi z)\,dz$	2	(D.3)

Array	Integral	Index (K)	
T3(3,N,M,L)	$= \int_0^1 z \cos(n\pi z) \sin(m\pi z) \cos(\ell\pi z)\, dz$	3	(D.4)
T3(4,N,M,L)	$= \int_0^1 z \sin(n\pi z) \sin(m\pi z) \sin(\ell\pi z)\, dz$	4	(D.5)

The array indices N, M, and L vary from one to NEQ, where NEQ is the number of terms retained in the series expansion(s) of the dependent variable(s). As coded in this report, NEQ $\leq$ 10. It is recommended that a value of NEQ = 10 be used regardless of the number of terms in the series. The reason for this choice is discussed in the section of this appendix entitled "Recommendations on Program Usage".

A standard Simpson's rule numerical integration algorithm (see, for example, Conte[18]) is used to evaluate the integrals. In this procedure, the interval [0,1] is divided into 2N subintervals of length h and the integral is evaluated using the following equation:

$$\int_0^1 f(z)\, dz = \frac{h}{3}\left[f_0 + 4f_1 + 2f_2 + 4f_3 + \ldots + 4f_{2N-1} + f_{2N}\right]$$

The error involved in this numerical integration scheme is of the order of h^4. The user specifies h, and h must be such that the interval [0,1] is divided into an even number of subintervals.

Input and Output

The required input data consist of the number of terms in the series expansion(s) of the dependent variable(s), NEQ, and the integration step size, HI. The input data is read into the computer from two data cards:

Card 1: NEQ, integer, is right justified in columns 1-10 (Format I10) and NEQ ≤ 10

Card 2: HI, floating point number, in columns 1-10 (Format F10.0)

The computed integrals are stored in an assigned data file (see the section on the Deck set-up) and are printed in a straightforward output format. The notation used in the printed output is self-explanatory: L, N, and M are array indices (M = 0 for integral (D,1)) and K is the index which defines the integrand (e.g., K = 0 for integral (D.1), etc.).

A typical set of input data and a portion of the printed output are respectively shown in Tables D-1 and D-2.

Deck Set-up

The deck set-up described herein is for the Univac 1108 Exec 8 system used at Georgia Tech. The manner in which data files are assigned might be different at other computer facilities. The important thing to note is that the data file number (I/O unit) assigned to the output data of this program is used as the input data file number in program WAVES. This program uses I/O unit 2 to store the data file.

Deck Set-up:

1. Run Card (I.D. Card)

TABLE D-1. Sample Input For Program SPAINT

COLUMN		
1-10	11-20	
10		
.02		

TABLE D-2. Sample Output From Program SPAINT

SPACE INTEGRALS STEP SIZE = .020 L = 1

OUTPUT FORMAT INTEGRAL FROM 0 TO 1 OF F(X)

K=0 IS F(X) = X*SIN(M*PI*X)*COS(L*PI*X)
K=1 IS F(X) = SIN(M*PI*X)*SIN(M*PI*X)*COS(L*PI*X)
K=2 IS F(X) = COS(M*PI*X)*COS(M*PI*X)*COS(L*PI*X)
K=3 IS F(X) = X*COS(M*PI*X)*SIN(M*PI*X)*COS(L*PI*X)
K=4 IS F(X) = X*SIN(M*PI*X)*SIN(M*PI*X)*SIN(L*PI*X)

K	N= M	1	2	3	4	5	6	7	8	9	10
0	0	-.7958-01	.2122+00	-.1194+00	.4488-01	-.6632-01	.5457-01	-.4643-01	.4044-01	-.3583-01	.3218-01
1	1	-.2196-07	.2500+00	-.1317-07	-.9289-10	.7199-09	-.8316-09	-.1478-08	-.4532-08	.6824-09	.3639-08
1	2	.2500+00	-.3278-07	.2500+00	-.8438-08	-.1608-09	-.1994-09	-.3811-08	.6109-08	.3478-08	-.2187-08
1	3	-.1317-07	.2500+00	-.3504-07	.2500+00	-.1333-07	.1317-08	.3451-08	-.6779-08	-.6782-08	.7750-08
1	4	-.9289-10	-.8438-08	.2500+00	-.2993-07	.2500+00	-.8669-08	-.8070-08	.3699-08	.3429-08	-.5864-08
1	5	.7199-09	-.1608-09	-.1333-07	.2500+00	-.3095-07	.2500+00	.3922-08	-.1686-08	-.1145-08	-.2232-08
1	6	-.8316-09	-.1994-09	.1317-08	-.8669-08	.2500+00	-.3208-07	.2500+00	-.1153-07	-.2927-08	-.1245-08
1	7	-.1478-08	-.3811-08	.3451-08	-.8070-08	.3922-08	.2500+00	-.3030-07	.2500+00	-.1406-07	.1227-07
1	8	-.4532-08	.6109-08	-.6779-08	.3699-08	-.1686-08	-.1153-07	.2500+00	-.3462-07	.2500+00	-.1918-07
1	9	.6824-09	.3478-08	-.6782-08	.3429-08	-.1145-08	-.2927-08	-.1406-07	.2500+00	-.3974-07	.2500+00
1	10	.3639-08	-.2187-08	.7750-08	-.5864-08	-.2232-08	-.1245-08	.1227-07	-.1918-07	.2500+00	-.3338-07
2	1	.9191-06	.2500+00	.9509-06	-.9668-06	.9592-06	-.9656-06	.9672-06	-.9588-06	.9652-06	-.9636-06
2	2	.2500+00	.9362-06	.2500+00	.9505-06	-.9596-06	.9620-06	-.9692-06	.9561-06	-.9644-06	.9644-06
2	3	.9509-06	.2500+00	.9326-06	.2500+00	.9509-06	-.9628-06	.9724-06	-.9694-06	.9632-06	-.9672-06
2	4	-.9668-06	.9505-06	.2500+00	.9294-06	.2500+00	.9481-06	-.9700-06	.9608-06	-.9604-06	.9620-06
2	5	.9592-06	-.9596-06	.9509-06	.2500+00	.9330-06	.2500+00	.9700-06	-.9688-06	.9644-05	-.9632-06
2	6	-.9656-06	.9620-06	-.9628-06	.9481-06	.2500+00	.9286-06	.2500+00	.9545-06	-.9692-06	.9604-06
2	7	.9672-06	-.9692-06	.9724-06	-.9700-06	.9700-06	.2500+00	.9322-06	.2500+00	.9517-06	-.9523-06
2	8	-.9588-06	.9561-06	-.9604-06	.9608-06	-.9688-06	.9545-06	.2500+00	.9362-06	.2500+00	.9553-06
2	9	.9652-06	-.9644-06	.9632-06	-.9604-06	.9644-06	-.9692-06	.9517-06	.2500+00	.9441-06	.2500+00
2	10	-.9636-06	.9644-06	-.9672-06	.9620-06	-.9632-06	.9604-06	-.9523-06	.9553-06	.2500+00	.9386-06
3	1	.1061+00	-.1989-01	-.6366-01	.2652-01	-.1516-01	.9944-02	-.7069-02	.5299-02	-.4127-02	.3307-02
3	2	-.9947-01	.4244-01	.6630-02	-.7882-01	.3647-01	-.2222-01	.1524-01	-.1120-01	.8606-02	-.6836-02
3	3	.1495+00	-.7295-01	.2729-01	.1657-01	-.8589-01	.4177-01	-.2635-01	.1845-01	-.1391-01	.1087-01
3	4	-.9234+01	.1334+00	-.6300-01	.2022-01	.2167-01	-.9901-01	.4507-01	-.2906-01	.2081-01	-.1582-01
3	5	.6973-01	-.8290-01	.1263+00	-.5770-01	.1609-01	.2518-01	-.9272-01	.4733-01	-.3097-01	.2245-01
3	6	-.5537-01	.6266-01	-.7760-01	.1222+00	-.5441-01	.1338-01	.2741-01	-.9943-01	.4897-01	-.3239-01
3	7	.4750-01	-.5108-01	.5853-01	-.7429-01	.1195+00	-.5214-01	.1147-01	.2908-01	-.9605-01	.5021-01
3	8	-.4113-01	.4338-01	-.4777-01	.5582-01	-.7203-01	.1176+00	-.5050-01	.1005-01	.3032-01	-.9714-01
3	9	.3631-01	-.3782-01	.4067-01	-.4551-01	.5391-01	-.7039-01	.1162+00	-.4926-01	.8965-02	.3127-01
3	10	-.3253-01	.3360-01	-.3556+01	.3876-01	-.4387-01	.5249-01	-.6916-01	.1151+00	-.4830-01	.8114-02
4	1	.2122+00	-.5968-01	-.4244-01	.1326-01	-.6064-02	.3317-02	-.2022-02	.1328-02	-.9203-03	.6651-03
4	2	-.5968-01	.1698+00	-.4642-01	-.4851-01	.1658-01	-.8086-02	.4645-02	-.2943-02	.1993-02	-.1417-02
4	3	.4244-01	-.4642-01	.1637+00	-.4310-01	-.5053-01	.1791-01	-.9007-02	.5310-02	-.3439-02	.2374-02
4	4	.1326-01	-.4851-01	-.4310-01	.1617+00	-.4177-01	-.5145-01	.1857-01	-.9503-02	.5691-02	-.3739-02
4	5	-.6064-02	.1658-01	-.5053-01	-.4177-01	.1608+00	-.4111-01	-.5195-01	.1895-01	-.9803-02	.5931-02
4	6	.3317-02	-.8086-02	.1791-01	-.5145-01	-.4111-01	.1603+00	-.4073-01	-.5224-01	.1919-01	-.9999-02
4	7	-.2022-02	.4645-02	-.9007-02	.1857-01	-.5195-01	-.4073-01	.1600+00	-.4049-01	-.5244-01	.1936-01
4	8	.1328-02	-.2943-02	.5310-02	-.9503-02	.1895-01	-.5224-01	-.4049-01	.1598+00	-.4033-01	-.5258-01
4	9	-.9203-03	.1993-02	-.3439-02	.5691-02	-.9803-02	.1919-01	-.5244-01	-.4033-01	.1596+00	-.4021-01
4	10	.6651-03	-.1417-02	.2374-02	-.3739-02	.5931-02	-.9999-02	.1936-01	-.5258-01	-.4021-01	.1595+00

2. I/O unit assignment cards.
3. Main Program, MAIN. This program reads the input, calls subroutine SUMM, and outputs the computed integrals.
4. Subroutine SUMM. This program specifies the integrand function, f(x), and calls subroutine SIMPSN.
5. Subroutine SIMPSN. This program performs the Simpson rule integration of f(x). f(x) is defined in the External Real Function Subprogram FOFX.
6. Real Function Subprogram FOFX. This program defines the integrand function f(x) according to the integral index, K.
7. Input Data Cards.

Recommendations on Program Usage

Experience with this program has shown that an integration step size of HI = .02 produces good results. Although NEQ can be varied from 1 to 10, it is recommended that NEQ = 10 be used for the following reason: Using this approach, one data set can be used to compute nonlinear solutions (using program WAVES) for values of NEQ between one and ten. Program WAVES is set-up to use the output generated by program SPAINT in this manner. In summary, it is recommended that values of HI = .02 and NEQ = 10 be used. Approximately 60 seconds of computation time on a U-1108 are required in this case.

FORTRAN Listing of Program SPAINT

```
C
C       THIS PROGRAM EVALUATES THE INTEGRAL OF F(X) FROM 0 TO 1
C       USING SIMPSON RULE
C
C       THE MAIN PROGRAM READS THE INPUT, CALLS SUBROUTINE SUMM,
C       AND OUTPUTS THE COMPUTED INTEGRALS. THE INTEGRALS ARE
C       PRINTED AND STORED IN FILE 3 USING THE FASTRAN SYSTEM.
C       THE F(X) ARE DEFINED WITH THE PRINTED OUTPUT
C       THE SIMPSON RULE INTEGRATION IS PERFORMED IN
C       SUBROUTINE SUMM. THE F(X) ARE DEFINED IN THE EXTERNAL
C       FUNCTION SUBPROGRAM FOFX.
C
C       INPUT DATA
C         CARD 1  IN COL. 1-10 THE STEP SIZE, HI  (ABOUT .01 TO .02)
C         CARD 2  RIGHT JUSTIFIED IN COL. 1-10 THE NUMBER OF
C                 TERMS IN THE SERIES EXPANSION  NEQ< OR = 10
C
C       THE OUTPUT DATA IS DEFINED IN THE PRINTED OUTPUT
C
C       THE COMPUTATION TIME ON THE U-1108 IS ABOUT 60 SEC FOR
C       HI = .02  AND  NEQ = 10.
C
      COMMON/INTER/  T2(1,10,10),T3(4,10,10,10)
  400 FORMAT (8I10)
  402 FORMAT (10X,'OUTPUT FORMAT   INTEGRAL FROM 0 TO 1 OF F(X)',/ )
  403 FORMAT (10X,'K=0 IS F(X) = X*SIN(N*PI*X)*COS(L*PI*X)')
  405 FORMAT (10X,'K=1 IS F(X) = SIN(N*PI*X)*SIN(M*PI*X)*COS(L*PI*X)')
  406 FORMAT (10X,'K=2 IS F(X) = COS(N*PI*X)*COS(M*PI*X)*COS(L*PI*X)')
  407 FORMAT (10X,'K=3 IS F(X) = X*COS(N*PI*X)*SIN(M*PI*X)*COS(L*PI*X)')
  408 FORMAT (10X,'K=4 IS F(X) = X*SIN(N*PI*X)*SIN(M*PI*X)*SIN(L*PI*X)')
  410 FORMAT (BF10.0)
  430 FORMAT (1H1,   10X,'SPACE INTEGRALS    STEP SIZE = ',F5.3,
     1        4X,'L =',I2,/)
  440 FORMAT (2I5,10E10.4)
  450 FORMAT (/,8X,2HN=,   I5, 9I10, )
  460 FORMAT ('   K    M'/)
  800 FORMAT (5E15.8)
      READ (5,410) HI
      READ (5,400) NEQ
C        INTEGRATION OF SPACE INTEGRALS
      CALL SUMM (NEQ,     HI)
      DO 200 L=1,NEQ
      WRITE (6,430) HI,L
      WRITE (6,402)
      WRITE (6,403)
      WRITE (6,405)
      WRITE (6,406)
      WRITE (6,407)
      WRITE (6,408)
      WRITE (6,450) (I,I=1,NEQ)
      WRITE (6,460)
      M = 0
      K = 1
      J = 0
      WRITE (2,800)     (T2(K,N,L),N=1,NEQ)
```

```
      WRITE (6,440) J,M,(T2(K,N,L),N=1,NEQ)
      DO 220 K=1,4
      DO 230 M=1,NEQ
      WRITE (2,800)      (T3(K,N,M,L),N=1,NEQ)
  230 WRITE (6,440) K,M,(T3(K,N,M,L),N=1,NEQ)
  220 CONTINUE
  200 CONTINUE
      WRITE (2,800) HI
      STOP
      END



      SUBROUTINE SUMM (NEQ,     HI)
      COMMON/INTER/  T2(1,10,10),T3(4,10,10,10)
      NSM=1./HI + 1.01
      DO 100 K=1,5
      IF (K.GT.1) GO TO 1
      MSTP=1
      GO TO 3
    1 MSTP=NEQ
    3 DO 200 L=1,NEQ
      AL = L*3.14159
      DO 210 N=1,NEQ
      AN = N*3.14159
      DO 220 M=1,MSTP
      AM = M*3.14159
      CALL SIMPSN (K,AL,AM,AN,SUM,      NSM,HI)
      IF (K.GT.1) GO TO 4
      T2(K,N,L) = SUM
      GO TO 5
    4 KK = K-1
      T3(KK,N,M,L) = SUM
    5 CONTINUE
  220 CONTINUE
  210 CONTINUE
  200 CONTINUE
  100 CONTINUE
      RETURN
      END
```

```
      SUBROUTINE SIMPSN (K,AL,AM,AN,SUM,      NSM,HI)
      EXTERNAL FOFX
      X = 0.0
      SUM = 0.0
      DO 1 I=1,NSM
      C = 1.0
      IF (I.EQ.1) GO TO 2
      IF (I.EQ.NSM) GO TO 2
      C = 4.0
      ID = 2*(I/2) - I
      IF (ID.EQ.0) GO TO 2
      C = 2.0
    2 SUM = SUM + C*FOFX(K,X,AL,AM,AN)
    1 X = X+HI
      SUM = HI*SUM/3.0
      RETURN
      END
```

```
      REAL FUNCTION FOFX (K,X,AL,AM,AN)
      GO TO (1,2,3,4,5),K
    1 FOFX = X*SIN(AN*X)*COS(AL*X)
      GO TO 100
    2 FOFX = SIN(AN*X)*SIN(AM*X)*COS(AL*X)
      GO TO 100
    3 FOFX = COS(AN*X)*COS(AM*X)*COS(AL*X)
      GO TO 100
    4 FOFX = COS(AN*X)*SIN(AM*X)*COS(AL*X)*X
      GO TO 100
    5 FOFX = SIN(AN*X)*SIN(AM*X)*SIN(AL*X)*X
  100 CONTINUE
      RETURN
      END
```

APPENDIX E

PROGRAM WAVES: COMPUTES THE COMBUSTION INSTABILITY OSCILLATION WAVEFORMS

Statement of the Problem

Program WAVES computes the combustion instability oscillation waveforms for combustors having a linear steady state velocity distribution, $\bar{u}(z) = \bar{u}_e z$, for which $\bar{u}_e$ is small. Before this program can be used, the space integrals must be evaluated using program SPAINT. The computed integrals, together with the specification of the engine operating conditions (i.e., $\hat{n}$, $\bar{\tau}$, $\bar{u}_e$, γ, etc.), initial conditions, and certain program control numbers, make up the required input data for program WAVES.

Program WAVES performs the following functions:

1. For an initial peak pressure amplitude, initial values of the mode-amplitude functions are computed.
2. The time-dependent mode-amplitude functions are found by a Runge-Kutta-type numerical integration.
3. Perturbation pressures and velocities are computed.
4. A check for limit cycle conditions is made.
5. Printed and/or plotted output data is generated.

The program provides the user with various options. For instance, function (3) may be omitted if only the behavior of the mode-amplitude functions is desired. Similarly, function (4) is omitted when only the

transient behavior of the instabilities is required. The use of these and other user options are discussed in this appendix.

Three nonlinear solutions have been developed in this report: (1) a second order analysis using a nonlinear wave equation; (2) a second order analysis using a set of two conservation equations; and (3) a large amplitude analysis using a set of three conservation equations. Consequently, three computer programs are required. These programs have been written in a manner which permits a good deal of commonality. In particular, the required input data is the same for all programs. In order to achieve the commonality between the programs, the definitions shown in Table E.1 have been made.

The relations defining the behavior of the functions $A_n(t)$, $B_n(t)$, and $C_n(t)$ are listed in Table E.2.

Program WAVES consist of 11 elements: MAIN, START, POFX, TREND, FLOW, POUT2, POUT, RUNG, EQTN, PRMTRS, and WOUT1. The first seven elements are the same for the three nonlinear solutions. The last four elements are different for each nonlinear solution technique. The functions performed by these elements are discussed in the following paragraphs.

MAIN: Element MAIN serves the twofold functions of (1) reading the data required to compute the nonlinear waveforms, and (2) calling the required subroutines.

START and POFX: These two subroutines provide the initial values of the mode-amplitude functions required for the integration of the ordinary differential equations describing the behavior of the mode-

TABLE E.1. Definition of the Mode-Amplitude Functions Used in Program WAVES

Array	Parameter	Description
A(N)	$A_n(t)$	Specific volumn mode-amplitude function, used only in the large amplitude analysis.
B(N)	$B_n(t)$	Pressure mode-amplitude function. In the analysis using the nonlinear wave equation, $B_n(t)$ represents the time derivative of the velocity potential mode-amplitude function.
C(N)	$C_n(t)$	Acoustic-type velocity mode-amplitude function. In the nonlinear wave equation solutions, $C_n(t)$ represents the velocity potential mode-amplitude function.

TABLE E.2. Equations Governing the Mode-Amplitude Functions

Parameter	Equation Number		
	Wave Equation	2nd Order Equations	Large Amplitude
$A_n(t)$	—	—	4.53
$B_n(t)$	3.9	4.28	4.54
$C_n(t)$	3.9	4.29	4.55

amplitude functions. It is assumed that the combustor is operating in a steady manner until time $t = 0$, at which time a pressure disturbance is impulsively introduced inside the combustor. The perturbation velocity at $t = 0$ is zero. The user may specify a spacially continuous initial pressure disturbance in any axial mode, or a spacially discontinuous fundamental mode disturbance, with the discontinuity located at $z = .5$ at $t = 0$. The analytical expressions used to find the initial conditions, found by a Fourier analysis of the initial waveform, are given in the following equations:

(1) Spacially Continuous Pulse in the ℓth Axial Mode.

$$C_\ell(t = 0) = 0 \qquad \ell = 1,\ldots,N \tag{C.1}$$

$$B_\ell(t = 0) = \begin{cases} 0 & n \neq \ell \\ p_i & n = \ell \end{cases} \tag{C.2}$$

(2) Spacially Discontinuous Pulse.

$$C_\ell(t = 0) = 0 \qquad \ell = 1,\ldots,N \tag{C.3}$$

$$B_\ell(t = 0) = \frac{4p_i}{(\ell\pi)} \sin\left(\frac{\ell\pi}{2}\right) \tag{C.4}$$

where in both cases,

$$C_\ell(t) = B_\ell(t) = 0, \quad \text{for } -\bar{\tau} \leq t < 0, \quad \ell = 1,\ldots,N \tag{C.5}$$

An initial condition on $A_\ell(t)$ is required for the large amplitude analysis. Consideration of the linear behavior of the system shows that $\nu = -p/\gamma$; consequently the following relation is used for an initial condition on $A_\ell(t = 0)$:

$$A_\ell(t = 0) = -B_\ell(t = 0)/\gamma \tag{C.6}$$

In the solution using the nonlinear wave equation, Eqs. (C.2) and (C.4) merely approximate the spacial dependence of the initial impulse. Specifically, these equations are based on a linear representation of the initial disturbance, and the computed wave amplitude differs by a factor of γ from the specified p_i.

TREND: This subroutine determines whether or not limit cycle conditions have been reached. This task is accomplished by evaluating the summation $S = \sum_{n=1}^{NEQ} B_n(t)$ and examining the behavior of the summation. Note that S represents the behavior of the injector face pressure. Subroutine TREND performs the following functions:

1) Determines the maximum (positive) peak amplitude of one cycle of S.
2) Finds two successive average values of S for two cycles, $\bar{S}_1$ and $\bar{S}_2$, respectively.
3) Compares the absolute difference, $|\Delta\bar{S}|$, between the two successive averages with a user specified percentage, ϵ, of the latter value of the average S. If the $|\Delta\bar{S}| < \epsilon\bar{S}_2$ then limit cycle conditions have been reached.
4) Makes the appropriate change in the internal program control index

which tells the program that limit cycle conditions have been reached.

FLOW: Subroutine FLOW computes the summations used to find the perturbation flow field, outputs the computed pressure and velocity, and calls subroutine POUT2. The summations computed are:

$$SUMA = \sum_{n=1}^{NEQ} A_n(t)\cos(n\pi z)$$

$$SUMB = \sum_{n=1}^{NEQ} B_n(t)\cos(n\pi z)$$

$$SUMC = \sum_{n=1}^{NEQ} C_n(t)\sin(n\pi z)$$

$$SUMJ = \sum_{n=1}^{NEQ} (n\pi)C_n(t)\sin(n\pi z)$$

These summations are used in subroutine PRMTRS to calculate the perturbation flow field.

POUT2 and POUT: Subroutines POUT and POUT2 plot the temporal behavior of B(N) (the pressure mode-amplitude functions) and the temporal behavior of the pressure oscillations, respectively. The mode-amplitude functions to be plotted are specified by the user. The axial location(s) of the pressure plots are also user specified. The programs have been developed for use on a CALCOMP plotter.

RUNG: Subroutine RUNG is a modified Runge-Kutta numerical integration algorithm. The modification accounts for the presence of the retarded time variable. In this modification, the retarded variable is treated as a known quantity; that is, it is treated in the same manner as the independent variable. Two algorithms, based on the Runge-Kutta equations developed in reference (19), are used. One algorithm is used to integrate a set of second order O.D.E.'s; the other is used to integrate a set of first order O.D.E.'s. The required expressions are given in the following equations:

(1) First order O.D.E.'s; $y_\ell'^{(j)} = f_\ell^{(j)}\left[y_n, y_n(t-\bar{\tau})\right]$:

$$y_\ell^{(j+1)} = y_\ell^{(j)} + \frac{1}{6}\left\{K_{1_\ell} + K_{4_\ell} + 2\left[K_{2_\ell} + K_{3_\ell}\right]\right\}$$

where

$$K_{1_\ell} = hf_\ell^{(j)}\left[y_n, y_n(t-\bar{\tau})\right]$$

$$K_{2_\ell} = hf_\ell^{(j)}\left[\left(y_n + K_{1_n}/2\right), y_n\left(t-\bar{\tau}+h/2\right)\right]$$

$$K_{3_\ell} = hf_\ell^{(j)}\left[\left(y_n + K_{2_n}/2\right), y_n\left(t-\bar{\tau}+h/2\right)\right]$$

$$K_{4_\ell} = hf_\ell^{(j)}\left[\left(y_n + K_{3_n}\right), y_n\left(t-\bar{\tau}+h\right)\right]$$

and where

$$y_{\ell}^{(j)} = y_{\ell}(t)$$

$$y_{\ell}^{(j+1)} = y_{\ell}(t+h)$$

and $f_{\ell}^{(j)}$ is the function evaluated at t.

(2) Second order O.D.E.'s; $y_{\ell}'' = f_{\ell}\left[y_n, y_n', y_n'(t-\bar{\tau})\right]$

$$y_{\ell}'^{(j+1)} = y_{\ell}'^{(j)} + \frac{1}{6}\left\{K_{1_{\ell}} + K_{4_{\ell}} + 2\left[K_{2_{\ell}} + K_{3_{\ell}}\right]\right\}$$

$$y_{\ell}^{(j+1)} = y_{e}^{(j)} + h\left\{y_{\ell}'^{(j)} + \frac{1}{6}\left[K_{1_{\ell}} + K_{2_{\ell}} + K_{3_{\ell}}\right]\right\}$$

where

$$K_{1_{\ell}} = hf_{\ell}^{(j)}\left[y_n, y_n', y_n'(t-\bar{\tau})\right]$$

$$K_{2_{\ell}} = hf_{\ell}^{(j)}\left[\left(y_n + \frac{h}{2}y_n' + \frac{h}{8}K_{1_n}\right), \left(y_n' + \frac{1}{2}K_{1_n}\right), y_n'\left(t - \bar{\tau} + \frac{h}{2}\right)\right]$$

$$K_{3_{\ell}} = hf_{\ell}^{(j)}\left[\left(y_n + \frac{h}{2}y_n' + \frac{h}{8}K_{1_n}\right), \left(y_n' + \frac{1}{2}K_{2_n}\right), y_n'\left(t - \bar{\tau} + \frac{h}{2}\right)\right]$$

$$K_{4_\ell} = hf_\ell^{(j)}\left[\left(y_n + hy_n' + \frac{h}{2}K_{3_n}\right),\ \left(y_n' + K_{3_n}\right),\ y_n'\left(t - \bar{\tau} + h\right)\right]$$

and where

$$y_\ell^{(j)} = y_\ell(t) \quad ; \quad y_\ell'^{(j)} = y_\ell'(t)$$

$$y_\ell^{(j+1)} = y_\ell(t+h) \quad ; \quad y_\ell'^{(j+1)} = y_\ell'(t+h)$$

The equations defining the numerical integration of a set of first order O.D.E.'s is used in the solutions of the conservation equations. The second order O.D.E. equations are used to solve the nonlinear wave equation. The functional form of f_ℓ is defined in element EQTN.

In order to use the equations with the retarded variable, the integration step size, h, must be selected such that h divides the time lag, $\bar{\tau}$, into K equal increments. Thus $\bar{\tau} = Kh$, and the retarded variables become:

$$y_n(t - \bar{\tau}) = y_n(t - Kh)$$

$$y_n\left(t - \bar{\tau} + \frac{h}{2}\right) = y_n\left(t - Kh + \frac{h}{2}\right)$$

$$y_n(t - \bar{\tau} + h) = y_n(t - Kh + h)$$

It has been found that an integration step size of the order $h \simeq .05$ produces satisfactory results. The program selects the integration step size by forming the ratio $\bar{\tau}/.05$, rounding off the result to the nearest integer, and dividing $\bar{\tau}$ by the resulting integer, that is:

$$\text{integer} = (\bar{\tau}/.05) + .01$$

$$h = \bar{\tau}/\text{integer}.$$

The computation of h is performed in element MAIN.

EQTN: Subroutine EQTN defines the functions, f_ℓ, used in subroutine RUNG to evaluate the K terms. The particular equations defined in EQTN depend upon the problem under consideration (i.e., nonlinear wave equation, etc.). These functions are defined in Table C.2.

PRMTRS: Subroutine PRMTRS uses the summations, SUMA, SUMB, SUMC, and SUMU, computed in subroutine FLOW to calculate the perturbed flow field. The current program is coded to compute the perturbation pressure and velocity, using the following equations:

(1) Nonlinear wave equation solutions:

$$u'(z,t) = -\text{SUMU}$$

$$p'(z,t) = \frac{\gamma}{2}\left[\text{SUMB}(\text{SUMB}-2) + \text{SUMU}(2\bar{u}(z) - \text{SUMU})\right]$$

(2) Second order conservation equation solutions:

$$p'(z,t) = \text{SUMB}$$

$$u'(z,t) = \text{SUMC} + \frac{\gamma-1}{2\gamma}\,\bar{u}_e Z\ \text{SUMB}$$

(3) Large amplitude solutions:

$$p'(z,t) = \text{SUMB}$$

$$u'(z,t) = \text{SUMC} + \left[1 - \frac{\gamma+1}{4\gamma}\,\text{SUMB}\right]\frac{\gamma-1}{2\gamma}\,\bar{u}_e Z\ \text{SUMB}$$

WOUT1: This program writes the output of the mode-amplitude functions.

Input Data

The required input data consist of the integral values computed by program SPAINT, the engine operating conditions, and program control numbers. The data from program SPAINT is automatically read from data file 2. The remain data is read from user supplied data cards. These cards are described in this section.

Card 1 (Format 8I10)

Column[1]	Term	Data Type[2]	Information	Restrictions
10	NEQ	I	No. of terms in the series expansion of the dependent variables	≤ 10
20	NX	I	No. of axial locations at which flow field is to be computed	≤ 11
30	LIN	I	LIN = 1 to compute linear solutions LIN ≠ 1 nonlinear solutions	
40	IPLOT	I	IPLOT = 1 if any data is to be plotted IPLOT ≠ 1 no plots	
50	INPT	I	INPT = 1 to write the space integrals INPT ≠ 1 space integrals are not written	

Card 2 (Format 8I10)

Column	Term	Data Type	Information	Restrictions
10	LC1	I	LC1 = 1 to write the mode-amplitude functions LC1 ≠ 1 mode-amplitude functions are not written	
20	LC2	I	LC2 = 1 to plot pressure mode-amplitude functions LC2 = 4 no plot of mode-amplitudes	
30	LC4	I	Number of terms to be plotted	≤ 10
40	LC5	I	Incremental index between terms to be plotted	≤ 9

1. For integer data, indicates the column in which data is right justified.
2. I denotes integer data; F denotes floating point (decimal) data.

Card 3 (Format 8I10)

Column	Term	Data Type	Information	Restrictions
10	LP1	I	LP1 = 1 to calculate p' and u' LP1 ≠ 1 flow field is not calculated	
20	LP2	I	LP2 = 1 to write p' and u' LP2 ≠ 1 p' and u' are not written	
30	LP3	I	LP3 = 1 to plot p' vs t LP3 = 4 no flow field (p') plot	
40	LP4	I	Number of axial locations at which p' vs t is to plotted	≤4

Card 4 (Format 8I10)

Column	Term	Data Type	Information	Restrictions
10	NTAU	I	Number of $\bar{\tau}$ to be run	

Card 5 (Format 8F10.0)

Column	Term	Data Type	Information	Restrictions
1-10	UE	F	Exit Mach number	small, << 1
11-20	GAMMA	F	Specific heat ratio	
21-30	EPS	F	Limit cycle amplitude percent error	EPS = $\mathcal{O}(.01)$

Card 6 (Format 8F10.0)

Column	Term	Data Type	Information	Restrictions
1-10	TBEGIN	F	Normalized time at which output is begun, and at which flow field calculation is started	see discussion

Column	Term	Data Type	Information	Restrictions
11-20	TEND	F	Normalized time at which computations are terminated	see discussion
21-30	TLMCY	F	Normalized time at which limit cycle check is begun	see discussion
31-40	DELTAT	F	Normalized time increment for output of limit cycle conditions	see discussion
41-50	TSMP	F	Normalized time at which plot of pressure mode-amplitude is begun	
51-60	DELPT	F	Normalized time increment for plot of pressure mode-amplitude, B(N) vs t	see discussion

Discussion of Card 6:

(1) BEGIN must be greater than or equal zero. TEND must be such that the ratio (TBEGIN-TEND)/H is less than 300. This ratio can be estimated using a value of H = .05. Experience has shown that a time increment of TBEGIN-TEND ≐ 12. is sufficient to determine the behavior of the solutions.

(2) If a limit cycle check is not desired, then set TLYMCY > TEND.

(3) DELTAT must be such that DELTAT/H < 300. Usually, a DELTAT ≐ 6 is sufficient to verify that limit cycle conditions have been reached. In this case, approximately three fundamental mode cycles are computed.

(4) If a limit cycle check is made, and if limit cycle conditions are found, TSMP is automatically set equal to the initial time at

which limit cycle conditions are found, if LC2 = 1.

(5) DELPT must be such that DELPT/H < 100. Good results have been obtained using DELPT ≐ 3.9.

(6) If a limit cycle check is made, and limit cycle conditions are not found, the data output begins at TBEGIN and ends at TEND.

Card 7 (Format 8F10.0)

Column	Term	Data Type	Information	Restrictions
1-10	X(1)	F	Axial location at which p' and u' are computed	≤1
11-20	X(2)	F	Axial location at which p' and u' are computed	≤1
⋮	⋮	⋮	⋮	⋮
⋮	X(NX)	⋮	⋮	⋮

Discussion:

If NX > 8, then two cards are required to complete the input of X(I). In this case, X(9) is in columns 1-10 of card 7B, and so on.

Card 8 (Format 8I10)

This card is included in the data set only when LP3 = 1.

Column	Term	Data Type	Information	Restrictions
10	IPX(1)	I	Index of X(I) at which a p' vs t plot is made	≤10
20	IPX(2)	I	Index of X(I) at which a p' vs t plot is made	≤10
⋮				
40	IPX(LP4)	I	Index of X(I) at which a p' vs t plot is made	≤10

Discussion:

Plots can be made at any four (or fewer) axial locations at which p' is calculated.

Card 9 (8)[1] (F10.0, 2I10)

Column	Term	Data Type	Information	Restrictions
1-10	TAU	F	Sensitive time lag	
20	NNB	I	Number of $\hat{n}$ to be run at the specified $\bar{\tau}$	≤ 10
30	LCUT	I	Highest mode in which energy feedback is permitted	see discussion

Discussion:

This number is used to eliminate the secondary zones of instability. For fundamental mode investigations, LCUT = 2 is usually appropriate. For $\bar{\tau} > 1$, energy feedback is only permitted in the fundamental mode.

Card 10 (9) (8F10.0)

Column	Term	Data Type	Information	Restrictions
1-10	ANR(1)	F	First value of $\hat{n}$	
11-20	ANR(2)	F	Second $\hat{n}$	
⋮	⋮		⋮	
⋮	ANR(NNB)	F	Final value of $\hat{n}$	

Discussion:

If NNB > 8, then two cards are used to input the ANR(I).

1. Number in parenthesis is the card number if card 8 (IPX(I) card) is omitted.

Card 11 (10) (8I10)

Column	Term	Data Type	Information	Restrictions
10	NPI	I	Number of initial disturbances for each $\hat{n}$-$\bar{\tau}$ condition	

Card 12 (11) (F10.0, 8I10)

Column	Term	Data Type	Information	Restrictions
1-10	PI	F	Initial disturbance peak amplitude	
20	IPOP	I	If IPOP ≤ 10, then an initial disturbance in the IPOP mode is generated If IPOP = 11, then a spacially discontinuous fundamental mode wave, with the discontinuity at z = .5, is generated	

This completes the description of the input data cards. If NPI > 1, then card 12(11) is repeated NPI times. When NNB > 1, then cards 11(10) and 12(11) must be repeated NNB times. Similarly, when NTAU > 1, card 10(9) through 12(11) must be repeated NTAU times. An example input data set is shown in Table C.3.

Using the input data shown in Table E.3, program WAVES performs the following functions:

1. Nonlinear solutions are found at two axial locations using eight term expansion(s). The exit Mach number is $\bar{u}_e = 0.2$, and $\gamma = 1.2$.
2. The mode-amplitude functions are printed, and the first pressure mode-amplitude function is plotted.
3. The perturbation pressure and velocity are computed at z = 0.0 and

TABLE E-3. Sample Input Data For Program WAVES

COLUMN					
1-10	11-20	21-30	31-40	41-50	51-60
8	2	2	1	1	
1	1	1	1		
1	1	1	1		
2					
0.2	1.2	0.01			
30.0	42.0	5.0	6.0	30.0	3.9
0.0	0.25				
1					
1.30	2	2			
1.18	1.30				
2					
.025	1				
.05	1				
1					
.15	11				
1.0	1	2			
1.10					
1					
.1	11				

$z = 0.25$. The results are printed and the temporal dependence of the pressure oscillation is plotted at $z = 0.0$.

4. A limit cycle check is initiated at $t = 5.0$. If limit cycle conditions are reached prior to $t = 30.0$, the required data is output in a time interval of $\Delta t = 6.0$ after the establishment of limit cycle conditions. On the other hand, if a limit cycle is not reached by $t = 30.0$, the data is output in the time interval $30 \leq t \leq 42.0$. The pressure mode-amplitude function is plotted over at time interval of $\Delta t = 3.9$.

5. Solutions are to be calculated for two values of $\bar{\tau}$. At the first $\bar{\tau}$ ($\bar{\tau} = 1.30$), the computations are to be made for two $\hat{n}$ ($\hat{n} = 1.18$ and $\hat{n} = 1.30$). The computations at $\bar{\tau} = 1.30$, $\hat{n} = 1.18$ are to be made using two initial disturbances; a .025 and a .05 peak amplitude 1L pressure wave. The computations at $\bar{\tau} = 1.30$, $\hat{n} = 1.30$ are made for a discontinuous 1L pressure wave of peak amplitude equal to .15. At the second $\bar{\tau}$ ($\bar{\tau} = 1.0$), the computations are made for an $\hat{n} = 1.10$ and a discontinuous, .1 peak amplitude pressure wave.

6. In both cases, energy feedback is only permitted in the first two axial modes.

Output Data

The following data output options are available:

(1) INPT = 1 causes the space integrals used in the computations to be written.

(2) LC1 = 1 results in a tabulated output of the mode-amplitude

functions.

(3) LP2 = 1 results in the listing of p' and u' as functions of t at each axial location specified by X(I).

(4) LC2 = 1 causes plots of B(N) vs time to be made, with the N's specified by the user.

(5) LP3 = 1 causes plots of p' vs time to be made at the axial locations X(I) specified by the indices IPX(I).

The output limitations have been discussed in the data input section of this appendix. The output symbols are described in Table E.4. Portions of an example output is shown in Table E.5.

Deck Set-up

The data set described herein is for the Univac 1108 Exec. 8 system as used at Georgia Tech. The important points are:

1. Unit 2 must be assigned to the data file SPAINT.
2. Unit 3 must be assigned to the CALCOMP PLOT subroutines.

It is convenient to group the program elements in the sequence in which they are discussed in the first section of this appendix (i.e., page 153). The program is then adapted to the solution of a particular formulation of the problem (i.e., second order wave equation, etc.) by changing the last four subroutines.

TABLE E.4. Output Symbols

Symbol	
A	(1) potential mode-amplitude function, or (2) specific volume mode-amplitude function
AP	time derivative of the potential mode-amplitude
B	pressure mode-amplitude function
C	velocity mode-amplitude function
LINEAR	LINEAR = 1, solutions are linear LINEAR $\neq$ 1, solutions are nonlinear
L	axial mode number
M	axial mode number
N	(1) axial mode number, or (2) interaction index
NEQ	number of terms used in the solutions
P	normalized perturbation pressure
PINITIAL	peak amplitude of the initial disturbance
TAU	sensitive interaction index, $\bar{\tau}$
Z	axial station

TABLE E-5. Sample Output From Program WAVES:
Part of the Space Integrals Used in the Calculations

SPACE INTEGRALS STEP SIZE = .020 L = 1

OUTPUT FORMAT INTEGRAL FROM 0 TO 1 OF F(X)

K=0 IS F(X) = X*SIN(N*PI*X)*COS(L*PI*X)
K=1 IS F(X) = SIN(N*PI*X)*SIN(M*PI*X)*COS(L*PI*X)
K=2 IS F(X) = COS(N*PI*X)*COS(M*PI*X)*COS(L*PI*X)
K=3 IS F(X) = X*COS(N*PI*X)*SIN(M*PI*X)*COS(L*PI*X)
K=4 IS F(X) = X*SIN(N*PI*X)*SIN(M*PI*X)*SIN(L*PI*X)

K	N= M	1	2	3	4	5	6	7	8
0	0	-.7958-01	.2122+00	-.1194+00	.8888-01	-.6632-01	.5457-01	-.4643-01	.4044-01
1	1	-.2196-07	.2500+00	-.1317-07	-.9240-10	.7199-09	-.8316-09	-.1478-08	-.4532-08
1	2	.2500+00	-.3278-07	.2500+00	-.8438-08	-.1608-09	-.1994-09	-.3811-08	-.6109-08
1	3	-.1317-07	.2500+00	-.3504-07	.2500+00	-.1333-07	.1317-08	.3451-08	-.6779-08
1	4	-.9289-10	-.8438-08	.2500+00	-.2993-07	.2500+00	-.8669-08	-.8070-08	.3699-08
1	5	.7199-09	-.1608-09	-.1333-07	.2500+00	-.3095-07	.2500+00	.3952-08	-.1686-08
1	6	-.8316-09	-.1994-09	.1317-08	-.8669-08	.2500+00	-.3288-07	.2500+00	-.1153-07
1	7	-.1478-08	-.3811-08	.3451-08	-.8070-08	.3922-08	.2500+00	-.3030-07	.2500+00
1	8	-.4532-08	.6109-08	-.6779-08	.3699-08	-.1686-08	-.1153-07	.2500+00	-.3462-07
2	1	.9191-06	.2500+00	.9509-06	-.9660-06	.9592-06	-.9656-06	.9672-06	-.9588-06
2	2	.2500+00	.9362-06	.2500+00	.9505-06	-.9596-06	.9620-06	-.9692-06	.9561-06
2	3	.9509-06	.2500+00	.9326-06	.2500+00	.9509-06	-.9628-06	.9734-06	-.9604-06
2	4	-.9668-06	.9505-06	.2500+00	.9299-06	.2500+00	.9481-06	-.9720-06	.9608-06
2	5	.9592-06	-.9596-06	.9509-06	.2500+00	.9330-06	.2500+00	.9704-06	-.9688-06
2	6	-.9656-06	.9620-06	-.9628-06	.9481-06	.2500+00	.9286-06	.2500+00	.9545-06
2	7	.9672-06	-.9692-06	.9734-06	-.9720-06	.9708-06	.2500+00	.9332-06	.2500+00
2	8	-.9588-06	.9561-06	-.9604-06	.9608-06	-.9688-06	.9545-06	.2500+00	.9362-06
3	1	.1061+00	-.1989-01	-.6366-01	.2652-01	-.1516-01	.9994-02	-.7069-02	.5299-02
3	2	-.9947-01	.4294-01	-.6630-02	-.7882-01	.3647-01	-.2222-01	.1524-01	-.1120-01
3	3	.1485+00	-.7295-01	.2729-01	.1657-01	-.8989-01	.4177-01	-.2655-01	.1855-01
3	4	-.9284-01	.1334+00	-.4310-01	.1617+00	-.4177-01	.5195-01	.1857-01	-.2906-01
3	5	.6973-01	-.8290-01	.1263+00	-.5770-01	.1609-01	.2518-01	-.9272-01	.4733-01
3	6	-.5637-01	.6286-01	-.7760-01	.1222+00	-.5446-01	.1338-01	.2748-01	-.9463-01
3	7	.4750-01	-.5108-01	.5853-01	-.7429-01	.1195+00	-.5214-01	.1147-01	.2908-01
3	8	-.4113-01	.4338-01	-.4777-01	.5582-01	-.7203-01	.1176+00	-.5250-01	.1005-01
4	1	.2122+00	-.5968-01	-.4244-01	.1326-01	-.6064-02	.3317-02	-.2092-02	.1328-02
4	2	-.5968-01	.1695+00	-.9682-01	-.4851-01	.1658-01	-.8086-02	.4645-02	-.2943-02
4	3	-.4244-01	-.9682-01	.1637+00	-.4310-01	-.5053-01	.1791-01	-.9007-02	.5310-02
4	4	.1326-01	-.4851-01	-.4310-01	.1617+00	-.4177-01	-.5195-01	.1857-01	-.9503-02
4	5	-.6064-02	.1658-01	-.5053-01	-.4177-01	.1608+00	-.4111-01	-.5195-01	.1895-01
4	6	.3317-02	-.8086-02	.1791-01	-.5195-01	-.4111-01	.1603+00	-.4073-01	-.5224-01
4	7	-.2092-02	.4645-02	-.9007-02	.1857-01	-.5195-01	-.4073-01	.1600+00	-.4044-01
4	8	.1328-02	-.2943-02	.5310-02	-.9503-02	.1895-01	-.5224-01	-.4044-01	.1598+00

TABLE E-5 (cont.). Sample Output From Program WAVES: Initial Pressure Pulse

INITIAL PRESSURE DISTRIBUTION

Z	P
.00000	.09216
.10000	.10684
.20000	.09628
.30000	.09790
.40000	.11386
.50000	.00000
.60000	-.11386
.70000	-.09790
.80000	-.09628
.90000	-.10684
1.00000	-.09216
1.10000	-.10684

TABLE E-5 (cont.). Sample Output From Program WAVES: Part of the Mode-Amplitude Output

TIME DEPENDENT COEFFICENTS OF THE NONLINEAR WAVE EQUATION PHI = A(T)*COS(N*PI*Z)

LINEAR= 2 NEG= 8 N= 1.10000 TAU= 1.00000
EXIT MACH= .200 GAMMA =1.200 PINITIAL =.1000

TIME	A1	A2	A3	A4	A5	A6	A7	A8	A9	A10
TIME	AP1	AP2	AP3	AP4	AP5	AP6	AP7	AP8	AP9	AP10
-.000	.0000	.0000	.0000	.0000	.0000	.0000	.0000	.0000		
-.000	.1273+00	-.4685-06	-.4244-01	.4685-06	.2546-01	-.4685-06	-.1819-01	.4685-06		
.050	.6344-02	-.6014-04	-.2026-02	.7293-04	.1135-02	-.7628-04	-.7025-03	.2252-04		
.050	.1258+00	-.2797-02	-.3715-01	.2498-02	.1759-01	-.2265-02	-.7514-02	.4591-03		
.100	.1252-01	-.2486-03	-.3579-02	.2026-03	.1566-02	-.1221-03	-.6213-03	.7215-06		
.100	.1208+00	-.3786-02	-.2382-01	.2302-02	-.1244-02	.1102-02	.1013-01	-.1298-02		
.150	.1837-01	-.4508-03	-.4315-02	.2662-03	.1026-02	.4913-04	.8884-04	-.6046-04		
.150	.1124+00	-.4226-02	-.4982-02	-.5158-04	-.1915-01	.5260-02	.1561-01	-.6534-03		
.200	.2372-01	-.6562-03	-.4052-02	.1742-03	.1300-03	.2975-03	.6341-03	-.1770-04		
.200	.1011+00	-.3805-02	-.1533-01	-.3720-02	-.2457-01	.3592-02	.4439-02	.2285-02		
.250	.2843-01	-.8089-03	-.2844-02	-.9135-04	-.1159-02	.3110-03	.4624-03	.1084-03		
.250	.8693-01	-.2079-02	.3196-01	-.6517-02	-.1449-01	-.3353-02	-.1045-01	.2065-02		
.300	.3236-01	-.8415-03	-.9987-03	-.4117-03	-.1432-02	-.7751-06	-.1935-03	.1084-03		
.300	.6956-01	.9952-03	.4020-01	-.5562-02	.3955-02	-.8178-02	-.1347-01	-.2241-02		
.350	.3534-01	-.6938-03	.1004-02	-.5762-03	-.8198-03	-.3670-03	-.6043-03	-.7294-04		
.350	.4961-01	.4967-02	.3828-01	-.5672-03	.1912-01	-.5263-02	-.1806-02	-.4180-02		
.400	.3731-01	-.3579-03	.2683-02	-.4554-03	.2697-03	-.4309-03	-.3372-03	-.1905-03		
.400	.2088-01	.8170-02	.2771-01	.5166-02	.2221-01	.2927-02	.1141-01	.1090-03		
.450	.3924-01	.7984-04	.3681-02	-.1124-03	.1167-02	-.1182-03	.3250-03	-.4796-04		
.450	.8549-02	.8882-02	.1163-01	.7883-02	.1199-01	.8625-02	.1241-01	.4977-02		
.500	.3818-01	.4912-03	.3826-02	.2620-03	.1355-02	.2948-03	.6508-03	.1798-03		
.500	-.1049-01	.7307-02	-.5579-02	.6511-02	-.4656-02	.6702-02	-.4865-03	.3078-02		
.550	.3723-01	.7942-03	.3177-02	.4935-03	.7662-03	.4511-03	.2709-03	.1718-03		
.550	-.2703-01	.4702-02	-.1967-01	.2491-02	-.1762-01	-.8130-03	-.1348-01	-.3345-02		
.600	.3556-01	.9496-03	.1943-02	.4992-03	-.2253-03	.2310-03	-.4314-03	-.6971-04		
.600	-.4192-01	.1423-02	-.2802-01	-.2207-02	-.2022-01	-.7306-02	-.1254-01	-.5179-02		

TABLE E-5 (concluded). Sample Output From Program WAVES: Part of the Perturbation Flow Output

FLOW PRARAMETERS Z= .000

LINEAR= 2 NEG= 8 N= 1.10000 TAU= 1.00000
EXIT MACH= .200 GAMMA =1.200 PINITIAL =.1000

TIME	PRESSURE	VELOCITY
-.000	-.1055+00	.0000
.050	-.1104+00	.0000
.100	-.1154+00	.0000
.150	-.1185+00	.0000
.200	-.1082+00	.0000
.250	-.9654-01	.0000
.300	-.9807-01	.0000
.350	-.1142+00	.0000
.400	-.1213+00	.0000
.450	-.8656-01	.0000
.500	-.2861-02	.0000
.550	.9295-01	.0000
.600	.1479+00	.0000
.650	.1447+00	.0000
.700	.1144+00	.0000
.750	.9950-01	.0000
.800	.1125+00	.0000
.850	.1308+00	.0000
.900	.1309+00	.0000
.950	.1168+00	.0000
1.000	.1003+00	.0000
1.050	.1145+00	.0000
1.100	.1176+00	.0000
1.150	.1094+00	.0000
1.200	.9893-01	.0000
1.250	.9826-01	.0000
1.300	.1007+00	.0000
1.350	.9221-01	.0000
1.400	.7471-01	.0000
1.450	.5890-01	.0000
1.500	.3819-01	.0000
1.550	-.4975-02	.0000
1.600	-.6246-01	.0000
1.650	-.1002+00	.0000
1.700	-.1010+00	.0000
1.750	-.3786-01	.0000
1.800	-.9498-01	.0000
1.850	-.1201+00	.0000
1.900	-.1309+00	.0000
1.950	-.1133+00	.0000
2.000	-.9116-01	.0000
2.050	-.9565-01	.0000

FORTRAN Listing of Program WAVES

```
C
C    THE SPACE INTEGRALS ARE STORED IN THE ARRAYS T2 AND T3. PROVISION
C    IS MADE FOR ONE N BY N INTEGRAL, AND FOUR N BY N BY N INTEGRALS.
C    MORE INTEGRALS CAN BE TREATED BY CHANGING THE APPROPRIATE DIMENSION
C    STATEMENT.
C
C    THE MODE AMPLITUDES ARE STORED IN THE ARRAYS A, B, AND C. THE RETARDED
C    VARIABLE IS STORED IN ARRAY BS. THE RETARDED VARIABLES REQUIRED AT
C    THE INTEGRATION STEP IN QUESTION ARE STORED IN ARRAYS BR1, BR2, AND BR3.
C    THE TERMS STORED IN THESE ARRAYS DEPENDS ON THE PROBLEM FORMULATION.
C      1. FOR THE NONLINEAR WAVE EQUATION
C           A = BLANK
C           B = TIME DERIVATIVE OF MODE AMPLITUDE
C           C = MODE-AMPLITUDE FUNCTION
C      2. FOR THE SECOND ORDER CONSERVATION EQUATIONS
C           A = BLANK
C           B = PRESSURE MODE-AMPLITUDE
C           C = VELOCITY MODE-AMPLITUDE
C      3. FOR THE LARGE AMPLITUDE ANALYSIS
C           A = SPECIFIC VOLUME MODE-AMPLITUDE
C           B = PRESSURE MODE-AMPLITUDE
C           C = VELOCITY MODE-AMPLITUDE
C
      DIMENSION ANR(10),DATA(2500)
      COMMON/COMP1/ QP1,QP2,QP3,QP4,QP5,QP7
      COMMON/COM51/ Q1,Q2,GP1,GT1
      COMMON/FLODA/ NEQ,UE,ANB,TAU,GAMMA,PI,LIN,TN(10),IPOP
      COMMON/PLTDA/ TARY(100),BARY(10,100)
      COMMON/COM2/ B(10),C(10),BR1(10),BR2(10),BR3(10),BS(10,110),A(10)
      COMMON/COM3/ H,HD2,HD6,HD8
      COMMON/COM4/ T2(1,10,10),T3(4,10,10,10)
      COMMON/COM5/ X(11),IPX(4)
      COMMON/COM6/ TSTART,TSTOP,TLYMCY
  400 FORMAT (8I10)
  402 FORMAT (10X,'OUTPUT FORMAT   INTEGRAL FROM 0 TO 1 OF F(X)',/ )
  403 FORMAT (10X,'K=0 IS F(X) = X*SIN(N*PI*X)*COS(L*PI*X)')
  405 FORMAT (10X,'K=1 IS F(X) = SIN(N*PI*X)*SIN(M*PI*X)*COS(L*PI*X)')
  406 FORMAT (10X,'K=2 IS F(X) = COS(N*PI*X)*COS(M*PI*X)*COS(L*PI*X)')
  407 FORMAT (10X,'K=3 IS F(X) = X*COS(N*PI*X)*SIN(M*PI*X)*COS(L*PI*X)')
  408 FORMAT (10X,'K=4 IS F(X) = X*SIN(N*PI*X)*SIN(M*PI*X)*SIN(L*PI*X)')
  410 FORMAT (8F10.0)
  430 FORMAT (1H1,    10X,'SPACE INTEGRALS    STEP SIZE = ',F5.3,
     1          4X,'L =',I2,/)
  431 FORMAT (/,8X,2HN=,   I5, 9I10, )
  432 FORMAT ('   K    M'/)
  433 FORMAT (2I5,10E10.4)
  450 FORMAT (1H1,///,10X,'DIVERGENT SOLUTION',//)
  460 FORMAT (/,10X,5HTAU= ,F10.5,5X,6HNBAR= ,F10.5,5X,4HUE= ,F10.5,
     15X,7HGAMMA= ,F10.5,5X,10HPINITIAL= ,F10.5,
     2//,10X,6HTIME= ,F10.5,5X,6HB(N)= ,E10.4,5X,6HC(N)= ,E10.4)
  800 FORMAT (5E15.8)
  420 FORMAT (F10.0,2I10)
C
C    READ SPACE INTEGRALS FROM FILE 2
C
```

```
      DO 200 L=1,10
      K = 1
      READ (2,800) (T2(K,N,L),N=1,10)
      DO 210 K=1,4
      DO 220 M=1,10
  220 READ (2,800) (T3(K,N,M,L),N=1,10)
  210 CONTINUE
  200 CONTINUE
      READ (2,800) HI
C
C   READ INPUT DATA (EXCEPT COMB. PARAMETERS AND INITIAL DISTURBANCE
C
C   FIRST DATA CARD
C        NEQ = NO. OF TERMS IN EXPANSIONS
C        NX = NO. OF X/L AT WHICH FLOW FIELD CALCULATED
C        LIN = 1 TO CALCULATE LINEAR RESULTS
C        IPLOT = 1 TO PLOT ANY OUTPUT
C        INPT = 1 TO WRITE THE SPACE INTEGRALS READ FROM FILE 2
C   SECOND DATA CARD
C        LC1 = 1 TO WRITE C(N) AND B(N)
C        LC2 = 1 TO PLOT B(N)
C            = 4 NO PLOT OF B(N)
C        LC4 = NUMBER OF TERMS TO BE PLOTTED
C        LC5 = INCREMENTAL INDEX BETWEEN TERMS TO BE PLOTTED
C   THIRD DATA CARD
C        LP1 = 1 TO CALCULATE U AND P
C        LP2 = 1 TO WRITE U AND P
C        LP3 = 1 TO PLOT P
C            = 4 NO PLOT OF P
C        LP4 = NO. OF X/L AT WHICH P OR U TO BE PLOTTED
C   FORTH DATA CARD
C        NTAU = NO. OF TAU TO BE RUN
C   FIFTH DATA CARD
C        UE = EXIT MACH NUMBER
C        GAMMA = SPECIFIC HEAT RATIO
C        EPS = AMPLITUDE PRECENT ERROR
C   SIXTH DATA CARD
C        TBEGIN = TIME TO START COMPUTATION OF FLOW VARIABLES AND
C                 TO START OUTPUT
C        TEND = STOP TIME
C        TLMCY = START TIME OF LIMIT CYCLE CHECK
C        DELTAT TIME DELTA FOR OUTPUT OF LIMIT CYCLE OSCILLATIONS
C        TSMPI = START TIME FOR PRESSURE MODE-AMPLITUDE PLOT
C        DELPT = TIME DELTA FOR PLOT OF P MODE-AMPLITUDE
C   SEVENTH DATA CARD
C        X(I) = AXIAL LOCATION AT WHICH FLOW FIELD IS TO BE CALCULATED
C   EIGHTH DATA CARD (USED ONLY IF LP3#4)
C        IPX(I) = INDEX OF X(I) FOR WHICH PRESSURE IS TO BE PLOTTED
C
      READ (5,400) NEQ,NX,LIN,IPLOT,INPT
      READ (5,400) LC1,LC2,    LC4,LC5
      READ (5,400) LP1,LP2,LP3,LP4
      READ (5,400) NTAU
      READ (5,410) UE,GAMMA,EPS
      READ (5,410) TBEGIN,TEND,TLMCY,DELTAT,TSMPI,DELPT
      READ (5,410) (X(I),I=1,NX)
      IF (LP3.EQ.4) GO TO 100
```

```
      READ (5,400) (IPX(I),I=1,LP4)
  100 CONTINUE
C
C    WRITE SPACE INTEGRALS IF INPT = 1
C
      IF (INPT.NE.1) GO TO 110
      DO 700 L=1,NEQ
      WRITE (6,430) HI,L
      WRITE (6,402)
      WRITE (6,403)
      WRITE (6,405)
      WRITE (6,406)
      WRITE (6,407)
      WRITE (6,408)
      WRITE (6,431) (I,I=1,NEQ)
      WRITE (6,432)
      M = 0
      K = 1
      J = 0
      WRITE (6,433) J,M,(T2(K,N,L),N=1,NEQ)
      DO 710 K=1,4
      DO 720 M=1,NEQ
  720 WRITE (6,433) K,M,(T3(K,N,M,L),N=1,NEQ)
  710 CONTINUE
  700 CONTINUE
  110 CONTINUE
C   CALL PLOT SUBROUTINE IF IPLOT = 1
C
      IF (IPLOT.NE.1) GO TO 600
      CALL PLOTS (DATA(1),2500,3)
  600 CONTINUE
C
C    CALCULATION OF SOME TERMS USED IN SOLUTION OF ODES
C
      P2 = 3.14159*3.14159
      QP1=6.28318*UE
      QP2=(GAMMA-1.)*UE/2.
      QP3=(GAMMA-1.)*P2
      QP4=2.*P2
      QP5=GAMMA*UE
      QP7=P2
      Q1 = .5*(GAMMA-1.)*UE/GAMMA
      GP1 = GAMMA + 1.
      GT1 = GAMMA*.5*(GAMMA-1.)*UE
      Q2 = -Q1*.25*GP1/GAMMA
C
      DO 1000 KTAU =1,NTAU
C
C    READ COMBUSTION PARAMETERS
C
      READ (5,420) TAU,NNB,LCUT
      READ (5,410) (ANR(I),I=1,NNB)
C
      LTEMP = TAU/.05 + .01
      H = TAU/LTEMP
      HD2 = H/2.
      HD6 = H/6.
```

```
      HDB = H/8.
      LTR = (TAU/H) + 1.01
      DO 2000 KK=1,NNB
      READ (5,400) NPI
      ANB= ANR(KK)
      DO 510 LLL =1,NEQ
      TN(LLL) = ANB
      IF (LLL.GT.LCUT) TN(LLL) = 0.0
      IF (TAU.LT.1) GO TO 510
      IF (LLL.NE.1) TN(LLL) = 0.0
  510 CONTINUE
      DO 3000 KKK=1,NPI
      READ (5,420) PI,IPOP
      TSTART = TBEGIN
      TSTOP = TEND
      TSMP = TSMPI
      KMT = 0
      KMTS = DELPT/H + 1.01
      KPLT = 2
      K2 = 2
      LGO = 2
      LOUT = 1
C
      CALL START (LTR,TX,H)
C
      KONTRL = 2
      L = LTR
      TSTOP1 = TSTOP + .10
  340 IF (TX.GT.TSTOP1) GO TO 130
      IF (L.NE.101) GO TO 140
      LTMP = 102 - LTR
      DO 150 L=1,LTR
      DO 160 I=1,NEQ
  160 BS(I,L) = BS(I,LTMP)
  150 LTMP = LTMP + 1
      L = LTR
  140 CONTINUE
C
      TEST = ABS(TX - TLMCY)
      IF (TEST.LT.0.03) K2=1
      IF (K2.NE.1) GO TO 320
      IF (LGO.EQ.1) GO TO 320
      PHI0 = 0.0
      DO 900 I=1,NEQ
  900 PHI0 = PHI0 + B(I)
      CALL TREND (TEST,PHI0,LGO,EPS)
      IF (LGO.EQ.2) GO TO 370
      TSMP = TX
      TSTART = TX
      TSTOP = TX + DELTAT
      TSTOP1 = TSTOP + .10
  370 CONTINUE
  320 CONTINUE
C
      CHECK = ABS(TX-TSTART)
      IF (CHECK.LT.0.04) KONTRL = 1
      IF (KONTRL.NE.1) GO TO 330
```

```
      IF (LC1.NE.1) GO TO 500
      CALL WOUT1 (H,TX)
  500 IF (LC2.EQ.4) GO TO 501
      IF (KMT.GT.KMTS) GO TO 501
      CHK1 = ABS(TX-TSMP)
      IF (CHK1.LE.0.04) KPLT = 1
      IF (KPLT.NE.1) GO TO 501
      KMT = KMT + 1
      TARY(KMT) = TX
      DO 504 K=1,10
      BARY(K,KMT) = B(K)
  504 CONTINUE
      IF (KMT.NE.KMTS) GO TO 501
      CALL POUT  (LC4,LC5,KMT)
      KPLT = 2
  501 IF (LP1.NE.1) GO TO 502
      CALL FLOW (NX,H,TX,LP2,LP3,LP4,LP5,LOUT)
  502 CONTINUE
      IF (LOUT.EQ.2) GO TO 3000
  330 CONTINUE
      L = L+1
      TX = TX + H
      LD0 = L-LTR
      LD1 = LD0 + 1
      DO 180 I=1,NEQ
      BR1(I) = BS(I,LD0)
      BR3(I) = BS(I,LD1)
  180 BR2(I) = (BR1(I)+BR3(I))/2.
C
      CALL RUNG  (NEQ)
C
      DO 300 I=1,NEQ
      BS(I,L) = B(I)
      CHK1 = B(I)
      CHK2 = C(I)
      IF (CHK1.LT.10.0.AND.CHK2.LT.10.0) GO TO 300
      WRITE (6,450)
      WRITE (6,460) TAU,ANB,UE,GAMMA,PI,TX,CHK1,CHK2
      GO TO 130
  300 CONTINUE
      GO TO 340
  130 CONTINUE
 3000 CONTINUE
 2000 CONTINUE
 1000 CONTINUE
      STOP
      END
```

```
      SUBROUTINE START (LTR,TX,H)
      EXTERNAL POFX
      COMMON/FLODA/ NEQ,UE,ANB,TAU,GAMMA,PI,LIN,T(10),IPOP
      COMMON/COM2/ B(10),C(10),BR1(10),BR2(10),BR3(10),BS(10,110),A(10)
  400 FORMAT (1H1,///,10X,'INITIAL PRESSURE DISTRIBUTION',///)
  410 FORMAT (12X,'Z', 9X 'P',/)
  420 FORMAT (5X,4F10.5)
      TX = -TAU
      DO 1 N=1,NEQ
      A(N) = 0.0
      C(N) = 0.0
    1 B(N) = 0.0
      DO 100 L =1,LTR
      TX = TX + H
      DO 110 N=1,NEQ
  110 BS(N,L) = 0.0
  100 CONTINUE
      TX = TX - H
      DO 120 I=1,NEQ
      B(I) = POFX (I,PI,IPOP)
      C(I) = 0.0
      A(I) = -B(I)/GAMMA
  120 BS(I,LTR) = B(I)
      WRITE (6,400)
      WRITE (6,410)
      X = 0.0
  150 SUMB = 0.0
      DO 140 I=1,NEQ
      ARG = 3.14159*X*I
      C1= COS(ARG)
      SUMB = SUMB + B(I)*C1
  140 CONTINUE
      P = SUMB
      WRITE (6,420) X,P
      IF (X.GE.1.0) GO TO 200
      X = X + .1
      GO TO 150
  200 CONTINUE
      RETURN
      END



      REAL FUNCTION POFX (I,PI,IPOP)
      IF (IPOP.EQ.11) GO TO 1
C
C        CONTINUOUS WAVE IN IPOP MODE
      POFX = 0.0
      IF (IPOP.EQ.I) POFX = PI
      GO TO 2
    1 CONTINUE
C        DISCONTINUOUS 1L WAVE
      C = 2.*PI
      A    = 1.5708*I
      POFX = C*SIN(A)/A
    2 CONTINUE
      RETURN
      END
```

```
      SUBROUTINE TREND (TEST,PHI0,LGO,EPS)
      DIMENSION PHIMAX(6)
      IF (TEST.GT.0.03) GO TO 1
      K=1
      M=1
    1 IF (M.NE.1) GO TO 10
      IF (PHI0.LE.0) GO TO 4
      PHIBIG = PHI0
      M=2
      GO TO 2
   10 IF (PHI0.LE.PHIBIG) GO TO 3
      PHIBIG=PHI0
      GO TO 2
    3 IF (PHI0.GT.0) GO TO 2
      SIGN = PHI0*PHIM1
      IF (SIGN.GT.0) GO TO 2
      PHIMAX(K)=PHIBIG
      M=1
      K=K+1
    2 PHIM1=PHI0
      IF (K.LE.4) GO TO 4
      AV1=0.0
      AV2=0.0
      DO 5 I=1,2
      AV1= AV1 + PHIMAX(I)
      IP2= I+2
    5 AV2 = AV2 +PHIMAX(IP2)
      K=1
      DELTA = ABS((AV2-AV1)/2.0)
      CHECK=  EPS*AV2/2.0
      IF (DELTA.GT.CHECK) GO TO 4
      LGO=1
      GO TO 6
    4 LGO=2
    6 CONTINUE
      RETURN
      END
```

```
      SUBROUTINE POUT2 (LP3,LP4,KSTOP,NX)
      COMMON/FLOOA/ NEQ,UE,ANB,TAU,GAMMA,PI,LIN,T(10)
      COMMON/COM3/ H
      COMMON/COM5/ X(11),IPX(4)
      COMMON/COM8/ ABC(303),ORDP(11,303),ORDU(11,303)
      COMMON/COM9/ ORD(303)
      CALL PLOT (0.0,2.0,-3)
      CALL PLOT (0.0,11.0,3)
      CALL PLOT (1.0,0.5,-3)
      TERMS = NEQ
      NPT = KSTOP
      J1 = NPT + 1
      J2 = NPT + 2
      SIZE = 0.10*NPT
      CALL SCALE (ABC,SIZE,NPT,1)
      DO 1 J=1,LP4
      DO 4 I=1,NX
      ICHK = IPX(J)
      IF (ICHK.NE.I) GO TO 4
      Z = X(I)
      DO 100 M=1,KSTOP
  100 ORD(M) = ORDP(I,M)
      GO TO 110
    4 CONTINUE
  110 CONTINUE
      CALL SCALE (ORD,4.0,NPT,1)
      IF (J.NE.3) GO TO 2
      DELX = SIZE + 4.0
      CALL PLOT (DELX,-6.3,-3)
    2 IF (J.EQ.2.OR.J.EQ.4) GO TO 3
      CALL SYMBOL (2.90,1.80,0.10,32HNORMALIZED PRESSURE TIME HISTORY,
     1             0.0,32)
      CALL SYMBOL (2.30,1.55,0.10, 3HN =,0.0,3)
      CALL SYMBOL (3.30,1.55,0.10, 4HTAU=, 0.0,4)
      CALL SYMBOL (4.50,1.55,0.10, 4HUE =,0.0,4)
      CALL SYMBOL (5.60,1.55,0.10, 6HGAMMA=, 0.0,6)
      CALL SYMBOL (2.30,1.30,0.10, 5HNEQ =,0.0,5)
      CALL SYMBOL (3.30,1.30,0.10, 3HH= ,0.0,3)
      CALL SYMBOL (4.50,1.30,0.10, 4HPI =,0.0,4)
      CALL NUMBER (2.60,1.55,0.10,ANB,0.0,4)
      CALL NUMBER (3.75,1.55,0.10,TAU,0.0,4)
      CALL NUMBER (4.95,1.55,0.10,   UE,0.0,3)
      CALL NUMBER (6.25,1.55,0.10,GAMMA,0.0,3)
      CALL NUMBER (2.80,1.30,0.10,TERMS,0.0,-1)
      CALL NUMBER (3.55,1.30,0.10,H,0.0,3)
      CALL NUMBER (4.95,1.30,0.10,PI,0.0,3)
    3 IF (J.EQ.2.OR.J.EQ.4) DELY = 5.3
      IF (J.EQ.1.OR.J.EQ.3) DELY = 4.0
      DELX = 0.0
      IF (J.EQ.1.OR.J.EQ.3) DELX = 2.0
      CALL PLOT (DELX,DELY,-3)
      CALL SYMBOL (1.80,-1.70,0.14,4HX/L=,  0.0 ,4)
      CALL NUMBER (2.40,-1.70,0.14,   Z,0.0,3)
      CALL FACTOR (0.788)
      CALL AXIS (0.0,0.0, 4HTIME,-4,SIZE,0.0,ABC(J1),ABC(J2))
```

```
      SUBROUTINE FLOW (NX,H,TX,LP2,LP3,LP4,LP,LOUT)
      COMMON/FLODA/ NEQ,UE,ANB,TAU,GAMMA,PI,LIN,T(10)
      COMMON/COM2/ B(10),C(10),AR1(10),R2(10),3R3(10),BS(10,110),A(10)
      COMMON/COM5/ X(11),IPX(4)
      COMMON/COM6/ TSTART,TSTOP,TLYMCY
      COMMON/COM8/ ABC(303),ORDP(11,303),ORDU(11,303)
  400 FORMAT (1H1, /,10X,'FLOW PRARAMETERS' ,10X,3HZ= ,F6.3,/ )
  410 FORMAT (10X,'LINEAR= ',I2,9X,'NEQ= ',I2, 9X,'N= ',F7.5, 9X,'TAU= '
     1 ,F7.5,/,10X,'EXIT MACH= ',F5.3,3X,'GAMMA =',F5.3, 4X,'PINITIAL ='
     2 ,F5.4,/)
  420 FORMAT (11X, 4HTIME,3X, 8HPRESSURE,3X,8HVELOCITY ,/ )
  430 FORMAT (10X,F7.3,11E10.4)
      TEST = ABS(TX-TSTART)
      IF (TEST.GT.0.03)  GO TO 1
      K=1
    1 CONTINUE
      DO 110 N=1,NX
      A1 = 3.14159*X(N)
      VEL=X(N)*UE
      SUMA = 0.0
      SUMB = 0.0
      SUMC = 0.0
      SUMU = 0.0
      DO 120 I=1,NEQ
      TA= A1*I
      ST = SIN(TA)
      CS = COS(TA)
      SUMA = SUMA + A(I)*CS
      SUMB = SUMB + B(I)*CS
      SUMC = SUMC + C(I)*ST
      SUMU = SUMU + C(I)*I*3.14159*ST
  120 CONTINUE
      CALL PRMTRS (N,K,SUMA,SUMB,SUMC,SUMU,VEL)
  110 CONTINUE
      ABC(K) = TX
      IF (TX.LT.TSTOP) GO TO 300
      LOUT = 2
      KSTOP = K
      IF (LP2.NE.1) GO TO 200
      DO 310 J=1,NX
      KOUNT = 44
      DO 220 L=1,KSTOP
      IF (KOUNT.NE.44) GO TO 210
      WRITE (6,400)  X(J)
      WRITE (6,410)  LIN,NEQ,ANB,TAU,UE,GAMMA,PI
      WRITE (6,420)
      KOUNT = 1
  210 CONTINUE
      WRITE (6,430) ABC(L),ORDP(J,L),ORDU(J,L)
      KOUNT = KOUNT + 1
  220 CONTINUE
  310 CONTINUE
  200 IF (LP3.EQ.4) GO TO 300
      CALL POUT2 (LP3,LP4,KSTOP,NX)
  300 CONTINUE
      K = K+1
      RETURN
      END
```

```
      CALL AXIS (0.0,-2.0, 8HPRESSURE,8,4.,90.,ORD(J1),ORD(J2))
      CALL PLOT (0.0,-2.0,-3)
      CALL LINE (ABC,ORD,NPT,1,1,1)
      CALL FACTOR (1.0)
    1 CONTINUE
      RETURN
      END

      SUBROUTINE POUT (NMDE,ISP,NPT)
      DIMENSION COEF(100)
      COMMON/FLOOA/ NEQ,UE,ANB,TAU,GAMMA,PI,LIN,T(10)
      COMMON/PLTDA/  TIM(100),  BS(10,100)
      COMMON/COM3/ H
      EQN = NEQ
      J1=NPT+1
      J2=NPT+2
      CALL SCALE (TIM,4.0,NPT,1)
      CALL PLOT (0.0,2.0,-3)
      CALL PLOT (0.0,11.0,3)
      CALL PLOT (0.0,0.5,-3)
      KOUNT = 1
      DO 110 I=1,NMDE,ISP
      L = 1
      DO 120 K=1,NPT
      COEF(K)=BS(I,L)
  120 L=L+1
      CALL SCALE (COEF,2.0,NPT,1)
      IF (KOUNT.NE.1) GO TO 1
      CALL SYMBOL (3.0,1.3,0.10,27HTIME DEPENDENT COEFFICIENTS,0.0,27)
      CALL SYMBOL (3.5,1.1,0.10,14HTERM EXPANSION,0.0,14)
      CALL SYMBOL (3.0,0.9,0.10,29HTAU=          NBAR=          H=,0.0,29)
      CALL SYMBOL (3.0,0.7,0.10,20HGAMMA=          MACH=,0.0,20)
      CALL NUMBER (3.0,1.1,0.10, EQN,0.0,-1)
      CALL NUMBER (3.5,0.9,0.10,TAU,0.0,3)
      CALL NUMBER (4.9,0.9,0.10,ANB,0.0,3)
      CALL NUMBER (6.0,0.9,0.10,H,0.0,3)
      CALL NUMBER (5.1,0.7,0.10,UE  ,0.0,3)
      CALL NUMBER (3.7,0.7,0.10,GAMMA,0.0,3)
      CALL PLOT (2.0,0.5,-3)
    1 Y=2.5
      CALL PLOT (0.0,Y,-3)
      CALL AXIS (.0,.0,4HTIME,-4,4.,0.0,TIM(J1),TIM(J2))
      CALL AXIS (0.0,-1.0,5HBN(T),5,2.0,90.0,COEF(J1),COEF(J2))
      CALL SYMBOL (4.5,0.0,0.10,2HN=,0.0,2)
      TERM = I
      CALL NUMBER (4.8,0.0,0.10,TERM, 0.0,-1)
      CALL PLOT (0.0,-1.0,-3)
      CALL LINE (TIM,COEF,NPT,1,0,1)
      CALL PLOT (0.0,1.0,-3)
      IF (KOUNT.NE.3) GO TO 20
      CALL PLOT ( 8.0,-8.0,-3)
      KOUNT =1
      GO TO 110
   20 KOUNT = KOUNT + 1
  110 CONTINUE
      CALL PLOT (8.0,0.0,-3)
      CALL PLOT (0.0,0.0,999)
      RETURN
      END
```

Section of the Program Used to Solve the Nonlinear Wave Equation

```
      SUBROUTINE RUNG (NEQ)
C
C     INTEGRATION OF SECOND ORDER ODE WITH RETARDED VARIABLE.
C     USE WITH SECOND ORDER WAVE EQUATION ANALYSIS.
C
      EXTERNAL EQTN
      DIMENSION R(10,4),BB(10),BPB(10),BB1(10),BPB1(10)
      COMMON/COM2/ BP(10),  B(10),R1(10),R2(10),R3(10),BS(10,110),DM(10)
      COMMON/COM3/ H,H2,H06,H8
      DO 100 I=1,NEQ
      R(I,1) = H*EQTN(I, R1,B,BP)
      BPB(I) = BP(I)+ R(I,1)/2.
  100 BB(I) = B(I) + H2*BP(I) + H8*R(I,1)
      DO 110 I=1,NEQ
      R(I,2) = H*EQTN(I, R2  ,BB,BPB)
      BPB1(I)= BP(I)+ R(I,2)/2.
  110 BB1(I)= B(I)+ H2*BP(I) +H8*R(I,1)
      DO 120 I=1,NEQ
      R(I,3)= H*EQTN(I,  R2 ,BB1,BPB1)
      BPB(I)= BP(I)+R(I,3)
  120 BB(I) = B(I) + H*BP(I) +H2*R(I,3)
      DO 130 I=1,NEQ
  130 R(I,4)= H*EQTN(I, R3  ,BB,BPB)
      DO 140 I=1,NEQ
      B(I) = H*(BP(I)+(R(I,1)+R(I,2)+R(I,3))/6.) + B(I)
  140 BP(I)= (R(I,1)+2.*(R(I,2)+R(I,3))+R(I,4))/6. +BP(I)
      RETURN
      END

      REAL FUNCTION EQTN(L,YPR,Y,YP)
C
C     SECOND ORDER WAVE EQUATION
C
      DIMENSION Y(10),YP(10),YPR(10)
      COMMON/COMP1/ Q1,Q2,Q3,Q4,Q5,Q7
      COMMON/COM44/ T2(1,10,10),T3(4,10,10,10)
      COMMON/FLODA/ NEQ,UE,ANB,TAU,GAMMA,PI,LIN,T(10)
      D1 = -L*L*Q7*Y(L) - Q5*(YP(L) - T(L)*(YP(L) - YPR(L)))
      SUM=.0
      DO 100 N=1,NEQ
      S1 = Q1*Y *YP(N)*T2(1,N,L)
      S2 =((-1)**(N+L ))*YP(N)*Q2
      SUM1=.0
      IF (LIN.EQ.1) GO TO 1
      DO 110 M=1,NEQ
      S3 = Q3* M*M *YP(N)*Y(M)*T3(2,N,M,L)
      S4 = Q4* N*M *Y(N)*YP(M)*T3(1,N,M,L)
  110 SUM1= SUM1+S3-S4
    1 CONTINUE
  100 SUM = SUM + SUM1 +S1-S2
      EQTN = D1 +2.*SUM
      RETURN
      END
```

```
      SUBROUTINE PRMTRS (N,K,SUMA,SUMB,SUMC,SUMU,VEL)
C
C   SUBROUTINE FOR CALCULATING FLOW PARAMETERS FOR WAVE EQUATION
C
      COMMON/FLODA/ NEQ,UE,ANB,TAU,GAMMA,PI,LIN,T(10)
      COMMON/COM5/ X(11),IFX(4)
      COMMON/COM8/ ABC(303),ORDP(11,303),ORDU(11,303)
      ORDU(N,K) = -SUMU
      IF (LIN.EQ.1) GO TO 1
      ORDP(N,K) = GAMMA*(SUMB*(SUMB-2.)+SUMU*(2.*VEL-SUMU))/2.
      GO TO 2
    1 ORDP(N,K) = GAMMA*(-SUMB + VEL*SUMU)
    2 CONTINUE
      RETURN
      END
```

```
      SUBROUTINE WOUT1 (H,TX)
      COMMON/FLODA/ NEQ,UE,ANB,TAU,GAMMA,PI,LIN,T(10)
      COMMON/COM2/ B(10),C(10),BR1(10),BR2(10),BR3(10),BS(10,110),A(10)
      COMMON/COM6/ TSTART,TSTOP,TLYMCY
  420 FORMAT (3X,F7.3,10E10.4)
  430 FORMAT (1H )
  440 FORMAT (1H1,10X,'TIME DEPENDENT COEFFICENTS OF THE ',
     1          ,'NONLINEAR WAVE EQUATION   PHI = A(T)*COS(N*PI*Z)',/ )
  451 FORMAT (5X,'TIME     AP1      AP2       AP3       AP4       AP5
     1    AP6       AP7       AP8       AP9       AP10')
  452 FORMAT (5X,'TIME      A1       A2        A3        A4        A5
     1    A6        A7        A8        A9        A10')
  410 FORMAT (10X,'LINEAR= ',I2,9X,'NEQ= ',I2, 9X,'N= ',F7.5, 9X,'TAU= '
     1 ,F7.5,/,10X,'EXIT MACH= ',F5.3,3X,'GAMMA =',F5.3, 4X,'PINITIAL ='
     2 ,F5.4,/)
      TEST = ABS(TX-TSTART)
      IF (TEST.GT.0.030) GO TO 10
      K = 16
   10 IF (K.NE.16) GO TO 2
      WRITE (6,440)
      WRITE (6,410) LIN,NEQ,ANB,TAU,UE,GAMMA,PI
      WRITE (6,452)
      WRITE (6,451)
      K=1
    2 WRITE (6,430)
      WRITE (6,420) TX,(C(I),I=1,NEQ)
      WRITE (6,420) TX,(B(I),I=1,NEQ)
      K=K+1
      RETURN
      END
```

Section of the Program Used in the Solution of the Second Order Conservation Equations

```
      SUBROUTINE RUNG  (NEQ)
      DIMENSION R1(20),R2(20),R3(20),R4(20),C1(10),C2(10),B1(10),B2(10)
      COMMON/COM2/ B(10),C(10),BR1(10),BR2(10),BR3(10),BS(10,110)
      COMMON/COM3/ H,HD2,HD6
      CALL EQTN (B,C,BR1,R1)
      DO 100 I =1,NEQ
      IP = I+NEQ
      B1(I) = B(I) + HD2*R1(I)
  100 C1(I) = C(I) + HD2*R1(IP)
      CALL EQTN (B1,C1,BR2,R2)
      DO 110 I=1,NEQ
      IP = I+NEQ
      B2(I) = B(I) + HD2*R2(I)
  110 C2(I) = C(I) + HD2*R2(IP)
      CALL EQTN (B2,C2,BR2,R3)
      DO 120 I=1,NEQ
      IP = I+NEQ
      B1(I) = B(I) + H*R3(I)
  120 C1(I) = C(I) + H*R3(IP)
      CALL EQTN (B1,C1,BR3,R4)
      DO 130 I=1,NEQ
      IP = I+NEQ
      B(I) = B(I) + HD6*(R1(I)+R4(I)+2.*(R2(I)+R3(I)))
  130 C(I) = C(I) + HD6*(R1(IP)+R4(IP)+2.*(R2(IP)+R3(IP)))
      RETURN
      END
```

```
      SUBROUTINE EQTN (B,C,BR,R)
      DIMENSION C(10),B(10),BR(10),R(20),F1(10),F2(10)
      COMMON/COMS1/ Q1,Q2,GP1,GT1
      COMMON/FLODA/ NEQ,UE,ANB,TAU,GAMMA,PI,LIN,T(10)
      COMMON/COM4/ T2(1,10,10),T3(3,10,10,10)
      LSIGN = -1
      DO 110 L=1,NEQ
      PIL = L*3.14159
      S1 = -UE*C(L) + PIL*B(L)/GAMMA
      R1 = -GAMMA*(PIL*C(L)+  UE*B(L)-T(L) *UE*(B(L)-BR(L)))
      R5 = -GAMMA*Q1*B(L)
      SUMN1 = 0.0
      SUMN2 = 0.0
      DO 120 N=1,NEQ
      PIN = N*3.14159
      S4 =   UE*PIN*T2(1,N,L)*C(N)
      R2 =   UE*PIN*T2(1,L,N)*B(N)
      R6 = GAMMA*Q1*PIN*T2(1,L,N)*B(N)
      SUMM1 = 0.0
      SUMM2 = 0.0
      IF (LIN.EQ.1) GO TO 300
      DO 130 M=1,NEQ
      PIM = M*3.14159
      S5 = PIM*T3(1,N,M,L)*C(N)*C(M)
      S6 = PIN*    T3(1,N,M,L)*B(N)*B(M)/(GAMMA*GAMMA)
      R3 = PIM*T3(1,N,L,M)*B(M)*C(N)
      R4 = PIM*T3(3,N,M,L)*B(N)*C(M)
      SUMM2 = SUMM2 + R3 - GAMMA*R4
  130 SUMM1= SUMM1 + S5 + S6
  300 CONTINUE
      SUMN2 = SUMN2 + R2 + SUMM2 + R6
  120 SUMN1 = SUMN1 + S4 + SUMM1
      F1(L) = S1    -2.*SUMN1
      F2(L) = R1 + 2.*SUMN2 + R5
      LSIGN = -1*LSIGN
  110 CONTINUE
      DO 210 L=1,NEQ
      LP = L + NEQ
      R(L) = F2(L)
      S = 0.0
      DO 200 N=1,NEQ
  200 S = S + T2(1,N,L)*F2(N)
      R(LP) = F1(L) - 2.*Q1*S
  210 CONTINUE
      RETURN
      END
```

```
      SUBROUTINE PRMTRS (N,K,SUMA,SUMB,SUMC,SUMU,VEL)
C
C   SUBROUTINE FOR ACLCULATING FLOW PARAMETERS FOR 2ND OREDER CONSER. EQS.
C
      COMMON/COMS1/ Q1,Q2,GP1,GT1
      COMMON/COMS/ X(11),IPX(4)
      COMMON/COMB/ ABC(303),ORDP(11,303),ORDU(11,303)
      ORDP(N,K) = SUMB
      ORDU(N,K) = SUMC +  Q1*SUMB*X(N)
      RETURN
      END
```

```
      SUBROUTINE WOUT1 (H,TX)
      COMMON/FLODA/ NEQ,UE,ANB,TAU,GAMMA,PI,LIN,T(10)
      COMMON/COM2/ B(10),C(10),BR1(10),BR2(10),BR3(10),BS(10,110),A(10)
      COMMON/COMS1/ Q1,Q2,GP1,GT1
      COMMON/COM6/ TSTART,TSTOP,TLYMCY
  420 FORMAT (3X,F7.3,10E10.4)
  430 FORMAT (1H )
  440 FORMAT (1H1,10X,'TIME DEPENDENT COEFFICENTS OF THE ',
     1  'SECOND ORDER CONSERVATION EQS. SOLUTIONS',/)
  450 FORMAT (5X,'TIME      B1        B2        B3        B4        B5
     1      B6        B7        B8        B9        B10')
  451 FORMAT (5X,'TIME      C1        C2        C3        C4        C5
     1      C6        C7        C8        C9        C10')
  410 FORMAT (10X,'LINEAR= ',I2,9X,'NEQ= ',I2, 9X,'N= ',F7.5, 9X,'TAU= '
     1 ,F7.5,/,10X,'EXIT MACH= ',F5.3,3X,'GAMMA =',F5.3, 4X,'PINITIAL ='
     2 ,F5.4,/)
        TEST = ABS(TX-TSTART)
        IF (TEST.GT.0.030) GO TO 10
        K = 16
   10 IF (K.NE.16) GO TO 2
        WRITE (6,440)
        WRITE (6,410) LIN,NEQ,ANB,TAU,UE,GAMMA,PI
        WRITE (6,450)
        WRITE (6,451)
        K=1
    2 WRITE (6,430)
        WRITE (6,420) TX,(B(I),I=1,NEQ)
        WRITE (6,420) TX,(C(I),I=1,NEQ)
        K=K+1
        RETURN
        END
```

Section of the Program Used in the Analysis of Large Amplitude Oscillations

```
      SUBROUTINE RUNG  (NEQ)
C
C   INTEGRATION OF FIRST ORDER ODE WITH RETARDED VARIABLE
C   USE WITH LARGE AMPLITUDE ANALYSIS
C
      DIMENSION RA1(10),RA2(10),RA3(10),RA4(10),RB1(10),RB2(10),RB3(10),
     1RB4(10),RC1(10),RC2(10),RC3(10),RC4(10),A1(10),A2(10),B1(10),
     2B2(10),C1(10),C2(10)
      COMMON/COM2/ B(10),C(10),BR1(10),BR2(10),BR3(10),BS(10,110),A(10)
      COMMON/COM3/ H,HD2,HD6
      CALL EQTN (A,B,C,BR1,RA1,RB1,RC1)
      DO 100 I =1,NEQ
      A1(I) = A(I) + HD2*RA1(I)
      B1(I) = B(I) + HD2*RB1(I)
      C1(I) = C(I) + HD2*RC1(I)
  100 CONTINUE
      CALL EQTN (A1,B1,C1,BR2,RA2,RB2,RC2)
      DO 110 I=1,NEQ
      A2(I) = A(I) + HD2*RA2(I)
      B2(I) = B(I) + HD2*RB2(I)
      C2(I) = C(I) + HD2*RC2(I)
  110 CONTINUE
      CALL EQTN (A2,B2,C2,BR2,RA3,RB3,RC3)
      DO 120 I=1,NEQ
      A1(I) = A(I) + H*RA3(I)
      B1(I) = B(I) + H*RB3(I)
      C1(I) = C(I) + H*RC3(I)
  120 CONTINUE
      CALL EQTN (A1,B1,C1,BR3,RA4,RB4,RC4)
      DO 130 I=1,NEQ
      A(I) = A(I) + HD6*(RA1(I)+RA4(I)+2.*(RA2(I)+RA3(I)))
      B(I) = B(I) + HD6*(RB1(I)+RB4(I)+2.*(RB2(I)+RB3(I)))
      C(I) = C(I) + HD6*(RC1(I)+RC4(I)+2.*(RC2(I)+RC3(I)))
  130 CONTINUE
      RETURN
      END
```

```
      SUBROUTINE PRMTRS (N,K,SUMA,SUMB,SUMC,SUMU,VEL)
C
C   SUBROUTINE FOR CALCULATING FLOW PARAMETERS FOR LARGE AMPLITUDE WAVES
C
      COMMON/FLODA/ NEQ,UE,ANB,TAU,GAMMA,PI,LIN,T(10)
      COMMON/COMS1/ Q1,Q2,GP1,GT1
      COMMON/COM5/ X(11),IPX(4)
      COMMON/COM3/ ABC(303),ORDP(11,303),ORDU(11,303)
      ORDP(N,K) = SUMB
      IF (LIN.EQ.1) GO TO 1
      ORDU(N,K) = SUMC + (Q1 + Q2*SUMB)*SUMB*X(N)
      GO TO 2
    1 ORDU(N,K) = SUMC + Q1*SUMB*X(N)
    2 CONTINUE
      RETURN
      END




      SUBROUTINE WOUT1 (H,TX)
      COMMON/FLODA/ NEQ,UE,ANB,TAU,GAMMA,PI,LIN,T(10)
      COMMON/COM2/ B(10),C(10),BR1(10),BR2(10),BR3(10),BS(10,110),A(10)
      COMMON/COMS1/ Q1,Q2,GP1,GT1
      COMMON/COM6/ TSTART,TSTOP,TLYMCY
  420 FORMAT (3X,F7.3,10E10.4)
  430 FORMAT (1H )
  440 FORMAT (1H1,10X,'TIME DEPENDENT COEFFICENTS OF THE ',
     1  'LARGE AMPLITUDE SOLUTIONS',/)
  450 FORMAT (5X,'TIME      B1        B2        B3        B4        B5
     1     B6        B7        B8        B9        B10')
  451 FORMAT (5X,'TIME      C1        C2        C3        C4        C5
     1     C6        C7        C8        C9        C10')
  452 FORMAT (5X,'TIME      A1        A2        A3        A4        A5
     1     A6        A7        A8        A9        A10')
  410 FORMAT (10X,'LINEAR= ',I2,9X,'NEQ= ',I2, 9X,'N= ',F7.5, 9X,'TAU= '
     1 ,F7.5,/,10X,'EXIT MACH= ',F5.3,3X,'GAMMA =',F5.3, 4X,'PINITIAL ='
     2 ,F5.4,/)
      TEST = ABS(TX-TSTART)
      IF (TEST.GT.0.030) GO TO 10
      K = 12
   10 IF (K.NE.12) GO TO 2
      WRITE (6,440)
      WRITE (6,410) LIN,NEQ,ANB,TAU,UE,GAMMA,PI
      WRITE (6,452)
      WRITE (6,450)
      WRITE (6,451)
      K=1
    2 WRITE (6,430)
      WRITE (6,420) TX,(A(I),I=1,NEQ)
      WRITE (6,420) TX,(B(I),I=1,NEQ)
      WRITE (6,420) TX,(C(I),I=1,NEQ)
      K=K+1
      RETURN
      END
```

```
      SUBROUTINE EQTN (A,B,C,BR,RA,RB,RC)
C
C     LARGE AMPLITUDE EQUATION
C
      DIMENSION A(10),B(10),C(10),BR(10),RA(10),RB(10),RC(10),F1(10),
     1F2(10),F3(10)
      COMMON/COMS1/ Q1,Q2,GP1,GT1
      COMMON/FLODA/ NEQ,UE,ANB,TAU,GAMMA,PI,LIN,T(10)
      COMMON/COM4/ T2(1,10,10),T3(4,10,10,10)
      DO 100 L=1,NEQ
      PIL = L*3.14159
      S01 =PIL*C(L) + Q1*B(L) - T(L)*UE*(B(L) - BR(L))
      S0 = -UE*A(L) + S01
      R0 = -GAMMA*(S01+ UE*B(L))
      U0 = PIL*B(L)/GAMMA - UE*C(L)
      SUMN1 = 0.0
      SUMN2 = 0.0
      SUMN3 = 0.0
      DO 110 N=1,NEQ
      PIN = N*3.14159
      S1 =  PIN*T2(1,N,L)*A(N)
      S2 = PIN*T2(1,N,L)*B(N)
      R1 =  PIN*T2(1,N,L)*B(N)
      U1 =  PIN*T2(1,L,N)*C(N)
      SUMM1 = 0.0
      SUMM2 = 0.0
      SUMM3 = 0.0
      IF (LIN.EQ.1) GO TO 200
      DO 130 M=1,NEQ
      PIM = M*3.14159
      S3 = PIM*T3(1,N,M,L)*C(N)*A(M)
      S4 = PIM*T3(2,N,M,L)*A(N)*C(M)
      S5 =  T3(2,N,M,L)*A(N)*A(M)
      S6 = PIM*T3(3,N,M,L)*(B(N)*A(M) - B(M)*A(N))
      S8 = T3(2,N,M,L)*A(N)*B(M)
      S9 = T3(2,N,M,L)*(B(N)-BR(N))*A(M)
      S10 = T3(2,N,M,L)*B(N)*B(M)
      S11 = PIM*T3(3,N,M,L)*B(N)*B(M)
      S12 = S10 - 2.*S11
      R2 = PIM*T3(1,N,M,L)*C(N)*B(M)
      R3 =  PIM*T3(2,N,M,L)*B(N)*C(M)
      R4 = T3(1,N,M,L)*C(N)*C(M)
      U2 = PIM*T3(1,L,M,N)*A(N)*B(M)
      U3 = T3(1,N,L,M)*C(N)*C(M)*PIM
      U4 =  PIM*T3(3,N,L,M)*B(N)*C(M)
      U5 = PIN*T3(4,N,L,M)*B(N)*C(M)
      U6 = T3(1,L,N,M)*B(N)*C(M)
      SUMM1 = SUMM1 + S3 + S4 - UE*S5 + Q1*(S6+S8) -2.*T(N)*UE*S9
     1        + Q2*S12
      SUMM2 = SUMM2 + R2 - GAMMA*R3 - GT1*R4 - Q1*(GAMMA*S10 - GP1*S11)
     1        - Q2*GAMMA*S12
      SUMM3 = SUMM3 + U2/GAMMA - U3 - Q1*(U4 - U5 + U6)
  130 CONTINUE
  200 CONTINUE
      SUMN1 = SUMN1 + SUMM1 + UE*S1 - Q1*S2
```

```
      SUMN2 = SUMN2 + SUMM2 + UE*R1 + GAMMA*Q1*S2
      SUMN3 = SUMN3 + SUMM3 - UE*U1
  110 CONTINUE
      F1(L) = S0 + 2.*SUMN1
      F2(L) = R0 + 2.*SUMN2
      F3(L) = U0 + 2.*SUMN3
  100 CONTINUE
      DO 300 L=1,NEQ
      U8N = 0.0
      DO 310 N=1,NEQ
      U8 = T2(1,L,N)*F2(N)
      U8M = 0.0
      IF (LLIN.EQ.1) GO TO 320
      DO 330 M=1,NEQ
      U9 = T3(3,N,L,M)*B(N)*F2(M)
  330 U8M = U8M + U9
  320 CONTINUE
      U8N = U8N - Q1*U8 - Q2*U8M*2.
  310 CONTINUE
      RA(L) = F1(L)
      RB(L) = F2(L)
      RC(L) = F3(L) + 2.*U8N
  300 CONTINUE
      RETURN
      END
```

LITERATURE CITED

1. Crocco, L., "The Relevance of a Characteristic Time in Combustion Instability," ICRPG 2nd Combustion Conference, pp. 115-138, May, 1966.

2. Crocco, L., and Sirignano, W. A., "Effect of the Transverse Velocity Component on the Nonlinear Behavior of Short Nozzles," AIAA J., 4, pp. 1428-1430, 1960.

3. Crocco, L., and Cheng, S. I., Theory of Combustion Instability in Liquid Propellant Rocket Motors, AGARD Monograph No. 8, Butterworths Scientific Pub., Ltd., London, 1956.

4. Zucrow, M. J., and Osborne, J. R., "An Experimental Study of High Frequency Combustion Pressure Oscillations," A.R.S. Journal, V. 28, No. 10, p. 654, 1958.

5. Crocco, L., "Aspects of Combustion Stability in Liquid Propellant Rocket Motors," J. American Rocket Soc., 21, p. 163, 1951, and 22, p. 7, 1952.

6. Reardon, F. H., "Application of Crocco Theory," ICRPG 2nd. Combustion Conference, pp. 155-162, May 1966.

7. Crocco, L., Grey, J., and Harrie, D. T., "Theory of Liquid Propellant Rocket Combustion Instability and its Experimental Verification, ARS J., 30, 159, 1960.

8. Sirignano, W. A., "A Theoretical Study of Nonlinear Combustion Ins bility: Longitudinal Mode," Princeton University AMS Tech. Rpt. No. 677, March 1964 (Ph.D. Thesis).

9. Mitchell, C. E., "Axial Mode Shock Wave Combustion Instability in Liquid Propellant Rocket Engines," Princeton University AMS Tech. Rpt. No. 798, (NASA CR 72259), July 1967, (Ph.D. Thesis).

10. Powell, E. A., and Zinn, B. T., "A Single Mode Approximation in the Solution of Nonlinear Combustion Instability Problems," Combustion Science and Technology, Vol. 3, pp. 121-132, 1971.

11. Zinn, B. T., and Powell, E. A., "Application of the Galerkin Method in the Solution of Combustion Instability Problems," IAF paper p. 69, Proc. 19th Congress of the Int. Ast. Federation, 1968.

12. Zinn, B. T., and Powell, E. A., "Nonlinear Combustion Instability in Liquid-Propellant Rocket Engines," Proc. Thirteenth Int. Symp. on Combustion, The Combustion Institute, 1970.

13. Powell, E. A., and Zinn, B. T., "Stable Limit Cycles and Triggering Limits of the First Radial Mode in Unstable Liquid Rockets," Israel Journal of Technology, Vol. 9, Nos. 1-2, pp. 177-188, 1971.

14. Powell, E. A., "Nonlinear Combustion Instability in Liquid Propellant Rocket Engines," Georgia Inst. of Tech. Rpt. GITAER 70-6, 1970, (Ph.D. Thesis).

15. Culick, F. E. C., "Non-Linear Growth and Limiting Amplitude of Acoustic Oscillations in Combustion Chambers," Combustion Science and Technology, Vol. 3, pp. 1-16, 1971.

16. Finlayson, B. A., and Scrivea, L. E., "The Method of Weighted Residuals - A Review," Applied Mechanics Reviews, Vol. 19, No. 9, Sept. 1966.

17. Ames, W. F., Nonlinear Partial Differential Equations in Engineering, Academic Press, 1965.

18. Conte, S. D., Elementary Numerical Analysis, McGraw-Hill, Co., 1965.

19. Berezin, I. S., and Zhidkov, N. P., Computing Methods, Vol. 2, Addison Wesley Pub. Co., 1965.

20. Temkin, S., "Propagating and Standing Sawtooth Waves," The Journal of the Acoustical Society of America, Vol. 45, No. 1, pp. 224-227, 1969.

21. Chester, W., "Resonant Oscillations in Closed Tubes," Journal of Fluid Mechanics, 18, 1964.

22. Frederickson, E., "Resonance - Behavior of Non-Linear One-Dimensional Gas Vibrations Analyzed by the Ritz-Galerkin Method," Ingenieur-Archiv, XXV, 1957.

23. Priem, R. J., and Heidmann, M. F., "Propellant Vaporization as a Design Criterion for Rocket-Engine Combustion Chambers," NASA TR-R-67, 1960.

VITA

Manuel Edward Lores was born in Havana, Cuba, on July 22, 1942. He was raised in Miami, Florida, and he was graduated from Archbishop Curley High School in Miami. In September of 1960, Mr. Lores entered the Georgia Institute of Technology and received the degree of Bachelor of Aerospace Engineering in June, 1964.

Mr. Lores was employed with the McDonnell-Douglas Company from 1964 to 1965. In September of 1965, he returned to the Georgia Institute of Technology and received the degree of Master of Science in Aerospace Engineering in December, 1966.

After two years with the Ling-Temco-Vought Aerospace Corporation, Mr. Lores entered the doctoral program in the School of Aerospace Engineering at the Georgia Institute of Technology.

On June 14, 1964, Mr. Lores married the former Lynda L. Rilovick of Columbua, Georgia. They have two children, Richard Edward and Christine Michelle.